

Copyright Warning & Restrictions

The copyright law of the United States (Title 17, United States Code) governs the making of photocopies or other reproductions of copyrighted material.

Under certain conditions specified in the law, libraries and archives are authorized to furnish a photocopy or other reproduction. One of these specified conditions is that the photocopy or reproduction is not to be “used for any purpose other than private study, scholarship, or research.” If a user makes a request for, or later uses, a photocopy or reproduction for purposes in excess of “fair use” that user may be liable for copyright infringement,

This institution reserves the right to refuse to accept a copying order if, in its judgment, fulfillment of the order would involve violation of copyright law.

Please Note: The author retains the copyright while the New Jersey Institute of Technology reserves the right to distribute this thesis or dissertation

Printing note: If you do not wish to print this page, then select “Pages from: first page # to: last page #” on the print dialog screen

The Van Houten library has removed some of the personal information and all signatures from the approval page and biographical sketches of theses and dissertations in order to protect the identity of NJIT graduates and faculty.

MOLECULAR MODELING OF SIGMA 1 AND SIGMA 2 RECEPTOR LIGANDS: PHARMACOPHORE DEVELOPMENT AND COMPARISON USING DISCOTECH AND BIOACTIVITY PREDICTION COMPARISON OF *AB INITIO* AND DENSITY FUNCTIONAL COMFA STUDIES FOR SPIRO AND OTHER RECEPTOR LIGANDS

ABSTRACT

by
Lisa M. Kardos

The role of the biological receptor is currently being studied by researchers in medicine. Information about sigma receptors in particular can be gained by studying the ligands associated with each type, sigma 1 or sigma 2. Sigma 1 receptor ligands consist of drug candidates that often have psychiatric and neurological applications; sigma 2 receptor ligands consist of drug candidates that have been linked with cancer treatment among other applications.

Molecular modeling of biological receptor ligands often encompasses pharmacophore development and Comparative Molecular Field Analysis (CoMFA). Pharmacophore models are developed to understand the unique features such as binding groups that make a ligand bioactive. CoMFA uses experimental data of molecules, considered to be a training set, to yield bioactivity prediction for those molecules; this is the internal validation piece. An external test set of molecules with known experimental data can then be used for validation of the CoMFA models. The resulting CoMFA models create contour maps which provide information about the sterics and electrostatics, resulting in the ability to apply this information during the design of new ligands. The new molecules can then be tested in the validated CoMFA models to yield bioactivity predictions.

This study describes the development of pharmacophore and Comparative Molecular Field Analysis (CoMFA) models for sigma 1 and sigma 2 receptor ligands. Distance Comparisons (DISCOtech) in SYBYL-X 2.1 is used as a tool for the pharmacophore development. A pharmacophore is developed for each individual class of molecules and for the entire set of sigma 1 molecules and sigma 2 molecules analyzed during this study, respectively. All compounds are calculated in SPARTAN '14 using *ab initio* and density functional calculation methods HF/6-31G* and B3LYP/6-31G* prior to model development. These calculations determine the geometry optimization and electrostatic charges for each molecule.

CoMFA studies, utilizing SYBYL-X 2.1, are performed for 41 sigma 1 receptor ligands using the radioligand [H³](+) pentazocine and for 31 sigma 2 receptor ligands using [H³](+) DTG in the presence of pentazocine. The CoMFA models developed confirm that bioactivity prediction comparison is reliable for both HF/6-31G* and B3LYP/6-31G* optimized geometries for both sigma 1 and sigma 2 ligands; this is verified via both internal and external validation methods. The CoMFA contour maps are utilized to design new sigma 1 and sigma 2 ligands; the newly designed ligands are predicted to be highly active according to the CoMFA models. This study also compares CoMFA models between the *ab initio* and density functional calculation levels for sigma 1 and sigma 2 ligands, respectively. The similarities and differences between sigma 1 and sigma 2 receptor ligands are also analyzed via the developed pharmacophore models and generated CoMFA contour maps.

**MOLECULAR MODELING OF SIGMA 1 AND SIGMA 2 RECEPTOR
LIGANDS: PHARMACOPHORE DEVELOPMENT AND COMPARISON
USING DISCOTECH AND BIOACTIVITY PREDICTION COMPARISON OF *AB
INITIO* AND DENSITY FUNCTIONAL COMFA STUDIES FOR SPIRO AND
OTHER RECEPTOR LIGANDS**

by
Lisa M. Kardos

**A Dissertation
Submitted to the Faculty of
New Jersey Institute of Technology
in Partial Fulfillment of the Requirements for the Degree of
Doctor of Philosophy in Chemical Engineering**

Otto H. York Department of Chemical, Biological and Pharmaceutical Engineering

January 2015

Copyright © 2015 by Lisa M. Kardos

ALL RIGHTS RESERVED

APPROVAL PAGE

**MOLECULAR MODELING OF SIGMA 1 AND SIGMA 2 RECEPTOR
LIGANDS: PHARMACOPHORE DEVELOPMENT AND COMPARISON
USING DISCOTECH AND BIOACTIVITY PREDICTION COMPARISON OF *AB
INITIO* AND DENSITY FUNCTIONAL COMFA STUDIES FOR SPIRO AND
OTHER RECEPTOR LIGANDS**

Lisa M. Kardos

Dr. Tamara Gund, Co-Dissertation Advisor Date
Professor of Chemistry and Environmental Science, NJIT

Dr. Norman W. Loney, Co-Dissertation Advisor Date
Professor and Chair of Chemical, Biological and Pharmaceutical
Engineering, NJIT

Dr. Piero Armenante, Committee Member Date
Distinguished Professor of Chemical, Biological and Pharmaceutical
Engineering, NJIT

Dr. Reginald Tomkins, Committee Member Date
Professor of Chemical, Biological and Pharmaceutical Engineering, NJIT

Dr. Cyril Migdal, Committee Member Date
Research and Development Director, Chemtura Corporation

BIOGRAPHICAL SKETCH

Author: Lisa M. Kardos
Degree: Doctor of Philosophy
Date: January 2015

Undergraduate and Graduate Education:

- Doctor of Philosophy in Chemical Engineering, New Jersey Institute of Technology, Newark, NJ, 2015
- Master of Science in Chemical Engineering, New Jersey Institute of Technology, Newark, NJ, 2006
- Bachelor of Science in Chemical Engineering, Magna Cum Laude Albert Dorman Honors College, Newark College of Engineering New Jersey Institute of Technology, Newark, NJ, 2004

Major: Chemical Engineering

Presentations and Publications:

Zhu L., Bozzelli, J.W and Kardos, L.M., "Thermochemical Properties, $\Delta_f H^\circ$ Degrees (298), S° Degrees (298), and C_p Degrees (T), for n-Butyl and n-Pentyl Hydroperoxides and the Alkyl and Peroxy Radicals, Transition States, and Kinetics for Intramolecular Hydrogen Shift Reactions of the Peroxy Radicals. *Journal of Physical Chemistry A*, **2007**, 111, 6361-6377.

Kardos, L., Andal, R. and Barat, R.B. *Applied Optics in Chemical Reaction Engineering*. AIChE Annual Meeting and Fall Showcase, Austin, TX, November 2004.

To my precious son, Gabriel Fernando Jusino and my beloved husband, Fernando Jusino. Gabriel, I am so blessed to be your mother; you are my inspiration. Fernando, thank you for your love, support and for being such a wonderful husband. I will love you both forever.

I also dedicate this thesis to my family who has given me so much love, support and encouragement. I am especially grateful to my role models, my parents and grandparents, for believing in me and for encouraging me to pursue my Ph.D.; Amelia and Joseph Kardos III and Elizabeth and John Papetti Sr., respectively. I thank my siblings, Donna Kardos Yesalavich and Joseph Kardos IV. I love you all dearly.

I would like to honor the memory of those who have passed on - dear friends, teachers and mentors. I am very thankful that they believed in me, cared about me and encouraged me to pursue my dreams. They live on in my heart; my advisor and professor, Dr. Dana Knox; distinguished chemical engineer Otto H. York; my professor, Joseph Kisutcza; my dear childhood friend, Lindsay Della Serra; my childhood librarian, Rosemary Chodack; my math teacher, Carol Fedoryk; and my history teacher, Lawrence Fuhro.

ACKNOWLEDGMENT

My deepest appreciation goes to my co-advisors, Dr. Tamara Gund and Dr. Norman Loney. I thank Dr. Gund for teaching me molecular modeling, medicinal chemistry and drug design; I have learned so much from her and recognize her not only as an innovative researcher, but also as someone who possesses a special kindness and heart. I thank Dr. Loney, Chair of the department, for his excellent leadership in the department and for his guidance for my dissertation and graduate education, for mentoring me through my career, for teaching me to solve problems innovatively and for helping me to develop my teaching skills; his mentorship has indeed enriched my life and skillset. I also thank Dr. Reginald Tomkins for serving on the committee and for all of his support over the years, particularly as the Graduate Advisor. The combined encouragement from Dr. Tomkins and Dr. Knox led me to pursue my Ph.D. degree following the completion of my M.S. degree at NJIT. I thank Dr. Piero Armenante for serving on my dissertation committee and for his support over the years. I am also very grateful to Dr. Cyril Migdal, Research and Development Director at Chemtura Corporation, for traveling out-of-state to serve on my committee and for all of his mentoring, support and leadership during my degree work and previously when I worked at Chemtura Corporation. I would additionally like to acknowledge Dr. Angelo Perna and Ms. Zara Williams of the Ronald E. McNair Post-Baccalaureate Achievement Program; the McNair program encouraged me to pursue my Ph.D.

I would like to thank the Graduate Studies office administrators for their guidance and support through my graduate education; I especially thank Ms. Clarisa Gonzalez-

Lenahan for her help. I am also thankful to Associate Provost Sotirios Ziavras and to the late Associate Provost Marino Xanthos.

I thank the Otto H. York Department of Chemical, Biological and Pharmaceutical Engineering – the faculty, staff and particularly Cynthia Wos for her help and support through the years. I also thank the staff at the Robert W. Van Houten Library, especially Mr. Bruce Slutsky and Mrs. Rosalind Yates, for their assistance.

Dr. Joel Bloom has played a key role in my education and success; now President of NJIT, Dr. Bloom was formerly Dean of the Albert Dorman Honors College when I was an undergraduate. He has always motivated me to pursue excellence in my endeavors. Assistant Dean Lois Chipepo of the Honors College has been a pivotal figure in my life; she has been extremely supportive these past fifteen years. I am blessed by her friendship.

I would also like to express my appreciation to the NJIT community; so many individuals, from peers, to staff, to faculty members to administrators, have touched my life. I thank fellow peers and friends from NJIT; I give special thanks to Dr. Laura Wirsza for her friendship and guidance in the area of molecular modeling.

I am also very thankful for the childhood I had in Cranford Township - from the valuable start I received in my education at Cranford Public Schools through their inspiring teachers to the lifelong friendships I have from growing up there. I am especially grateful for my friendships with Mrs. Sherry Lange and Mrs. Katherine Arcieri Walter, for they always encouraged and inspired me to pursue my education.

I, again, thank all of my friends and family members, many of whom are mentioned in my dedication, for enriching my life through their love and support.

TABLE OF CONTENTS

Chapter	Page
1 INTRODUCTION.....	1
1.1 Overview	1
2 BACKGROUND.....	2
2.1 Biological Activity and Interactions of Receptor Ligands.....	4
2.2 Pharmacophore Identification and QSAR Methodology.....	6
2.2.1 Partial Least Squares.....	8
2.2.2 Criteria for “Robust” CoMFA Models.....	9
2.3 Design of New Ligands.....	11
3 MOLECULAR MODELING OF SIGMA 1 RECEPTOR LIGANDS.....	12
3.1 Introduction.....	12
3.2 Selection of Ligands.....	14
3.3 Materials and Methods.....	25
3.4 Pharmacophore Derivation.....	26
3.4.1 Pharmacophore Models.....	26
3.5 Comparative Molecular Field Analysis.....	50
3.5.1 Geometry Optimization and Electrostatic Studies.....	50
3.5.2 Alignment.....	51
3.5.3 Quantitative Structure Activity Data Analysis.....	54
3.5.4 Contour Maps of CoMFA Models.....	63

TABLE OF CONTENTS
(Continued)

Chapter	Page
3.6 Design of New Sigma 1 Ligands.....	66
4 MOLECULAR MODELING OF SIGMA 2 RECEPTOR LIGANDS.....	88
4.1 Introduction.....	88
4.2 Selection of Ligands.....	89
4.3 Materials and Methods.....	99
4.4 Pharmacophore Derivation.....	100
3.4.1 Pharmacophore Models.....	100
4.5 Comparative Molecular Field Analysis.....	117
4.5.1 Geometry Optimization and Electrostatic Studies.....	117
4.5.2 Alignment.....	118
4.5.3 Quantitative Structure Activity Data Analysis.....	121
4.5.4 Contour Maps of CoMFA Models.....	130
4.6 Design of New Sigma 2 Ligands.....	133
5 COMPARISON OF SIGMA 1 AND SIGMA 2 RECEPTOR LIGANDS.....	138
5.1 Sigma 1 and Sigma 2 Receptor Ligand Differences.....	138
6 SUGGESTIONS FOR FURTHER WORK.....	142
APPENDIX A: ADDITIONAL CONTOUR MAPS FOR SIGMA 1 LIGANDS.....	144
APPENDIX B: ADDITIONAL CONTOUR MAPS FOR SIGMA 2 LIGANDS.....	147
APPENDIX C: ADDITIONAL CONTOUR MAPS FOR NEWLY DESIGNED SIGMA 2 LIGANDS.....	150

LIST OF TABLES

Table	Page
3.1 Binding and Functional Data of 1,2,3,4-tetrahydrospiro[naphthalene-1,4'-piperidine] Series.....	15
3.2 Binding and Functional Data of 1,4'-silaspiro[indane-1,4'-piperidine] Series.....	16
3.3 Binding and Functional Data of Spirocyclic Thienopyran System and Aminoethyl-substituted Tetrahydrobenzothiophenes.....	17
3.4 Binding and Functional Data of Spirocyclic Thienopyran System and Aminoethyl-substituted Tetrahydrobenzothiophenes.....	18
3.5 Binding and Functional Data of Fluoro-oligo-ethoxylated 4-benzylpiperazine Derivatives.....	19
3.6 Binding and Functional Data of Spirocyclic Thiophenes Series.....	20-22
3.7 Binding and Functional Data of Reference Compounds.....	23-24
3.8 Experimental and Predicted Bioactivities (pK _i) by the Training Set of Sigma 1 Compounds using <i>ab initio</i> and Density Functional Calculation Methods.....	57
3.9 Experimental and Predicted Bioactivities (pK _i) by the Test Set of Five Sigma 1 Compounds using <i>ab initio</i> and Density Functional Calculation Methods.....	58
3.10 Optimal Component Number and q ² by “Leave-One-Out” using SAMPLS by the Training Set of 36 Molecules.....	58
3.11 QSAR Reports by Non-Crossvalidation Using SAMPLS by the Training Set of 36 Molecules.....	59
3.12 A. Results for QSAR Robust Criteria Equations 2.5 – 2.9 for HF/6-31G* (Sigma 1).....	60
3.12 B. Results for QSAR Robust Criteria Equations 2.5 – 2.9 for B3LYP/6-31G* (Sigma 1).....	62

LIST OF TABLES
(Continued)

Table	Page
3.13 Spipethiane-based New Ligands.....	67
3.14 PD144418-based Ligands.....	78
3.15 Additional PD144418-based Ligands (Comparison With Second R Group).....	79
4.1 Binding and Functional Data of 4-(Tetralin-1-yl) and 4-(Naphthalen-1-yl)alkyl Derivatives of 1-Cyclohexylpiperazine.....	90
4.2 Binding and Functional Data of Substituted Aminobutyl-benzamides.....	91-92
4.3 Binding and Functional Data of Benzamide-isoquinoline Derivatives.....	93-94
4.4 Trishomocubane Subset of Compounds.....	95
4.5 1-aralkyl-4-benzylpiperazine Derivatives Subset.....	96
4.6 Binding and Functional Data of Reference and Other Compounds.....	98
4.7 Experimental and Predicted Bioactivities (pK _i) by the Training Set of Sigma 2 Compounds using <i>ab initio</i> and Density Functional Calculation Methods.....	124
4.8 Experimental and Predicted Bioactivities (pK _i) by the Test Set of Five Sigma 2 Compounds using <i>ab initio</i> and Density Functional Calculation Methods.....	125
4.9 Optimal Component Number and q ² by “Leave-One-Out” using SAMPLS by the Training Set of 26 Molecules.....	126
4.10 QSAR Reports by Non-Crossvalidation Using SAMPLS by the Training Set of 26 Molecules.....	126
4.11 Results for QSAR Robust Criteria Equations 2.5 – 2.9 for HF/6-31G* (Sigma 2)	128
4.12 Results for QSAR Robust Criteria Equations 2.5 – 2.9 for B3LYP/6-31G* (Sigma 2).....	130
4.13 Compound 19-based New Ligands.....	133

LIST OF FIGURES

Figure	Page
3.1 Gund pharmacophore for sigma 1 receptor ligands	13
3.2 Gund pharmacophore for sigma 1 receptor ligands	14
3.3 DISCOtech pharmacophore derivation and overlay of 1,2,3,4-tetrahydrospiro[naphthalene-1,4'-piperidine] and 1,4'-silaspiro[indane-1,4'-piperidine] series (compounds 1-8, hydrogen atoms hidden).....	27
3.4 DISCOtech pharmacophore derivation of 1,2,3,4-tetrahydrospiro[naphthalene-1,4'-piperidine] and 1,4'-silaspiro[indane-1,4'-piperidine] series (compounds 1-8) with lead compound 1, hydrogen atoms hidden.....	27
3.5 DISCOtech pharmacophore model of 1,2,3,4-tetrahydrospiro[naphthalene-1,4'-piperidine] and 1,4'-silaspiro[indane-1,4'-piperidine] series (compounds 1-8)....	28
3.6 DISCOtech pharmacophore derivation of spirocyclic thienopyran system and aminoethyl-substituted tetrahydrobenzothiophenes (compounds 9-14, hydrogen atoms hidden).....	29
3.7 DISCOtech pharmacophore derivation of spirocyclic thienopyran system and aminoethyl-substituted tetrahydrobenzothiophenes (compounds 9-14) with lead compound 9, hydrogen atoms hidden.....	29
3.8 DISCOtech pharmacophore model of spirocyclic thienopyran system and aminoethyl-substituted tetrahydrobenzothiophenes (compounds 9-14).....	30
3.9 DISCOtech pharmacophore derivation of fluoro-oligo-ethoxylated 4-benzylpiperazine derivatives (compounds 15-17, hydrogen atoms hidden).....	31
3.10 DISCOtech pharmacophore model of fluoro-oligo-ethoxylated 4-benzylpiperazine derivatives (compounds 15-17).....	31
3.11 DISCOtech pharmacophore model of fluoro-oligo-ethoxylated 4-benzylpiperazine derivatives (compounds 15-17).....	32
3.12 DISCOtech pharmacophore derivation of spirocyclic thiophenes (compounds 18-38, hydrogen atoms hidden).....	35
3.13 DISCOtech pharmacophore derivation of spirocyclic thiophenes (compounds 18-38, hydrogen atoms hidden) with lead compound 18.....	36

LIST OF FIGURES
(Continued)

Figure	Page
3.14 DISCOtech pharmacophore derivation of spirocyclic thiophenes (compounds 18-38).....	36
3.15 Alternate DISCOtech pharmacophore derivation of spirocyclic thiophenes (highest activity compounds of series; hydrogen atoms hidden - compounds 18, 19, 21, 22, 24, 25 and 32).....	37
3.16 Alternate DISCOtech pharmacophore derivation of spirocyclic thiophenes with compound 22, hydrogen atoms hidden.....	37
3.17 Meyer and coworkers' mapping of compound "3b" (compound 32) onto a 3D pharmacophore model.....	38
3.18 Distances for spirocyclic thiophene pharmacophore generated by Meyer and coworkers.....	38
3.19 Comprehensive DISCOtech pharmacophore derivation representing entire Sigma 1 class of molecules studied (hydrogen atoms hidden – compounds 1, 9, 15, 22, 41, 43 and 44).....	40
3.20 Comprehensive DISCOtech pharmacophore derivation for Sigma 1.....	41
3.21 Comprehensive DISCOtech pharmacophore derivation with reference compound 43, Spipethiane.....	44
3.22 Sigma 1 pharmacophore model for Laggner and coworkers.....	44
3.23 Pharmacophore model for Collina and coworkers.....	45
3.24 Alternate sigma 1 pharmacophore model with additional hydrophobic groups (green spheres) to compare with Laggner et al. model.....	45
3.25 Additional alternate sigma 1 pharmacophore model with additional hydrophobic group (green sphere) to compare with Laggner et al. model.....	46
3.26 Sigma 1 pharmacophore model for Glennon.....	46

LIST OF FIGURES
(Continued)

Figure	Page
3.27 Additional alternate sigma 1 pharmacophore model without lone pair of electrons to compare with Glennon model.....	47
3.28 Additional alternate sigma 1 pharmacophore model with lone pair of electrons to compare with the Glennon model.....	47
3.29 Caballero and coworkers' figure depicting comparisons between Glennon (a), Laggner (b) and their work (c).	49
3.30 Caballero and coworkers' GALAHAD pharmacophore model of MAPCC derivatives and molecular alignment of the compounds.....	49
3.31 Alignment of all 41 sigma 1 ligands at the HF/6-31G* calculation level.....	53
3.32 Alignment of all 41 sigma 1 ligands at the B3LYP/6-31G* calculation level.....	53
3.33 A. Histogram of frequency vs pK_i for sigma 1 ligands in training set.....	54
3.33 B. Histogram of frequency vs pK_i for sigma 1 ligands in test set.....	55
3.34 Graph of Predicted pK_i vs Experimental pK_i by the CoMFA model at HF/6-31G*.....	59
3.35 Graph of Experimental pK_i vs Predicted pK_i for Test Set by the CoMFA model at HF/6-31G*.....	60
3.36 Graph of Predicted pK_i vs Experimental pK_i by the CoMFA model at B3LYP/6-31G*.....	61
3.37 Graph of Experimental pK_i vs Predicted pK_i for Test Set by the CoMFA model at HF/6-31G*.....	62
3.38 Contour map of compound 43 (Spipethiane) at HF/6-31G*.	64
3.39 Contour map of compound 43 (Spipethiane) at B3LYP/6-31G*.....	64
3.40 Contour map of compound 41 (PD144418) at HF/6-31G*.....	65
3.41 Contour map of compound 41 (PD144418) at B3LYP/6-31G.....	65

LIST OF FIGURES
(Continued)

Figure	Page
3.42 Contour map of compound 45 at HF/6-31G*.....	68
3.43 Contour map of compound 45 at B3LYP/6-31G*.....	68
3.44 Contour map of compound 46 at HF/6-31G*.....	69
3.45 Contour map of compound 46 at B3LYP/6-31G*.....	69
3.46 Contour map of compound 47 at HF/6-31G*.....	70
3.47 Contour map of compound 47 at B3LYP/6-31G*.....	70
3.48 Contour map of compound 48 at HF/6-31G*.....	71
3.49 Contour map of compound 48 at B3LYP/6-31G*.....	71
3.50 Contour map of compound 49 at HF/6-31G*.....	72
3.51 Contour map of compound 49 at B3LYP/6-31G*.....	72
3.52 Contour map of compound 50 at HF/6-31G*.....	73
3.53 Contour map of compound 50 at B3LYP/6-31G*.....	73
3.54 Contour map of compound 51 at HF/6-31G*.....	74
3.55 Contour map of compound 51 at B3LYP/6-31G*.....	74
3.56 Contour map of compound 52 at HF/6-31G*.....	75
3.57 Contour map of compound 52 at B3LYP/6-31G*.....	75
3.58 Contour map of compound 53 at HF/6-31G*.....	76
3.59 Contour map of compound 53 at B3LYP/6-31G*.....	76
3.60 Contour map of compound 54 at HF/6-31G*.....	80
3.61 Contour map of compound 54 at B3LYP/6-31G*.....	80

LIST OF FIGURES
(Continued)

Figure	Page
3.62 Contour map of compound 55 at HF/6-31G*	81
3.63 Contour map of compound 55 at B3LYP/6-31G*	81
3.64 Contour map of compound 56 at HF/6-31G*	82
3.65 Contour map of compound 56 at B3LYP/6-31G*	82
3.66 Contour map of compound 57 at HF/6-31G*	83
3.67 Contour map of compound 57 at B3LYP/6-31G*	83
3.68 Contour map of compound 58 at HF/6-31G*	84
3.69 Contour map of compound 58 at B3LYP/6-31G*	84
3.70 Contour map of compound 59 at HF/6-31G*	85
3.71 Contour map of compound 59 at B3LYP/6-31G*	85
3.72 Contour map of compound 60 at HF/6-31G*	86
3.73 Contour map of compound 60 at B3LYP/6-31G*	86
4.1 DISCOtech pharmacophore derivation of 1-cyclohexylpiperazines (compounds 1-18, hydrogen atoms hidden)	101
4.2 DISCOtech pharmacophore derivation of 1-cyclohexylpiperazines (compounds 1-18), overlay with compound 5, PB 28 (hydrogen atoms hidden)	102
4.3 DISCOtech pharmacophore derivation of 1-cyclohexylpiperazines (compounds 1-18)	102
4.4 DISCOtech pharmacophore derivation of substituted aminobutyl-benzamides (compounds 19, 20, 22, 23, 25, and 28, hydrogen atoms hidden)	103
4.5 DISCOtech pharmacophore derivation of substituted aminobutyl-benzamides overlay with compound 20 – hydrogen atoms hidden	103
4.6 DISCOtech pharmacophore derivation of substituted aminobutyl-benzamides (compounds 19-28)	104

LIST OF FIGURES
(Continued)

Figure	Page
4.7 DISCOtech pharmacophore derivation of substituted benzamide-isoquinoline derivatives (compounds 29-37, hydrogen atoms hidden).....	105
4.8 DISCOtech pharmacophore derivation of substituted benzamide-isoquinoline derivatives (compounds 29-37), overlay with compound 37 - hydrogen atoms hidden.....	105
4.9 DISCOtech pharmacophore derivation of substituted benzamide-isoquinoline Derivatives (compounds 29-37).....	106
4.10 DISCOtech pharmacophore derivation of substituted trishmocubane subset (compounds 38-42, hydrogen atoms hidden).....	106
4.11 DISCOtech pharmacophore derivation of substituted trishmocubane subset (compounds 38-42), overlay with reference molecule compound 52 (hydrogen atoms hidden).....	107
4.12 DISCOtech pharmacophore derivation of substituted trishmocubane subset (compounds 38-42).....	107
4.13 DISCOtech pharmacophore derivation of 1-aralkyl-4-benzylpiperazine derivatives subset (compounds 43-49, hydrogen atoms hidden).....	108
4.14 DISCOtech pharmacophore derivation of 1-aralkyl-4-benzylpiperazine derivatives subset (compounds 43-49), overlay with compound 43 - hydrogen atoms hidden.....	109
4.15 DISCOtech pharmacophore derivation of 1-aralkyl-4-benzylpiperazine derivatives subset (compounds 43-49).....	109
4.16 Comprehensive DISCOtech pharmacophore derivation for Sigma 2 (compounds 5, 19, 37, 45, 50, 51 and 52 – hydrogen atoms hidden).....	111
4.17 Comprehensive DISCOtech pharmacophore derivation for Sigma 2, overlay with compound 5 (hydrogen atoms hidden).....	111
4.18 Comprehensive DISCOtech pharmacophore derivation for Sigma 2.....	112
4.19 Comparison of Comprehensive DISCOtech pharmacophore (a) from Figure 4.17 with pharmacophore derived by Patel (b).....	113

LIST OF FIGURES
(Continued)

Figure	Page
4.20 Comparison of Comprehensive DISCOtech pharmacophore (a) from Figure 4.17 with pharmacophore derived by Jung (b).....	114
4.21 Comparison of Comprehensive DISCOtech pharmacophore (a) from Figure 4.17 with pharmacophore derived by Wirpsza (b).....	115
4.22 Pharmacophore models by Rhoades and colleagues.....	117
4.23 Alignment of all 31 sigma 2 ligands at the HF/6-31G* calculation level.....	120
4.24 Alignment of all 31 sigma 2 ligands at the B3LYP/6-31G* calculation level.....	120
4.25 A. Histogram of frequency vs pK_i for sigma 2 ligands in training set.....	121
4.25 B. Histogram of frequency vs pK_i for sigma 2 ligands in test set.....	122
4.26 Graph of Predicted pK_i vs Experimental pK_i by the CoMFA model at HF/6-31G*.....	127
4.27 Graph of Experimental pK_i vs Predicted pK_i for Test Set by the CoMFA model at HF/6-31G*.....	127
4.28 Graph of Predicted pK_i vs Experimental pK_i by the CoMFA model at B3LYP/6-31G*.....	129
4.29 Graph of Experimental pK_i vs Predicted pK_i for Test Set by the CoMFA model at HF/6-31G*.....	129
4.30 CoMFA contour map of compound 5 (PB28) at HF/6-31G*.....	131
4.31 CoMFA contour map of compound 5 (PB28) at B3LYP/6-31G*.....	131
4.32 CoMFA contour map of compound 19 at HF/6-31G*.....	132
4.33 CoMFA contour map of compound 19 at B3LYP/6-31G*.....	132
4.34 CoMFA contour map of compound 54 at HF/6-31G*.....	134
4.35 CoMFA contour map of compound 54 at B3LYP/6-31G*.....	135
4.36 CoMFA contour map of compound 55 at HF/6-31G*.....	135

LIST OF FIGURES
(Continued)

Figure	Page
4.37 CoMFA contour map of compound 55 at B3LYP/6-31G*	136
4.38 CoMFA contour map of compound 58 at HF/6-31G*.....	136
4.39 CoMFA contour map of compound 58 at B3LYP/6-31G*.....	137
5.1 Haloperidol at HF/6-31G* sigma 1 CoMFA contour map.....	140
5.2 Haloperidol at HF/6-31G* in sigma 2 CoMFA contour map.....	140
5.3 Haloperidol at B3LYP/6-31G* in sigma 1 CoMFA contour map.....	141
5.4 Haloperidol at B3LYP/6-31G* in sigma 2 CoMFA contour map.....	141
A.1 Contour map of sigma 1 compound 1 at HF/6-31G*.....	145
A.2 Contour map of sigma 1 compound 1 at B3LYP/6-31G*.....	144
A.3 Contour map of sigma 1 compound 9 at HF/6-31G*.....	144
A.4 Contour map of sigma 1 compound 9 at B3LYP/6-31G*.....	145
A.5 Contour map of sigma 1 compound 22 at HF/6-31G*.....	146
A.6 Contour map of sigma 1 compound 22 at B3LYP/6-31G*.....	146
B.1 Contour map of sigma 2 compound 37 at HF/6-31G*.....	147
B.2 Contour map of sigma 2 compound 37 at B3LYP/6-31G*.....	147
B.3 Contour map of sigma 2 compound 43 at HF/6-31G*.....	147
B.4 Contour map of sigma 2 compound 43 at B3LYP/6-31G*.....	148
B.5 Contour map of sigma 2 compound 52 at HF/6-31G*.....	148
B.6 Contour map of sigma 2 compound 52 at B3LYP/6-31G*.....	148
B.7 Contour map of sigma 2 training set at HF/6-31G*.....	148
B.8 Contour map of sigma 2 training set B3LYP/6-31G*.....	149

LIST OF FIGURES
(Continued)

Figure	Page
C.1 Contour map of sigma 2 compound 56 at HF/6-31G*.....	150
C.2 Contour map of c sigma 2 compound 56 at B3LYP/6-31G*.....	150
C.3 Contour map of sigma 2 compound 57 at HF/6-31G*.....	150
C.4 Contour map of sigma 2 compound 57at B3LYP/6-31G*.....	151
C.5 Contour map of sigma 2 compound 58 at HF/6-31G*.....	151
C.6 Contour map of sigma 2 compound 58 at B3LYP/6-31G*.....	151
C.7 Contour map of sigma 2 compound 59 at HF/6-31G*.....	152
C.8 Contour map of sigma 2 compound 59 at B3LYP/6-31G*.....	152
C.9 Contour map of sigma 2 compound 60 at HF/6-31G*.....	152
C.10 Contour map of sigma 2 compound 60at B3LYP/6-31G*.....	152
C.11 Contour map of sigma 2 compound 61 at HF/6-31G*.....	153
C.12 Contour map of sigma 2 compound 61at B3LYP/6-31G*.....	153
C.13 Contour map of sigma 2 compound 62 at HF/6-31G*.....	153
C.14 Contour map of sigma 2 compound 62at B3LYP/6-31G*.....	153

CHAPTER 1

INTRODUCTION

1.1 Overview

Chemical engineering and chemistry as disciplines interestingly converge at certain points. In this particular study, this convergence occurs conceptually with molecular modeling related drug design as it pertains to chemical reaction kinetics and thermodynamics. These are the same fundamentals which drive the interaction of biological receptors and their ligands; the binding of ligands to receptors results in a cascade of biological and medicinal activity, hence the usefulness in designing drugs targeted to receptors (Sharma, 2012).

Sigma receptors have become key therapeutic targets in biological and medicinal chemistry studies. Sigma receptors are considered to be a unique receptor family that is localized in the cell cytoplasm of the brain; internal organs; and endocrine, immune and reproductive tissues and they are overexpressed by several tumor cell lines (Berardi et al., 2004). There are two sub-types that are currently identified in the literature, sigma 1 and sigma 2. Receptor ligands, particularly highly active ones, are critical since binding leads to biological effects (Patrick, 2005). The sigma 1 subtype is involved in socially important human diseases such as schizophrenia, depression, Alzheimer's disease and drug/alcohol dependence (Brune and Wunsch, 2013). The sigma 1 receptor is also being studied for the treatment of several pain conditions, either alone or in combination with known analgesics (Zamanillo et al., 2013). The sigma 2 subtype is currently being studied as a target for tumor apoptosis and as biomarkers in cancer imaging (Abate et al., 2014;

Berardi et al., 2004).

Computers have become an essential tool in modern medicinal chemistry and are important in both drug discovery and drug development (Patrick, 2005). Molecular modeling, including methods such as quantum mechanics, pharmacophore derivation and CoMFA (Comparative Molecular Field Analysis), yielded results for the following objectives:

- 1) Derive pharmacophore models for each selected series of active sigma 1 ligand classes
- 2) Derive a representative (comprehensive) pharmacophore for the selected sigma 1 ligand series
- 3) Perform an alignment of 41 compounds to construct a validated CoMFA for sigma 1 receptor ligands.
- 4) Compare density functional and ab initio calculations to the CoMFA studies on sigma 1 ligands.
- 5) Predict the bioactivities (binding affinities) of the selected sigma 1 receptor ligands.
- 6) Design new sigma 1 ligands (potential drug candidates) from CoMFA results.
- 7) Derive pharmacophore models for each selected series of active sigma 2 classes.
- 8) Derive a representative (comprehensive) pharmacophore for the selected sigma 2 series.
- 9) Perform an alignment of 31 compounds to construct a validated CoMFA for sigma 2 receptor ligands.
- 10) Compare density functional and ab initio calculations to the CoMFA studies on sigma 2 ligands.
- 11) Predict the bioactivities (binding affinities) of the selected sigma 2 receptor ligands.
- 12) Design new sigma 2 ligands (potential drug candidates) from CoMFA results.

13) Analyze the resulting pharmacophores and models determined by the aforementioned approaches to yield a comparison of the sigma 1 and sigma 2 receptor ligands.

CHAPTER 2

BACKGROUND

2.1 Biological Activity and Interactions of Receptor Ligands

The term receptor has been formally defined as a cellular macromolecule that is concerned directly and specifically with chemical signaling between and within cells; the combination of an appropriate ligand with its receptor(s) initiates a change in cell function (Cannon, 2007). Essentially a ligand is a drug and the affinity is a measure of how strongly a drug binds to a receptor (Patrick, 2005). The corresponding equation describing the drug-receptor relationship, Equation 2.1, along with the equation for K_d , Equation 2.2. the dissociation binding constant, are as follows (Silverman, 2004):



$$K_d = \frac{[\text{drug}][\text{receptor}]}{[\text{drug} - \text{receptor complex}]} \quad (2.2)$$

The dissociation constant is a measure of the strength of the interaction between the drug candidate and the receptor (target); K_d is often referred to as the inhibition constant, K_i , for an enzyme inhibitor (Berg and Stryer, 2005). It is important to note that the literature for sigma receptor ligands typically uses K_i to discuss the affinity values. After synthesizing drug targets, researchers use radioligand labelling where a ligand for the target receptor is labelled with radioactivity and is added to cells or tissue such that it can bind to the receptors present; once an equilibrium has been reached, the unbound ligands

are removed thereby allowing measurement of radioactivity which relates to the extent of binding (Patrick, 2005). After data is collected from experiments and plotted, a displacement or inhibition curve can be generated to yield an IC₅₀ value (Patrick, 2005). Some researchers use computer software to aid in this area in the literature. Note that IC₅₀ (or I₅₀) expresses the concentration of inhibitor required to produce 50 percent inhibition of an enzymatic reaction (Cheng and Prusoff, 1973). K_i is the same as the IC₅₀ value if non-competitive interactions are involved; for compounds that are in competition with the radioligand for the binding site, the K_i depends on the following equation (Cheng and Prusoff, 1973; Patrick, 2005):

$$K_i = \frac{IC_{50}}{1 + [L]_{tot}/K_d} \quad (2.3)$$

Note that competitive inhibition is the focus of this study. Competitive inhibition means that the inhibitor binds to the same site on the enzyme as the substrate, forming an abortive complex; the substrate and inhibitor compete for the same site so that only one enzyme-inhibitor complex is possible (Cornish-Bowden, 1976). pK_i is also a tool that has been used by the Gund group in previous work, particularly in CoMFA. pK_i is defined in Equation 2.4 as:

$$pK_i = -\log[K_i] \quad (2.4)$$

The pK_i values were calculated by the K_i values provided in the literature which were collected either in vitro or in vivo for the various compounds studied.

The aforementioned information regarding the basic enzyme-type kinetics of receptor ligands explains a piece of the drug-receptor complex. It is important to note that the interactions involved in the drug-receptor complex are the same forces experienced by all interacting organic molecules and include covalent bonding, ionic (electrostatic) interactions, ion-dipole and dipole-dipole interactions, hydrogen bonding, charge-transfer interactions, hydrophobic interactions, and van der Waals interactions (Silverman, 2004). Electrostatic properties of the receptor ligands will be discussed and studied when the CoMFA studies are complete, whereas some of the structure-activity relationships with the hydrophobic groups within the receptor ligands, a key property of the pharmacophore models in this study, will be discussed in Chapters 3 and 4.

2.2 Pharmacophore Identification and QSAR Methodology

Pharmacophore identification for the ligands in this study is a key aspect of the research. Pharmacophores allow us to understand drug-receptor interactions on the molecular level especially if there is not much information about the structure of the receptors themselves (Höltje, 1996). A pharmacophore represents the relative position of important binding groups in space and disregards the molecular structure that holds them there (Patrick, 2005). A majority of drugs exert their action via specific binding to biomacromolecules, hence the importance of the binding groups (Höltje, 1996). Typical binding sites include hydrophobic groups, aromatic rings, positive nitrogen atoms, acceptor sites (lone pair of electrons), donor sites and others.

When a pharmacophore has been identified, structures can be analyzed to determine if they can adopt a stable conformation which will contain the pharmacophore;

this approach, while ensuring that there are no steric clashes with the binding site, will help identify the active structures (Patrick, 2005). It is important to note that this process can be conducted manually or via a software program. This study uses the SYBYL suite which includes DISCOtech (DIStance COmparison) which will be discussed further in Chapters 3 and 4. Eventually the pharmacophore model can be useful to help identify other potential ligands if the ligands have a close fit to the model with the appropriate binding groups.

When beginning the pharmacophore identification process, one should determine the appropriate calculation levels to be used to minimize the energy (at the equilibrium geometry) for each molecule. More sophisticated methods include density functional and *ab initio* optimizations; both are used in this study.

QSAR (Quantitative Structure-Activity Relationship) models, particularly 3D methods, consider properties of a molecule as opposed to individual substituents or moieties, typically utilizing software and hardware to achieve this; the premise is based on the assumption that the most important features about a molecule are its size, shape and electrostatic properties (Patrick, 2005). There are several approaches to QSAR but the common one is CoMFA which is used in this study based on the assumption that the ligand-receptor interactions are non-covalent and that biological activity correlate with the changes in the steric and/or electrostatic fields of the drug molecules (Patrick, 2005).

The first steps in CoMFA include the aforementioned determination of the active conformations and consequently pharmacophore identification. The next step is to place the pharmacophore into a lattice where it will act as a reference when positioning other molecules into the lattice; each molecule will be matched up to the pharmacophore

(Patrick, 2005). The steric and electrostatic fields around each molecule are measured. The measurements are conducted by putting a probe atom (i.e. carbocation) and determining the attraction or repulsion between the probe and the molecule at each of the lattice points, consequently calculating steric, electrostatic and hydrophobic interaction energies shown through countour lines (Patrick, 2005). The CoMFA is not complete until statistical procedures are followed to validate the measurements to determine the prediction accuracy for biological activity (Martin and Lin, 1996; Patrick, 2005).

2.2.1 Partial Least Squares

Validation techniques are an important aspect of research. Particularly in this study, as with most research studies utilizing CoMFA or QSAR techniques, PLS (partial least squares) needs to be incorporated through cross-validation. The concept of cross-validation essentially means that one or more active ligands are left out during the process of the computer deriving an equation or relationship, in this case for biological activity; this is often referred to as the “leave-one-out” process (Martin and Lin, 1996). The resulting equation is then applied to predict the activity for the omitted ligand(s). When this process is complete, a final formula is obtained. The predictability of the final formula is represented by the cross-validated correlation coefficient, PRESS (Predictive Residual Sum of Squares), r^2 , which is often referred to as q^2 (Leach, 1996; Patrick, 2005). One can evaluate r^2 or q^2 as he or she typically would with common regression analysis; the higher the r^2 (closer to 1.0) the better the prediction. Therefore, the q^2 value and its graph are a key aspect to evaluate the data generated in the CoMFA study.

2.2.2 Criteria for “Robust” CoMFA Models

Molecular alignment plays a decisive role in CoMFA analysis, since the relative interaction energies depend strongly on relative molecular positions; CoMFA then uses statistical techniques for correlating several molecular features, such as steric and electrostatic properties with their biological activities (Zhang et al., 2011). As mentioned in Section 2.2.1, the “leave-one-out” process concerns cross-validation for the set of data presented, essentially verifying what is often referred to as the “training set.” The predictive q^2 value refers to the internal robustness of the model (Zhang et al., 2011). There is an understood minimum value for the q^2 value of 0.3 to deem a QSAR model as statistically significant (Jung et al., 2004; Park et al., 2009). In fact, Clark and Cramer presented findings that virtually any q^2 value greater than 0.25 from CoMFA can be accepted as very unlikely to have resulted from chance correlation; however there is some possibility that CoMFA and similar PLS-based approaches can overlook a “true” correlation within a set of data (1993). With the interest of establishing criteria for robust QSAR models, Tropsha and coworkers introduced a new validation criterion (Zhang et al., 2011). Many authors consider high q^2 (for instance, $q^2 > 0.5$) as an indicator or even as the ultimate proof that the model is highly predictive; however, the high q^2 does not imply automatically a high predictive ability of the model (Golbraikh and Tropsha, 2002). Golbraikh and Tropsha state that the use of an external set of compounds with known experimental data, often referred to as the “test set,” for the model validation is always necessary (2002). Further, the aforementioned validation criterion that was developed by Golbraikh and colleagues is centered on test set criterion (Golbraikh et al., 2002, 2003). Golbraikh and colleagues present that the satisfaction of Equations 2.5 - 2.9

conclude that a QSAR model has acceptable predictive power (2002, 2003).

$$q^2 > 0.5 \quad (2.5)$$

$$R^2 > 0.6 \quad (2.6)$$

$$\frac{(R^2 - R_0^2)}{R^2} < 0.1 \text{ and } 0.85 \leq k \leq 1.15 \quad (2.7)$$

or

$$\frac{(R^2 - R_0'^2)}{R^2} < 0.1 \text{ and } 0.85 \leq k' \leq 1.15 \quad (2.8)$$

$$|R_0^2 - R_0'^2| < 0.3 \quad (2.9)$$

Note that R^2 is the quantity characterizing linear regression (trendline) between the predicted and observed activities while R_0^2 is the quantity characterizing linear regression with the Y-intercept set to zero (k represents the slope of that line as in $Y = kX$; $R_0'^2$ is the same as R_0^2 but is related to observed vs predicted activities. k' is the slope of $Y = kx$ for $R_0'^2$) (Golbraikh et al., 2003). Additionally, Golbraikh and colleagues determined that an external test set needs to have at least five compounds.

2.3 Design of New Ligands

The development of pharmacophore models, CoMFA analysis, validation techniques and collected observations about the molecular properties, all aforementioned, combine to yield the design of new ligands with prediction of activities. CoMFA contour maps are the key to understanding where the enhancement of electrostatic or steric properties would benefit a molecule. Therefore, we can see the value in performing this research – to eventually design new potential drug candidates for receptors, in this case for sigma 1 and 2 receptors.

CHAPTER 3

MOLECULAR MODELING OF SIGMA 1 RECEPTOR LIGANDS

3.1 Introduction

Sigma receptors were originally and incorrectly characterized as a new subtype of opioid receptors in the 1970s (Collina et al., 2007; Marriott et al., 2012). It has been clarified that sigma receptors are different from opioid and N-methyl-D-aspartate (NMDA) phenycyclidine receptors, that they bind numerous xenobiotics of unrelated compound classes including clinical drugs used in psychiatric disorders, neurodegenerative disorders, pain, amnesia and abuse drugs such as cocaine (Marriott et al., 2012). Ligand binding experiments and biochemical analysis has differentiated the sigma 1 receptor from sigma 2 receptor (Rack et al., 2011). The sigma 1 receptor has been cloned and is a 25.3 kDa membrane bound protein; the amino acid sequence does not show any homology or similarity with any other known mammalian protein (Hanner et al., 1996, Rack et al., 2011). Sigma 2 receptors are understood to be smaller in size than the sigma 1 receptor and that they do not translocate as the sigma 1 receptor does (Marriott et al., 2012). There appears to be less information and knowledge of the sigma 2 receptor, however its molecular weight has been approximated to be 21.5 kDa (Jasper et al., 2012). Concerning the prominence of sigma 1 receptors, large amounts have been discovered in various organs and tissues including the heart, liver, kidney and the eye including some human tumor cell lines (Rack et al., 2011). The physiological function is still to be completely understood beyond calcium channels and neurotransmitter modulation; there is some agreement to consider its role more like an activator/inactivator as opposed to

anagonist/antagonist (Cobos et al., 2008; Collina et al., 2007).

In the present study, several classes of sigma 1 ligands were selected. It was desired to create a pharmacophore model for each class, compare the models, develop a comprehensive pharmacophore that represents all of the selected sigma 1 classes and then compare the comprehensive model with the findings previously determined by Gund and colleagues. Additional analysis to include comparison to other models by researchers was also pursued.

Gund and colleagues have developed several pharmacophore models through various studies. The model developed in 1991 by Gund was originally compared with the initial idea of Manallack and coworkers regarding hydrophobic and hydrophilic sites (Gund et al., 1991; Jung et al., 2004; Manallack et al., 1988). The model in 1991 had corresponding distances of 5.3-5.7 angstroms for N-C, 7.3-7.9 angstroms for C-lone pair and 2.7-3.0 for N or C – lone pair (Gund et al., 1991). This model was further developed by Jung, Floyd and Gund in 2004 with values for those distances, respectively, of 7.138, 8.662 and 2.508 angstroms. Note that Figure 3.2 presents that an additional electronegative feature, the oxygen, as a feature of the pharmacophore model at that time.

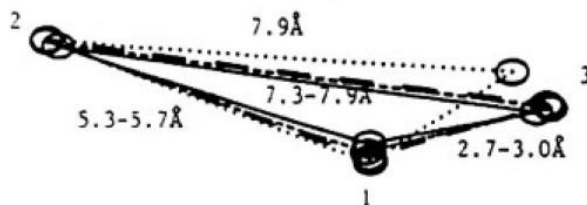


Figure 3.1 Gund pharmacophore for sigma 1 receptor ligands.

Source: Gund et al., 1991.

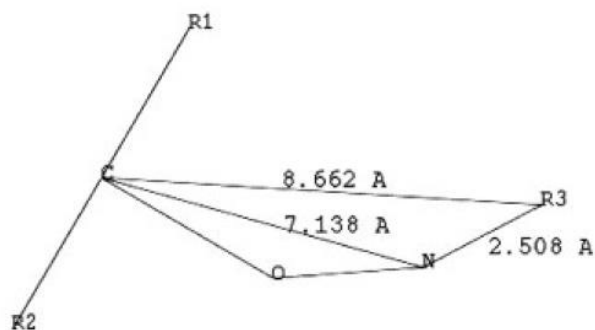


Figure 3.2 Gund pharmacophore for sigma 1 receptor ligands.
Source: Jung et al., 2004.

This study builds on the original Gund models from 1991 and 2003. The other models, which vary from researcher to researcher, are explored and compared with the new models generated in this study in Section 3.4.

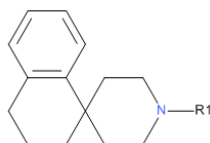
3.2 Selection of Ligands

Forty-four sigma 1 receptor ligands were selected for the present study – concerning sigma 1 - based on an extensive literature search. Considerations for selection included incorporating recently synthesized and researched ligands (from 2012 and 2013) that showed properties of moderate to high affinity values calculated via competitive radioligand binding studies using [³H](+)(-)pentazocine as a radioligand. Highly active ligands previously studied by Gund and colleagues were also included as references.

Tacke and coworkers focused on a series of high-affinity, selective sigma ligands of 1,2,3,4-tetrahydrospiro[naphthalene-1,4'piperidine] type along with related sigma ligands of the 1,4'-silaspiro[indane-1,4'-piperidine] type (Tacke et al., 2012). Note that silasubstitution was a key aspect of Tacke's study to determine the effect of replacing the carbon spirocenters with silicon atoms (Tacke et al., 2012). The corresponding molecules

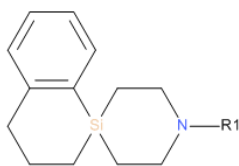
in these series are presented with their affinity data in Tables 3.1 and 3.2 for compounds 1-8.

Table 3.1 Binding and Functional Data of 1,2,3,4-tetrahydrospiro[naphthalene-1,4'-piperidine] Series



Compound	R1 group	$\sigma_1 K_i$ (nM)	$\sigma_2 K_i$ (nM)	σ_2 / σ_1
1*		2.0 ± 0.5	44 ± 21	22
2		3.8 ± 1.8	206 ± 71	54
3		8.0 ± 1.9	34 ± 4.7	4
4		1.8 ± 1.3	5.5 ± 1.5	3

*Indicates included in the comprehensive sigma 1 pharmacophore derivation.
Source: Tacke et al., 2012.

Table 3.2 Binding and Functional Data of 1,4'-silaspiro[indane-1,4'-piperidine] Series

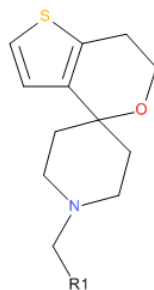
Compound	R1 group	$\sigma_1 K_i$ (nM)	$\sigma_2 K_i$ (nM)	σ_2 / σ_1
5		1.1 ± 0.5	243 ± 94	221
6		2.7 ± 0.5	460 ± 96	170
7		2.9 ± 0.8	39 ± 11.8	13
8		0.3 ± 0.2	19 ± 1.4	63

Source: Tacke et al., 2012.

For compounds 9-14, Harel and colleagues combined the pharmacophoric elements of potent sigma 1 ligands spirocyclic thienopyrans to result in aminoethyl substituted tetrahydrobenzothiophenes (Harel et al., 2013). Though the resulting molecules demonstrated a reduction in affinity (moderate to low), modeling this class, particularly by overlaying the molecules, can teach us visually how closely the new molecules overlay with the reference compounds when the pharmacophore is created.

Further, we can learn from the work of Harel and coworkers that essentially increasing the conformational flexibility of the aminoethyl side chain can explain the decrease in affinity in this class (Harel, et al., 2013). These molecules and corresponding data are shown in Tables 3.3 and 3.4.

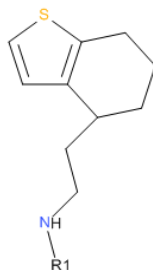
Table 3.3 Binding and Functional Data of Spirocyclic Thienopyran System and Aminoethyl-substituted Tetrahydrobenzothiophenes



Compound	R1 group	$\sigma_1 K_i$ (nM)	$\sigma_2 K_i$ (nM)	σ_2 / σ_1
9*	CH ₂ Ph	0.31 ± 0.06	13 ± 2.5	42
10	CH ₂ C ₆ H ₁₁	0.66 ± 0.16	3.3 ± 0.3	5

*Indicates included in the comprehensive sigma 1 pharmacophore derivation.
Source: Harel et al., 2013.

Table 3.4 Binding and Functional Data of Spirocyclic Thienopyran System and Aminoethyl-substituted Tetrahydrobenzothiophenes



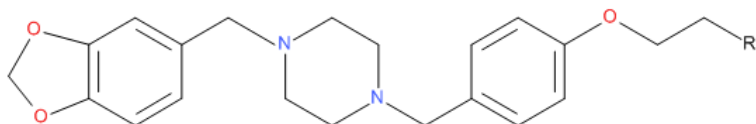
Compound	R1 group	$\sigma_1 K_i$ (nM)	$\sigma_2 K_i$ (nM)	σ_2 / σ_1
11	PhCH ₂	49 ± 2.0	149	3
12	PhCH ₂ CH ₂	126 ± 73	129 ± 20	1
13	PhCH ₂ CH ₂ CH ₂	132	166	1
14	C ₆ H ₁₁ CH ₂	5.0 ± 2.0	10 ± 1.0	2

Source: Harel et al., 2013.

Compounds 15-17 were studied by Wang and colleagues (2013) to evaluate potential radiotracers for imaging sigma 1 receptors with PET (Positron Emission Topography). Interestingly, the lead compound, 1-(1,3-benzodioxol-5-ylmethyl)-4-(9,9-difluoroethoxy)benzyl)piperazine) does not exhibit the highest activity compared to other compounds in this study (activity at 1.85 nM but comparable with references), however it has been identified as a suitable radiotracer and therefore is worth studying as it does have an impact for sigma-1 receptor-type applications (Wang et al., 2013). Compounds 16 and 17 were also studied as part of the series of fluoro-oligo-ethoxylated 4-

benzylpiperazine derivatives as potential sigma 1 receptor ligands. These molecules and corresponding data are shown in Table 3.5

Table 3.5 Binding and Functional Data of Fluoro-oligo-ethoxylated 4-benzylpiperazine Derivatives



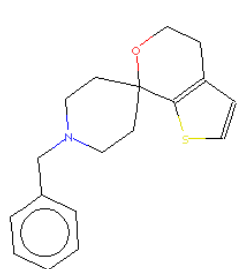
Compound	R1 group	$\sigma_1 K_i$ (nM)	$\sigma_2 K_i$ (nM)	σ_2 / σ_1
15*	F	1.85 ± 1.59	291 ± 111	157
16	OCH ₂ CH ₂ F	40.7 ± 22.8	666 ± 106	16.4
17	OCH ₂ CH ₂ OCH ₂ CH ₂ F	505 ± 120	1420 ± 160	2.81

*Indicates included in the comprehensive sigma 1 pharmacophore derivation.
Source: Wang et al., 2013.

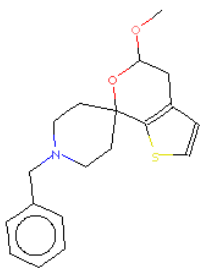
Compounds 18-38, spirocyclic thophenes, were studied by Meyer and coworkers (2012). This group studied pharmacophore models from various papers for sigma 1 and consequently tried to enlarge the lipophilic region of the thiophene moiety to achieve a higher sigma 1 affinity (Meyer et al., 2012). The sigma 1 affinity of the phenylated compounds is comparable or slightly reduced compared to the nonphenylated compounds; the placement of the S-atom appears to be a key aspect impacting affinity in this study, not necessarily increasing the lipophilicity of the thiophene moiety (Meyer et al., 2012). The spirocyclic thiophenes studied have reasonable sigma 1 affinities and due

to the focus of the impact of structural changes on the binding sites they are worth studying; the corresponding data and molecules are in Table 3.6.

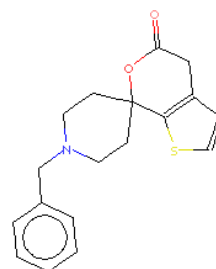
Table 3.6 Binding and Functional Data of Spirocyclic Thiophenes Series



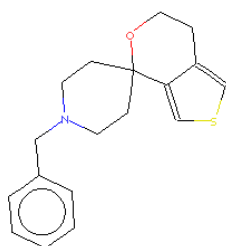
18



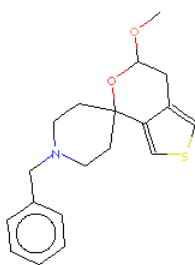
19



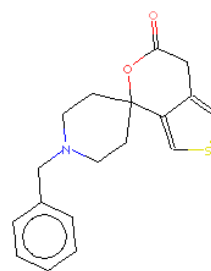
20



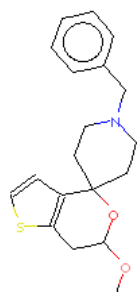
21



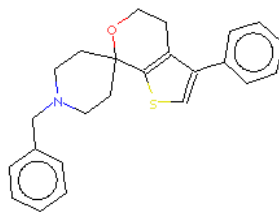
22



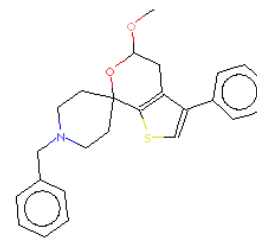
23



24



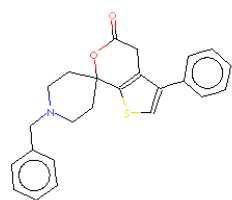
25



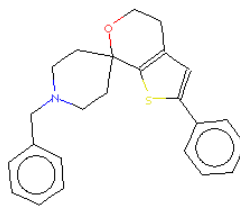
26

Source: Meyer et al., 2012

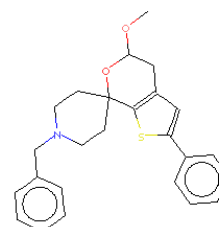
Table 3.6 (continued) Binding and Functional Data of Spirocyclic Thiophenes Series



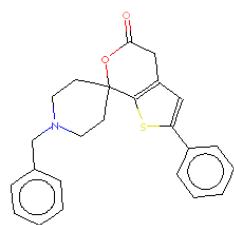
27



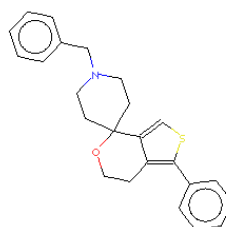
28



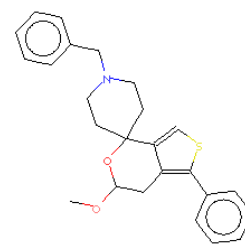
29



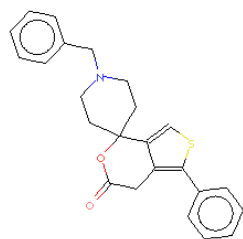
30



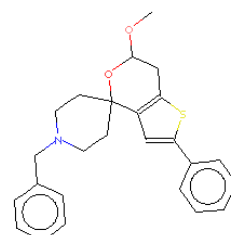
31



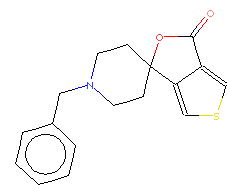
32



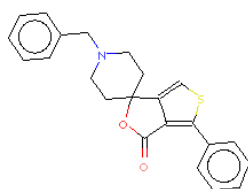
33



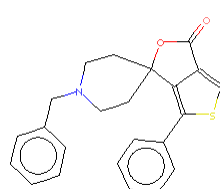
34



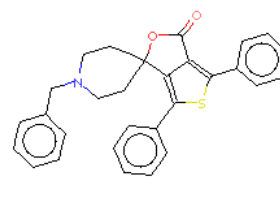
35



36



37



38

Source: Meyer et al., 2012

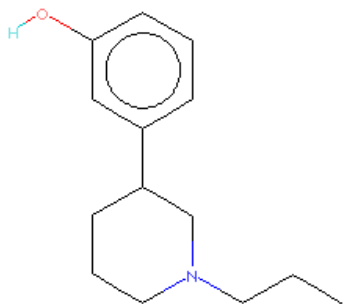
Table 3.6 (continued) Binding and Functional Data of Spirocyclic Thiophenes Series

Compound	$\sigma_1 K_i$ (nM)
18	1.0 ± 0.30
19	1.9 ± 0.44
20	255
21	0.35 ± 0.06
22	0.22 ± 0.06
23	40 ± 13
24	0.32 ± 0.10
25	1.6 ± 0.70
26	5.4 ± 0.97
27	5.3 ± 0.88
28	2.4 ± 0.69
29	16 ± 5.8
30	23 ± 9.9
31	4.5 ± 2.9
32	1.0 ± 0.4
33	2.5 ± 0.91
34	5.5 ± 1.5
35	16 ± 6.8
36	11 ± 3.2
37	483
38	87 ± 52

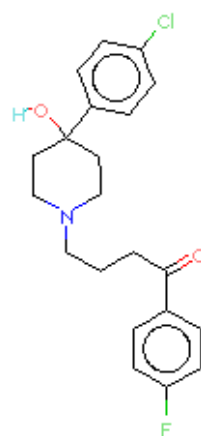
Source: Meyer et al., 2012

Since we are building on the foundation of Gund and colleagues, it is appropriate to use reference compounds from their work (Gund et al., 2004). Commonly researchers use rigid compounds for the pharmacophore modeling to help serve as templates since the rotatable bonds are more limited, reducing the number of potential conformers. In the selection of reference compounds, some rigid molecules were considered such as Spipethiane (43) and (+)-Pentazocine (44). An extremely highly active compound for sigma 1, PD144418 (41) is also included, however it has many conformers/rotatable bonds. The reference molecules included from Gund's previous work are in Table 3.7.

Table 3.7 Binding and Functional Data of Reference Compounds



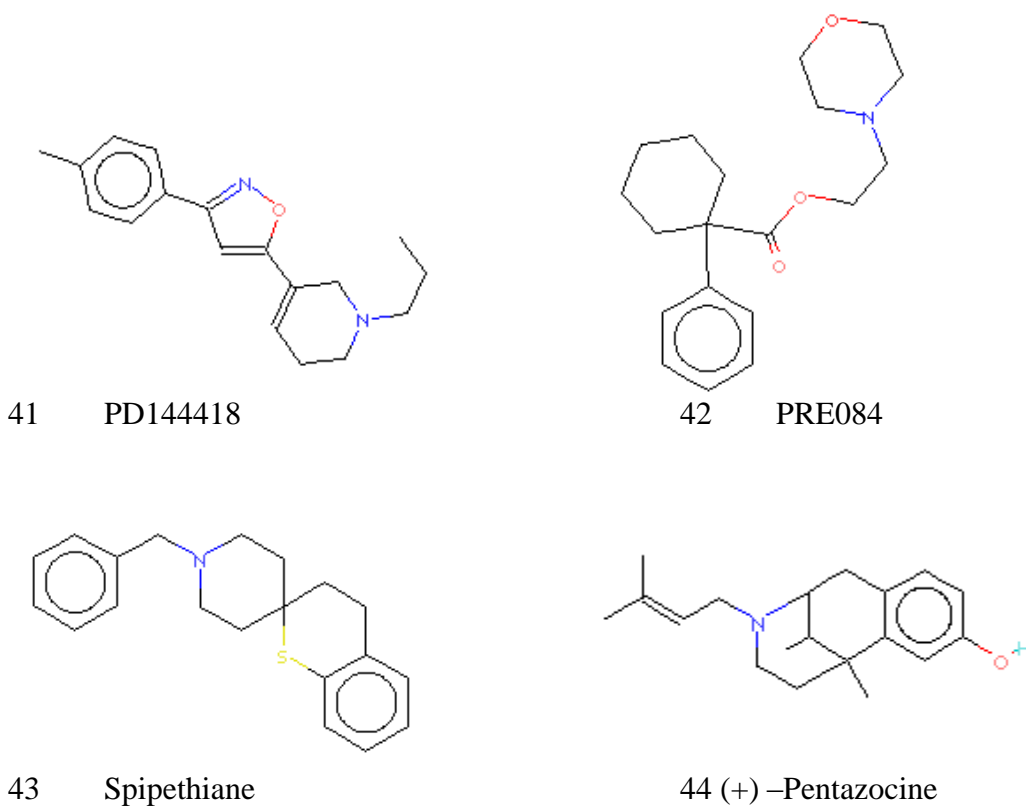
39 (+)3PPP



40 Haloperidol

Source: Gund, et al., 2003.

Table 3.7 (continued) Binding and Functional Data of reference compounds



Compound	$\sigma_1 K_i$ (nM)	$\sigma_2 K_i$ (nM)	σ_1 / σ_2	
39	23.7 ± 3.8	176.3 ± 23	7	(Jbilo et. al, 1997)
40	1.2 ± 0.20	26 ± 5.4	22	(Akunne et. al, 1997)
41*	0.08	1377	5.8×10^{-5}	(Akunne et. al, 1997)
42	44			(Su et. al, 1991)
43*	0.5 ± 0.02	416 ± 43	0.0012	(Quaglia et al., 1998)
44*	5.8 ± 1.0	1253 ± 519	0.0046	(Akunne et. al, 1997)

*Indicates included in the comprehensive sigma 1 pharmacophore derivation.
 Source: Gund, et al., 2003 (original data sources listed above as specified by Gund et al.).

3.3 Materials and Methods

All molecules were initially drawn in Spartan '14 and then optimized at the HF/6-31G* and B3LYP/6-31G* levels prior to being imported into the SYBYL-X 2.1 program. Molecular databases were created within SYBYL-X 2.1 to represent each class of compounds for the sigma 1 receptor ligands. DISCOtech, a tool within SYBYL-X 2.1, was then used to generate pharmacophores for each of the classes. Pharmacophore development for each set of selected molecules was conducted by utilizing the options within DISCOtech for feature selection (binding site), conformer searches, etc. to yield potential pharmacophore models. Following the development of pharmacophore models for each class, a database was created to include the most active/lead compounds with some rigid references and active references from the previous work by Gund and colleagues. This database was then utilized to develop a comprehensive pharmacophore to represent all of the sigma 1 ligand classes studied in this work. Once pharmacophore models were completed, the Comparative Molecular Field Analysis models were created for the sigma 1 molecules calculated at HF/6-31G* and B3LYP/6-31G* levels, respectively. New ligands were designed once the CoMFA models were determined to meet robust criteria; contour maps generated from the CoMFA models were studied during the new ligand design process. Additional information about the pharmacophore derivation, CoMFA and design of new ligands are in Sections 3.4, 3.5, and 3.6, respectively.

3.4 Pharmacophore Derivation

DISCOtech allows the researcher to manually select the binding features of each molecule to be considered for pharmacophore generation. For these classes, hydrophobic groups, positive nitrogen, lone pair and aromatic groups (same as the hydrophobic groups selected in these particular cases) were used. This was done via an iterative process. First, models were explored without constraints or features selected, and gradually various combinations of binding groups were included; eventually this iterative process yielded the typical models, in terms of binding sites, that Gund and coworkers had developed over the years (Jung et. al, 2004). Specifics regarding each class and the derivations are discussed in Section 3.4.1.

3.4.1 Pharmacophore Models

Pharmacophores were generated using DISCOtech in SYBYL-X 2.1 for each class of compounds and are shown as labelled in Figures 3.3 through 3.16 and Figures 3.19 through 3.21. As with the aforementioned Gund, Jung, Floyd models discussed (2003, 2004), the main binding sites are the nitrogen site, the lone pair of electrons and a hydrophobic/aromatic group. The distances between these groups for the various classes are on the order of the previous models which are in Figures 3.1 and 3.2; these models are more extensively analyzed during the discussion later in this section concerning the representative sigma 1 pharmacophore (Figures 3.19 – 3.21).

Figures 3.3 – 3.5 depict the model developed for the Tacke Series: 1,2,3,4-tetrahydrospiro[naphthalene-1,4'-piperidine] and 1,4'-silaspiro[indane-1,4'-piperidine] series (compounds 1-8). The distance from the N atom to the lone pair was 2.9 Å; from

the center of the aromatic/hydrophobic ring (phenyl) to the N atom the distance was 5.08 Å; and the distance from the lone pair to the center of the aromatic/hydrophobic ring was 6.89 Å.

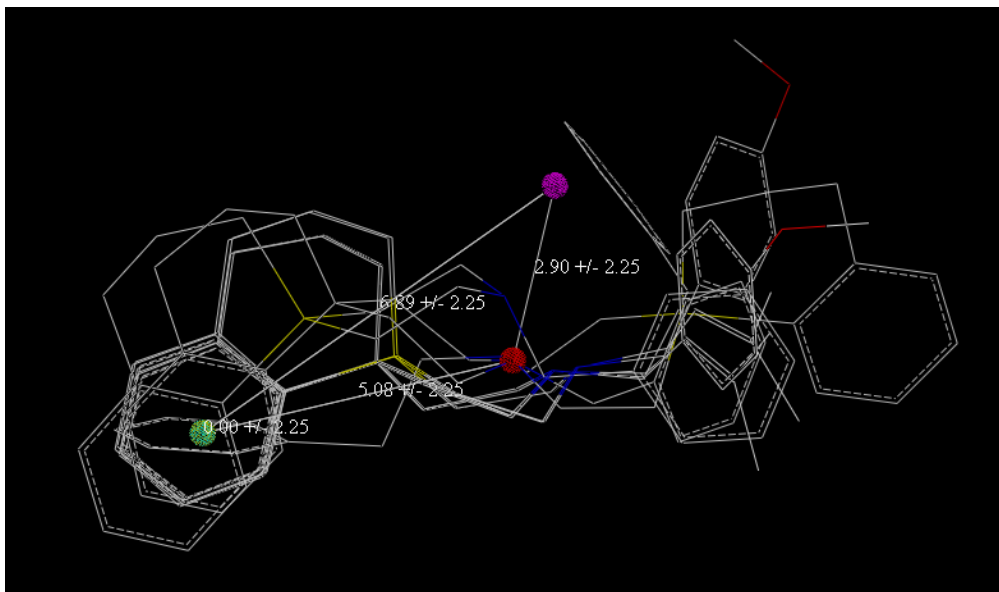


Figure 3.3 DISCOtech pharmacophore derivation and overlay of 1,2,3,4-tetrahydrospiro[naphthalene-1,4'-piperidine] and 1,4'-silaspiro[indane-1,4'-piperidine] series (compounds 1-8, hydrogen atoms hidden).

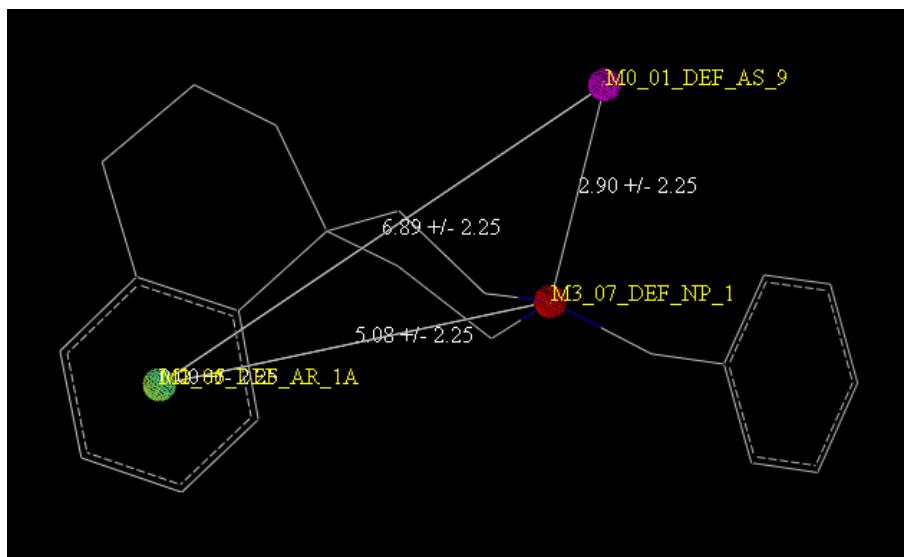


Figure 3.4 DISCOtech pharmacophore derivation of 1,2,3,4-tetrahydrospiro[naphthalene-1,4'-piperidine] and 1,4'-silaspiro[indane-1,4'-piperidine] series (compounds 1-8) with lead compound 1, hydrogen atoms hidden.

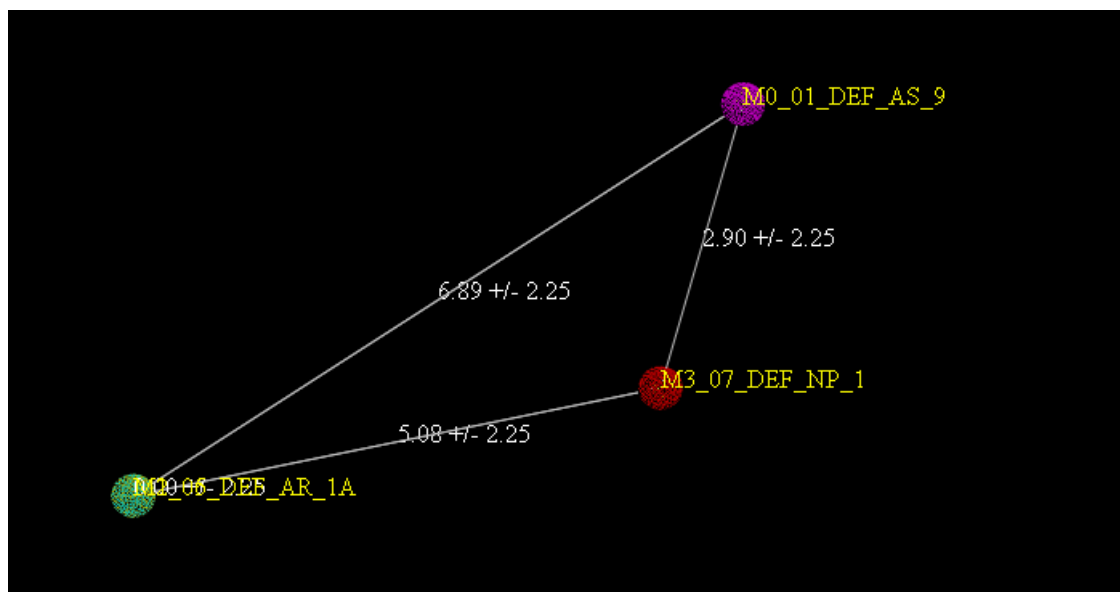


Figure 3.5 DISCOtech pharmacophore model of 1,2,3,4-tetrahydrospiro[naphthalene-1,4'-piperidine] and 1,4'-silaspiro[indane-1,4'-piperidine] series (compounds 1-8). Purple sphere = acceptor site, red sphere = positive nitrogen and green sphere = aromatic/hydrophobic center.

Figures 3.6 – 3.8 depict the pharmacophore derivation of the spirocyclic thienopyran system and aminoethyl-substituted tetrahydrobenzothiophenes (compounds 9-14). Note that in this case, the aromatic/hydrophobic ring consists of a thiophene ring. The distance from the N atom to the lone pair was 2.9 Å; from the center of the aromatic/hydrophobic ring to the N atom the distance was 5.53 Å; and the distance from the lone pair to the center of the aromatic/hydrophobic ring was 8.25 Å.

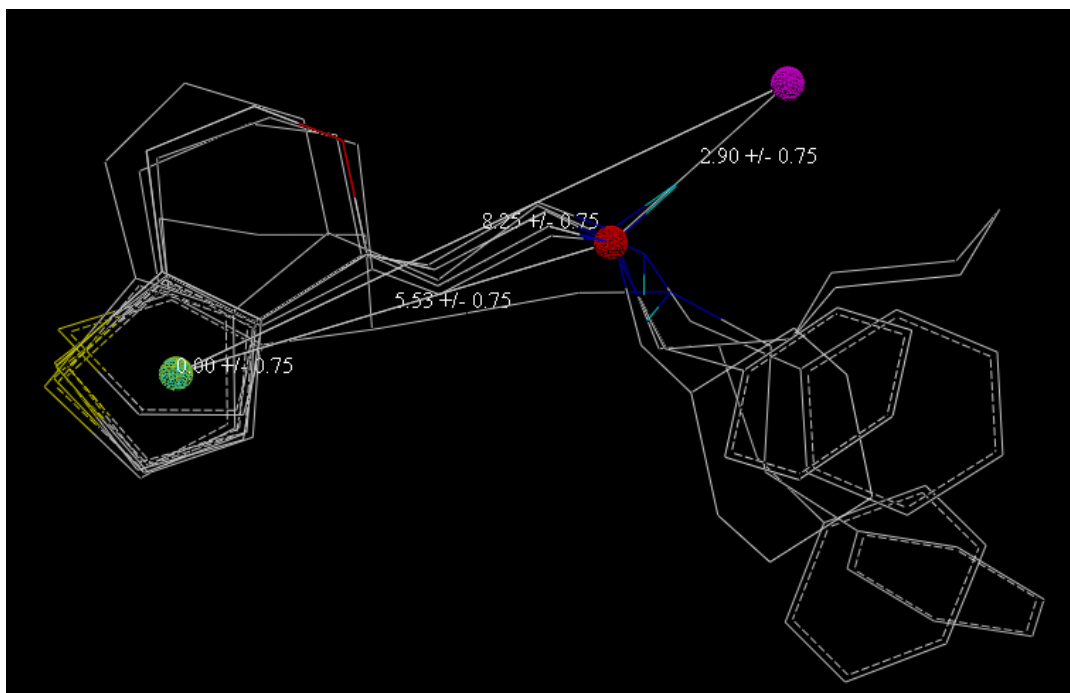


Figure 3.6 DISCOtech pharmacophore derivation of spirocyclic thienopyran system and aminoethyl-substituted tetrahydrobenzothiophenes (compounds 9-14, hydrogen atoms hidden).

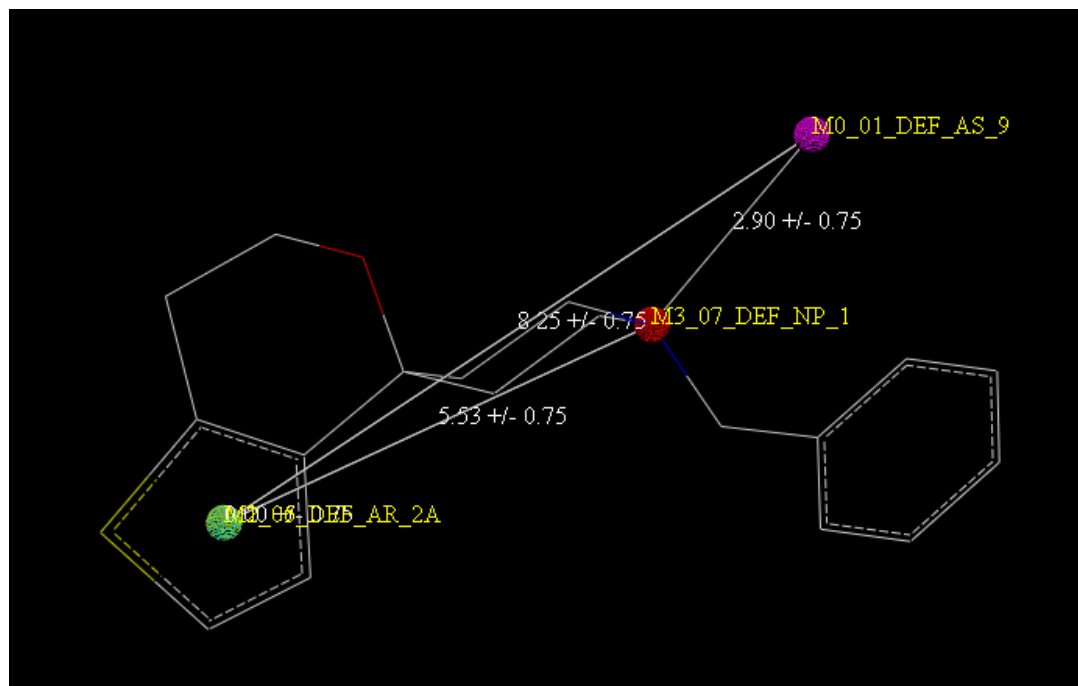


Figure 3.7 DISCOtech pharmacophore derivation of spirocyclic thienopyran system and aminoethyl-substituted tetrahydrobenzothiophenes (compounds 9-14) with lead compound 9, hydrogen atoms hidden.

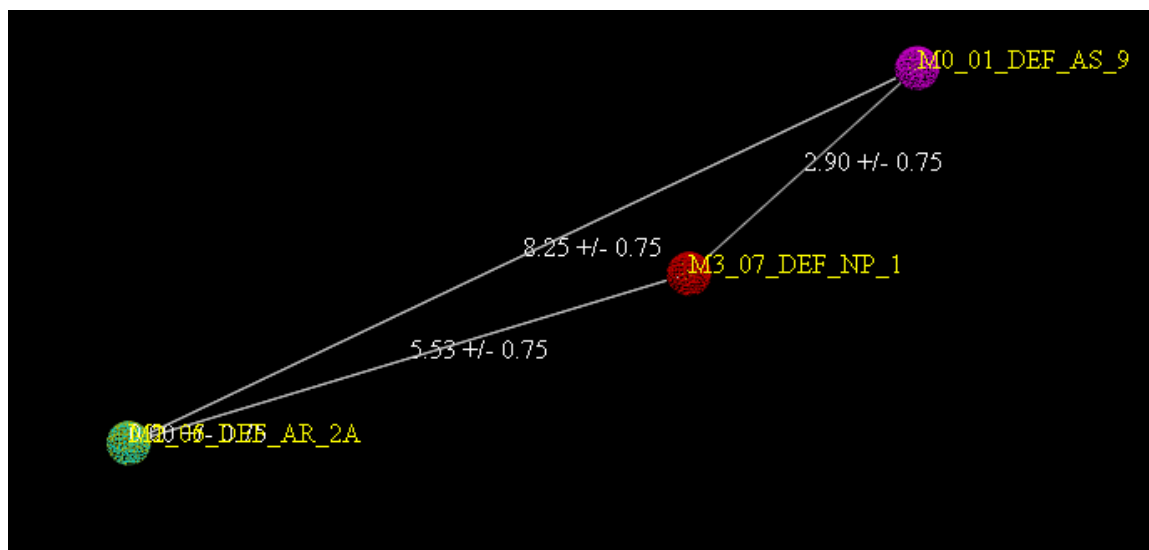


Figure 3.8 DISCOtech pharmacophore model of spirocyclic thienopyran system and aminoethyl-substituted tetrahydrobenzothiophenes (compounds 9-14). Purple sphere = acceptor site, red sphere = positive nitrogen and green sphere = aromatic/hydrophobic center.

Figures 3.9 – 3.11 depict the pharmacophore derivation of the fluoro-oligo-ethoxylated 4-benzylpiperazine derivatives (compounds 15-17). Note that in this case, the aromatic/hydrophobic ring consists of a phenyl ring. The distance from the N atom to the lone pair was 2.9 Å; from the center of the aromatic/hydrophobic ring to the N atom the distance was 5.91 Å; and the distance from the lone pair to the center of the aromatic/hydrophobic ring was 7.07 Å.

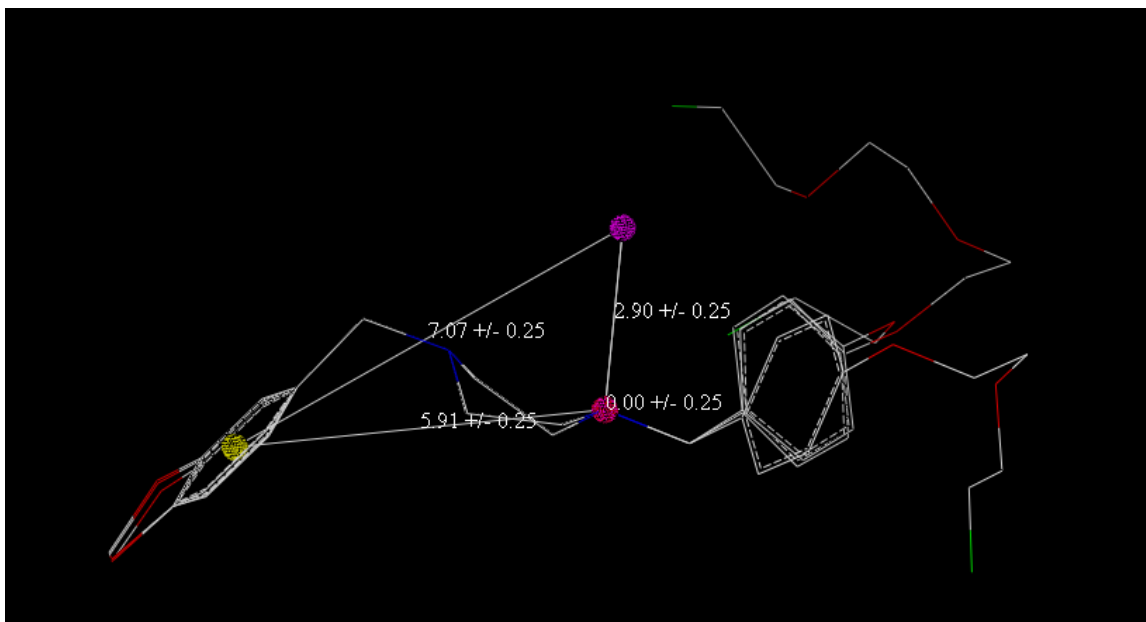


Figure 3.9 DISCOtech pharmacophore derivation of fluoro-oligo-ethoxylated 4-benzylpiperazine derivatives (compounds 15-17, hydrogen atoms hidden).

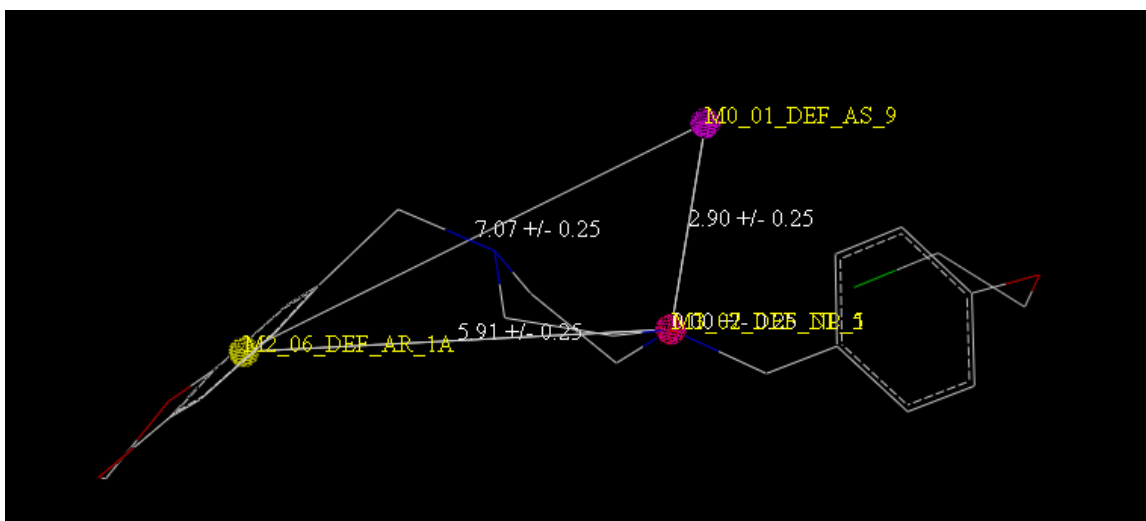


Figure 3.10 DISCOtech pharmacophore derivation of fluoro-oligo-ethoxylated 4-benzylpiperazine derivatives (compounds 15-17) with lead compound 15.

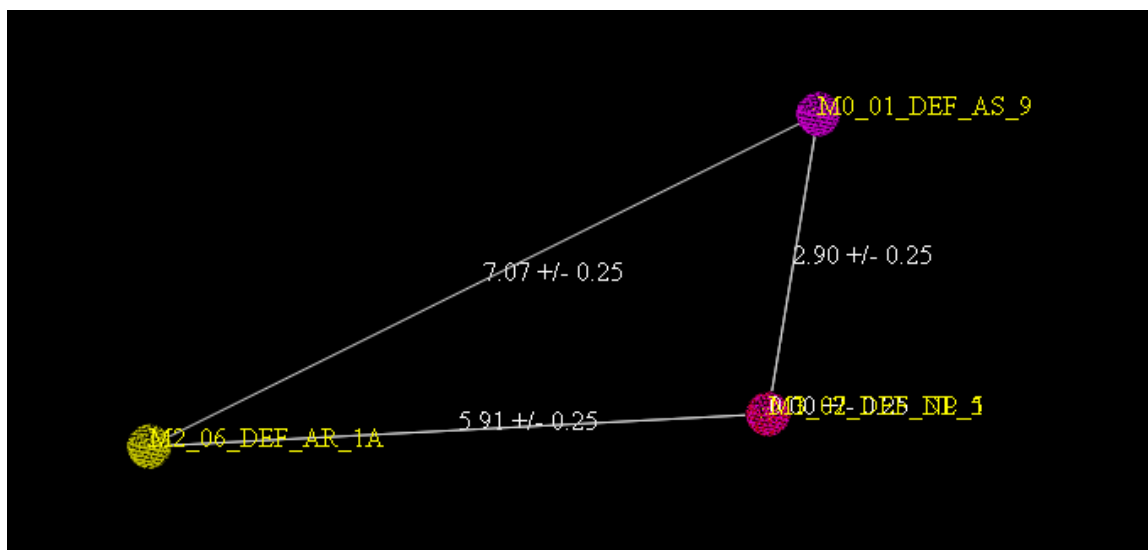


Figure 3.11 DISCOtech pharmacophore model of fluoro-oligo-ethoxylated 4-benzylpiperazine derivatives (compounds 15-17). Purple sphere = acceptor site, pink sphere = positive nitrogen and yellow sphere = aromatic/hydrophobic center.

The model for the spirocyclic thiophenes (Figures 3.12 – 3.14) shows a distance that is noticeably lower between the nitrogen and hydrophobic group as contrasted with other class pharmacophore models; this could be due to difficulty experienced by the researcher in directing DISCOtech to consider using the lipophilic groups Meyer and coworkers discussed (2012). Poor overlay can be visually observed of the thiophene moieties for the 21 spirocyclic thiophene molecules in Figure 3.12. The distance from the N atom to the lone pair was 2.9 Å; from the center of the aromatic/hydrophobic ring (phenyl) to the N atom the distance was 3.83 Å; and the distance from the lone pair to the center of the aromatic/hydrophobic ring (phenyl) was 6.46 Å. It is important to note that compound 22 from this class was used in the representative pharmacophore for sigma 1, and in that pharmacophore the thiophene moiety was used by DISCOtech as opposed to the phenyl ring as it is in the pharmacophore model in Figure 3.12. Therefore, an

alternate pharmacophore model was explored for this class as shown in Figures 3.15 and 3.16, where the seven most highly active spirocyclic thiophene compounds were chosen for the model (compounds 18, 19, 21, 22, 24, 25 and 32). This was a more inclusive model depicting additional hydrophobic groups with the objective to confirm that the thiophene moiety was a viable hydrophobic group for the pharmacophore as it occurred in the representative pharmacophore for sigma 1. Indeed, as shown in Figure 3.16, a pharmacophore model consisting of more than three points is possible for this class, and the highlighted section with the thiophene moiety, in this case for the most highly active ligand – compound 22 – is presented. In that case, the distance from the N atom to the lone pair was 2.9 Å; from the center of the thiophene ring to the N atom the distance was 5.36 Å; and the distance from the lone pair to the center of the thiophene ring was 7.54 Å. Therefore, it was determined that the spirocyclic thiophene class, depending on the ligands chosen, could have additional hydrophobic groups as part of the model. When the molecules were aligned with other molecules from other classes in CoMFA or used in the representative pharmacophore, it was interesting to note that the thiophene moiety aligned to the hydrophobic groups of the other molecules as opposed to the original phenyl ring used in DISCOtech for the spirocyclic thiophene specific pharmacophore. The features of the other molecules later used for the representative pharmacophore were a key reason that the approach on the part of the researcher for this study did not include other pharmacophoric features that other groups, such as Meyer coworkers, did in their 2012 work. Meyer and coworkers similarly used hydrophobic/aromatic points as well as the nitrogen atom, however they included additional hydrophobic centers in their molecule as pharmacophoric points which did not exist for every spirocyclic thiophene

molecule in this study or theirs (the additional phenyl ring attached to the thiophene ring, for instance) and also used donor atoms and corresponding acceptor sites outside of nitrogen and its lone pair, which again, did not always exist for the other sigma 1 ligands in our study (Meyer et al., 2012). Since the researcher in this study was aiming to develop consistency in the class pharmacophores with an overall, representative pharmacophore for sigma 1, features as seen in Figures 3.17 and 3.18 were not included. Work continues, as stated by Gund et al., in accordance with the suggestion that one pharmacophore may be sufficient to rationalize the binding of all sigma ligands (1992).

There seems to be agreement about the thiophene moiety being a viable binding group point as well as the nitrogen atom with the additional possibility of the phenyl group nearest the nitrogen atom being a hydrophobic/aromatic point; therefore these three points from our Figure 3.16 agree with the Meyer model depicted in Figure 3.17. Again, these models are more specific to spirocyclic thiophenes and are not necessarily representative to the overall sigma 1 pharmacophore; the “triangle” effect does exist in both the original and alternate spirocyclic thiophene pharmacophores in Figures 3.14 or Figure 3.16, with the difference in the hydrophobic/aromatic group being either the phenyl ring or thiophene ring, respectively. A final point on the Meyer and coworkers’ model is that a different approach and software was used for their pharmacophore modeling with the primary focus being spirocyclic thiophenes, specifically to explore the hydrophobic binding region of the sigma 1 receptor protein (Meyer et al., 2012).

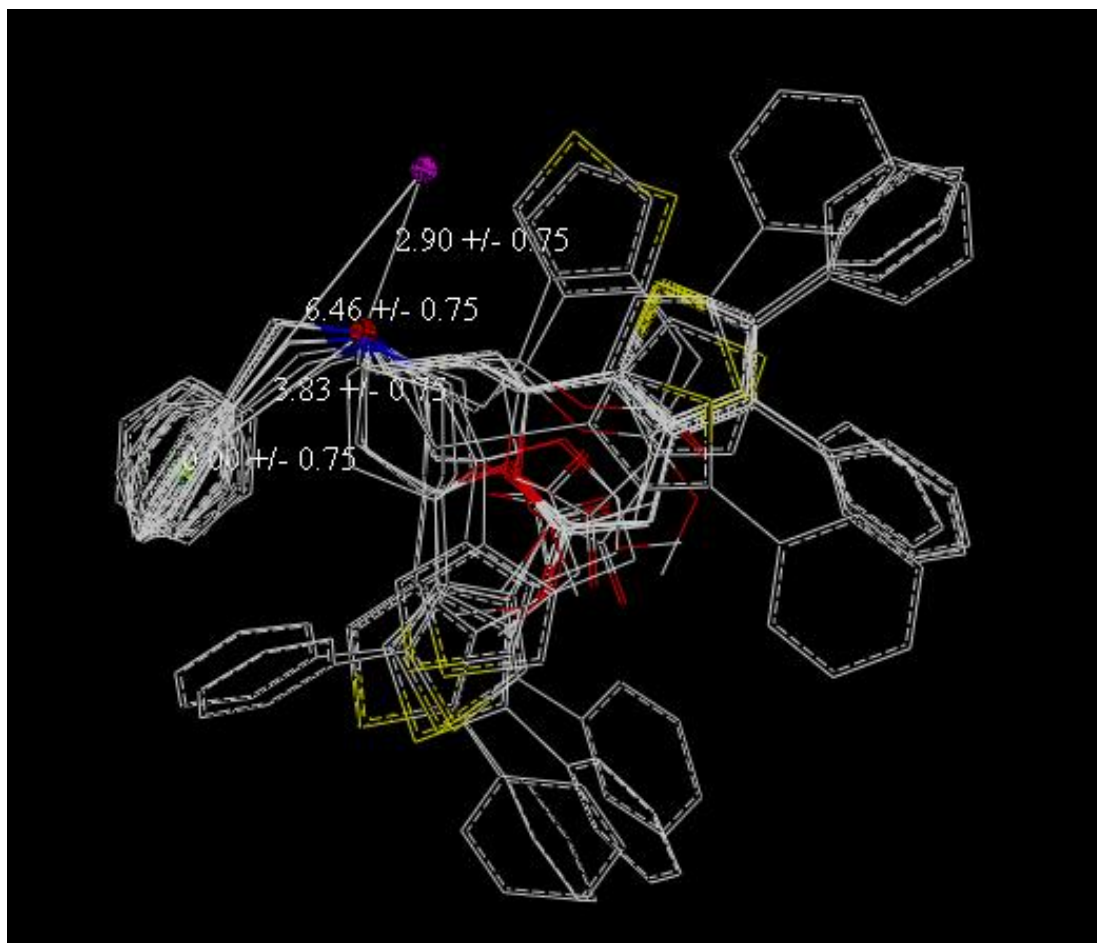


Figure 3.12 DISCOtech pharmacophore derivation of spirocyclic thiophenes (compounds 18-38, hydrogen atoms hidden).

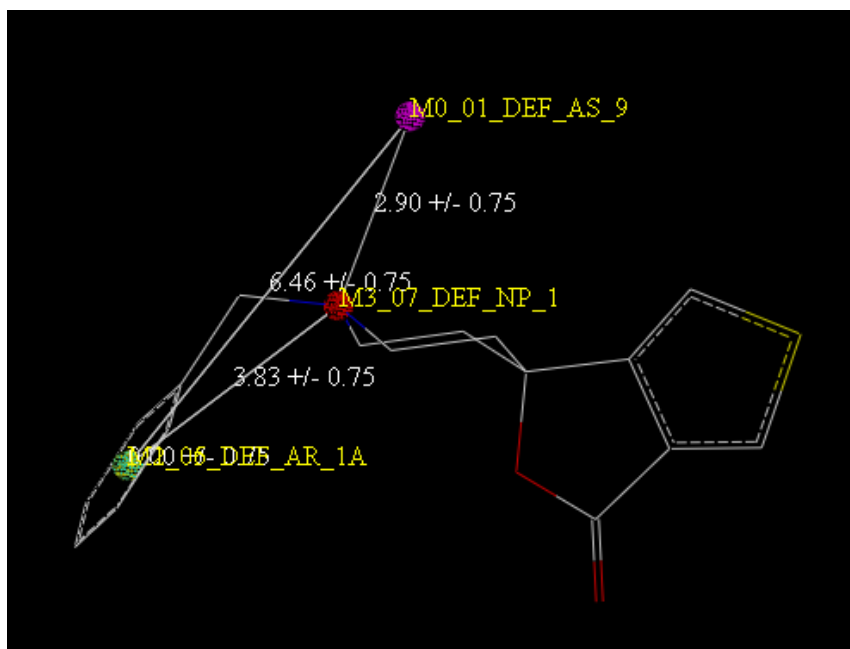


Figure 3.13 DISCOtech pharmacophore derivation of spirocyclic thiophenes (compounds 18-38, hydrogen atoms hidden) with lead compound 18.

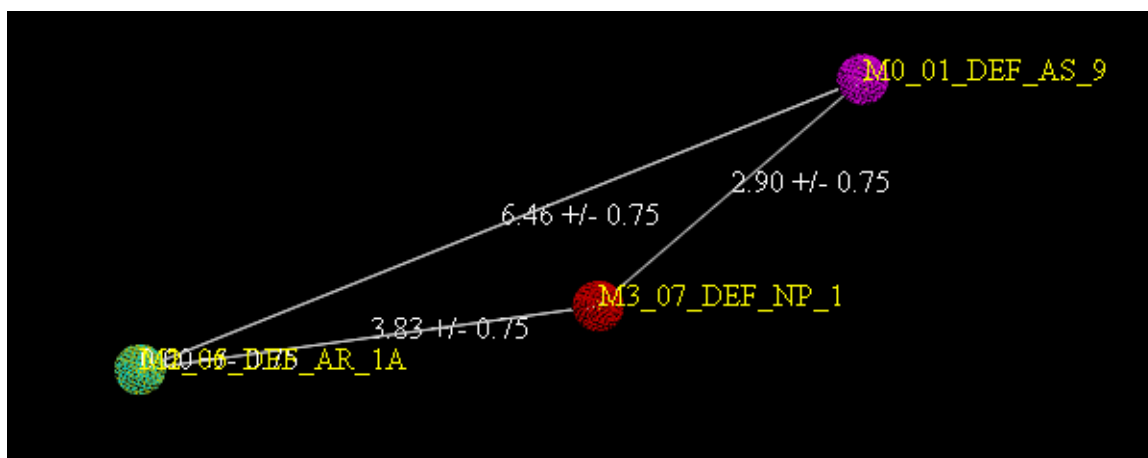


Figure 3.14 DISCOtech pharmacophore derivation of spirocyclic thiophenes (compounds 18-38). Purple sphere = acceptor site, red sphere = positive nitrogen and green sphere = aromatic/hydrophobic center.

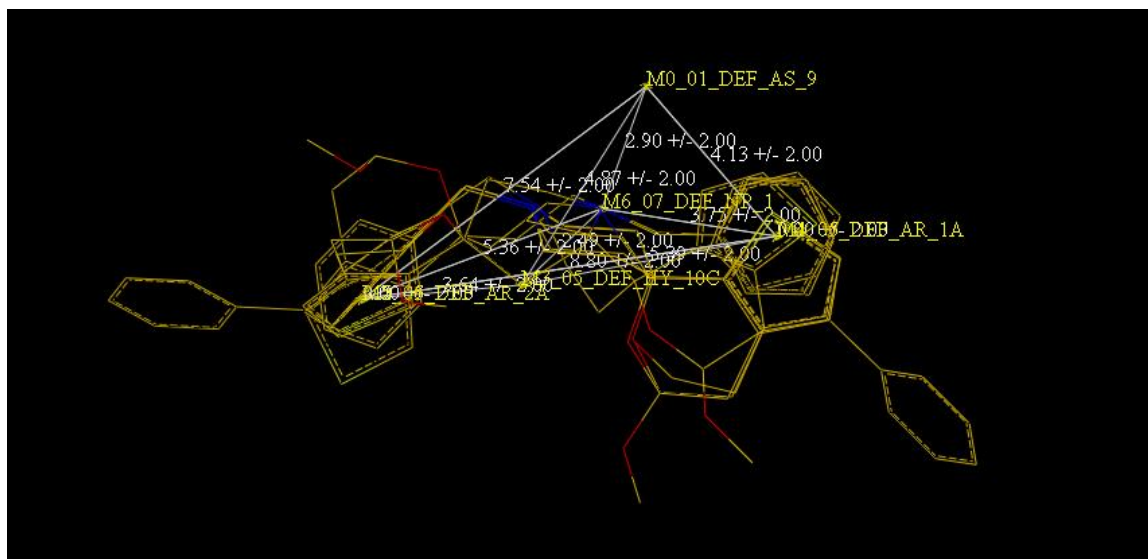


Figure 3.15 Alternate DISCOtech pharmacophore derivation of spirocyclic thiophenes (highest activity compounds of series; hydrogen atoms hidden - compounds 18, 19, 21, 22, 24, 25 and 32).

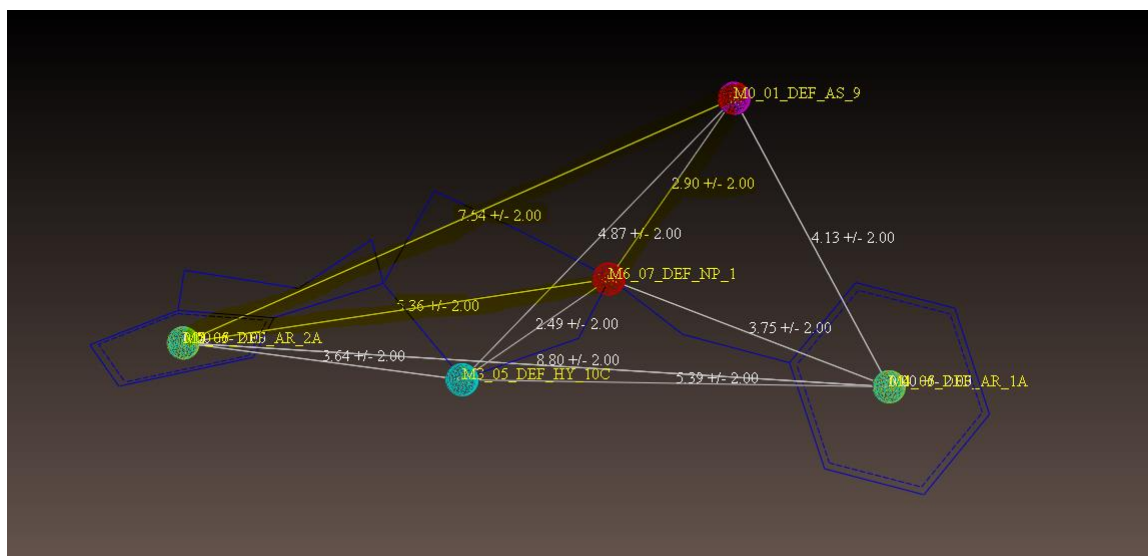


Figure 3.16 Alternate DISCOtech pharmacophore derivation of spirocyclic thiophenes with compound 22, hydrogen atoms hidden. Purple sphere = acceptor site, red sphere = positive nitrogen and green sphere = aromatic/hydrophobic center. Additional sphere in blue indicates a hydrophobic point. Highlight in yellow also depicts an alternate “triangle” pharmacophore.



Figure 3.17 Meyer and coworkers' mapping of compound "3b" (compound 32) onto a 3D pharmacophore model. Red sphere is the nitrogen/positive ionizable group, pink sphere is hydrogen/aromatic group and hydrogen bond acceptor is light green denoted as two spheres, the smaller being the location of the hydrogen bond acceptor on the ligand and the larger one being the location of the hydrogen bond donor on the receptor.
Source: Meyer et al., 2012.

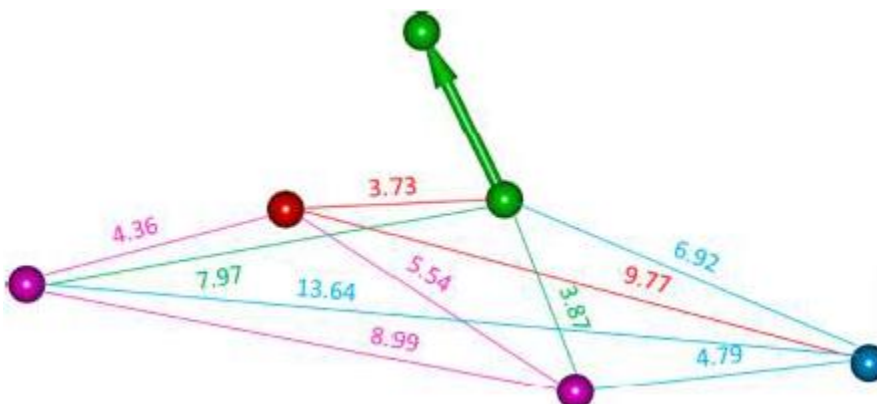


Figure 3.18 Distances for spirocyclic thiophene pharmacophore generated by Meyer and coworkers. Red sphere = nitrogen, pink sphere = hydrogen/aromatic group and hydrogen bond acceptor is light green denoted as two spheres, the smaller being the location of the hydrogen bond acceptor on the ligand and the larger one being the location of the hydrogen bond donor on the receptor).
Source: Meyer et al., 2012.

For the derivation of the sigma 1 representative pharmacophore as depicted in Figures 3.19 – 3.21, seven highly active ligands were used. Reference compounds from previous work in the Gund group included compound 43, Spipethiane (rigid), compound 44, (+)-Pentazocine (rigid) and compound 41, PD144418 (most active sigma 1 ligand

identified). The molecules additionally chosen from the new classes studied in this work for the representative pharmacophore included: compound 1 (lead compound for 1,2,3,4-tetrahydrospiro[naphthalene-1,4'-piperidine] and 1,4'-silaspiro[indane-1,4'-piperidine] series), compound 9 (lead compound for spirocyclic thienopyran system and aminoethyl-substituted tetrahydrobenzothiophenes), compound 15 (lead compound for fluoro-oligo-ethoxylated 4-benzylpiperazine derivatives) and compound 22 (highest activity spirocyclic thiophene molecule in this study). Spipethiane (compound 43) was designated as the reference molecule in DISCOtech since it was a rigid yet second highest active sigma 1 ligand of the compounds chosen. The resulting pharmacophore included the typical features aforementioned – the lone pair of electrons, the nitrogen atom and the center of a hydrophobic/aromatic ring. The distance from the N atom to the lone pair was 2.9 Å; from the center of the hydrophobic ring (varied from phenyl ring to thiophene ring depending on the molecule) to the N atom the distance was 6.80 Å; and the distance from the lone pair to the center of the thiophene ring was 8.45 Å. The last sigma 1 model from the Gund group in 2003 had proposed the pharmacophore to have similar distances for the same binding features. Therefore, the current model shows 8.45 Å vs 8.662 Å (previous model) for C-lone pair; 6.80 Å vs 7.135 Å (previous model) and 2.90 Å vs 2.508 Å (previous model) (Jung et al., 2004). The previous model in 2004 had used three main classes in addition to references. The three main classes were Spipethiane and its analogs, Piperidine and Piperazine Analogs and Benzothiazolone Analogs along with other ligands including PD144418 (Jung et al., 2004). The importance of the current work is that it essentially takes elements of the work in 1991 and 2004 and expands it to include more recent data on other sigma 1 ligands such as the

1,2,3,4-tetrahydrospiro[naphthalene-1,4'-piperidine] and 1,4'-silaspiro[indane-1,4'-piperidine] series, spirocyclic thienopyran system and aminoethyl-substituted tetrahydrobenzothiophenes and spirocyclic thiophene. The current model therefore continues to promote the idea of the original 1991 model of the “triangle” shaped pharmacophore, retaining the idea of the importance of the lone pair as an aspect of the model; the oxygen atom, though an element in some of the molecules studied and previously presented as an important aspect of previous pharmacophore models, is not part of the pharmacophore model created in this current study.

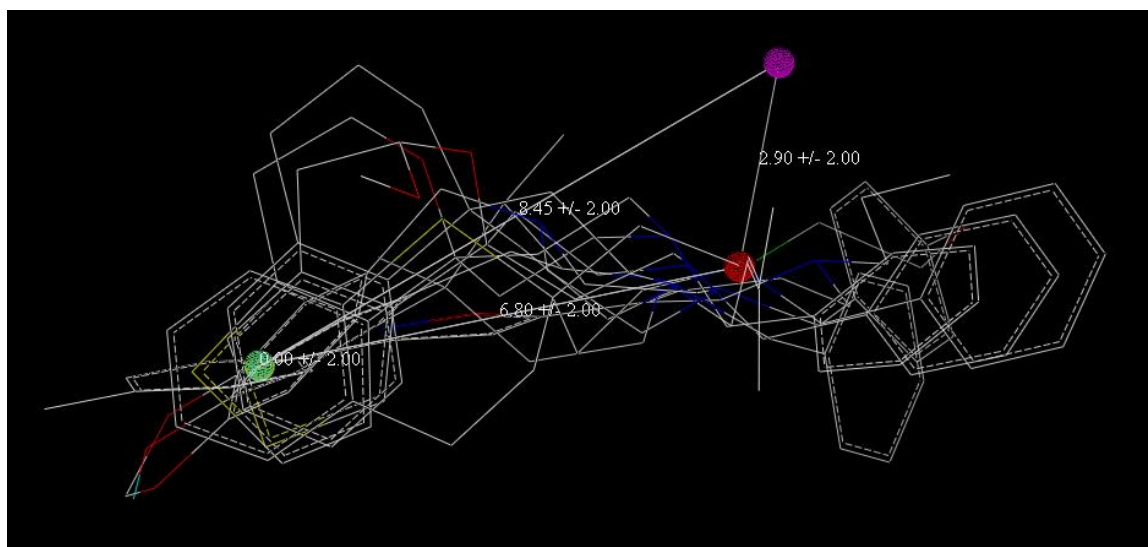


Figure 3.19 Comprehensive DISCOtech pharmacophore derivation representing entire Sigma 1 class of molecules studied (hydrogen atoms hidden – compounds 1, 9, 15, 22, 41, 43 and 44).

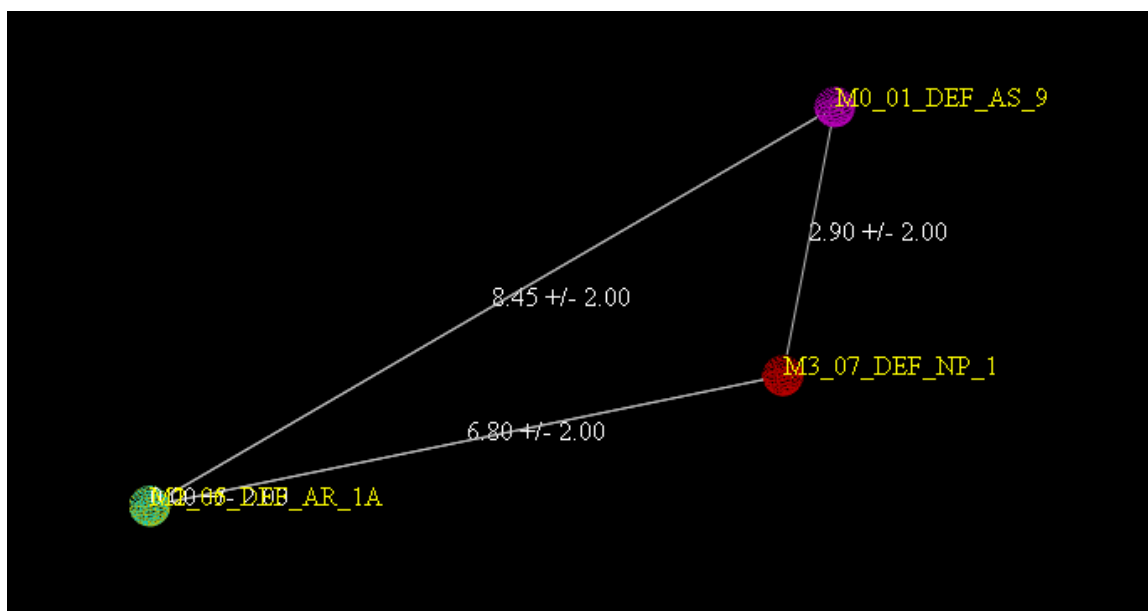


Figure 3.20 Comprehensive DISCOtech pharmacophore derivation for Sigma 1. Purple sphere = acceptor site, red sphere = positive nitrogen and green sphere = aromatic/hydrophobic center.

Certainly there is consistency, particularly with the aforementioned “triangle” shape in terms of distances and the main binding groups of the lone pair, nitrogen atom and center of a hydrophobic ring, in the pharmacophore modeling by the Gund group as the classes of sigma 1 compounds increased significantly over the years. Other researchers have proposed pharmacophore models as well for sigma 1 ligands; most of the other models developed have been designed by researchers who have synthesized sigma 1 ligands and therefore want to understand the relationship of the activities generated with the molecular structure of the synthesized molecules. Laggner and coworkers presented their pharmacophore model in Figure 3.22 featuring nitrogen and the phenyl group as important binding sites, however the additional hydrophobic groups featured are not in agreement in our model (2005). Though the additional hydrophobic features can be recognized in many of the molecules in this study, our model includes a

feature that Laggner's model does not have – that of the lone pair of electrons as seen in Figure 3.21. Note that the researcher did change the feature selection in DISCOtech in this study to simulate some of the other models for comparison and educational purposes. For instance, DISCOtech could not simulate Laggner's model because the representative sigma 1 ligands did not all have 4 hydrophobic features available, demonstrating that pharmacophore models can be very dependent on the molecules chosen. Instead, a modified version of Laggner's pharmacophore was created while including the additional feature of the lone pair of electrons as seen in Figure 3.24, however this model is not the leading or preferred model of the researcher since it does not represent the alignment approach later used for the Comparative Molecular Field Analysis (ComFA). The CoMFA, described in detail in Section 3.5, had the tightest alignment by approaching a fit primarily around the nitrogen atom and surrounding atoms (in an attempt to overlay the acceptor site and the N atoms of all of the molecules) while simultaneously trying to overlay the thiophene or phenyl moieties in the same binding site as the pharmacophore in Figure 3.19. Note that most other researchers do not show diagrams of how their molecules overlay; though supplemental data is available to address tolerances and distances for the binding groups, visually one cannot observe how the cyclohexyl (or N and surrounding atoms) align, specifically directionally. Our CoMFA and pharmacophore models align directionally for the cyclohexyl ring, with the objective for the lone pairs to overlap. Since the CoMFA models conducted in Section 3.5 are considered “robust” and highly predictive based on peer-reviewed journal criteria, the researcher for this study therefore postulates that the representative pharmacophore in Figure 3.19 is a key pharmacophore model for sigma 1 ligands since its inherent structure was used as a basis

for the successful CoMFA models.

Figure 3.23 depicts another pharmacophore model, in this case by Collina et al. (2007). Similar to Laggner's model in Figure 3.22, this model is depicting nitrogen as a positive ionizable feature with the remaining three features being hydrophobic binding sites.

For completeness, additional DISCOtech iterations were considered to include additional hydrophobic groups since other researchers included them. The model that is most similar to our lead pharmacophore from Figure 3.19 is in Figure 3.25 where an additional hydrophobic group (near the aromatic/primary hydrophobic groups as postulated by other researchers) is shown. This model, however, does not visually appear to align as closely for the thiophene/phenyl rings for the aromatic/hydrophobic binding site.

Literature often cites the Glennon model shown in Figure 3.23 (2005). This model was recreated in DISCOtech as seen in Figure 3.27 with similar distances; the N atom to the primary hydrophobic region being 6.8 Å, consistent with the Glennon range of 6-10 Å as well as the N to secondary hydrophobic region being 3.72 Å, consistent with the Glennon range of 2.5-3.9 Å. Glennon is another researcher who does not include the concept of the lone pair of electrons in his model. If the model is forced to include it, as shown in Figure 3.28, the distances between the primary hydrophobic region and the N atom reduces to 4.54 Å.

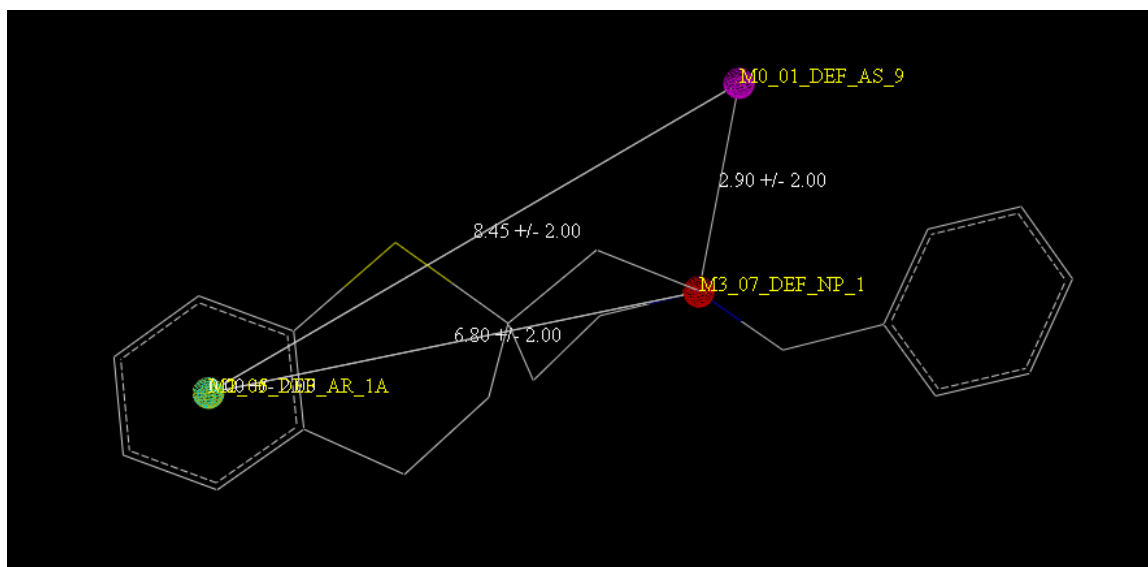


Figure 3.21 Comprehensive DISCOtech pharmacophore derivation with reference compound 43, Spipethiane.

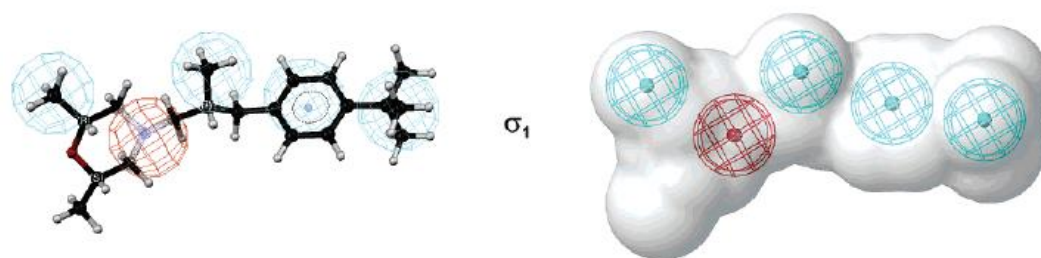


Figure 3.22 Sigma 1 pharmacophore model for Laggner and coworkers.
Source: Laggner et al., 2005.

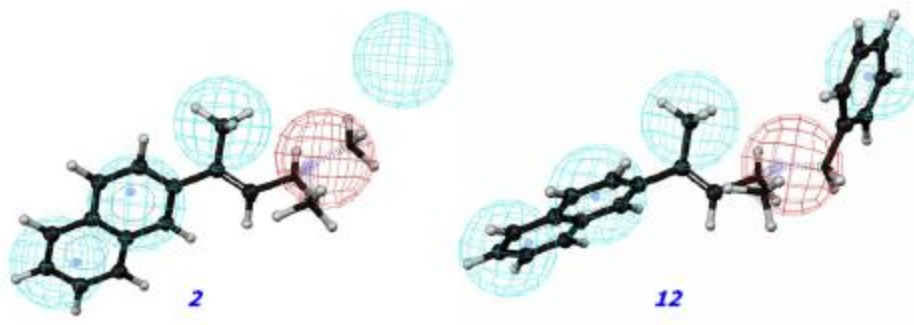


Figure 3.23 Pharmacophore model for Collina and coworkers. Molecules 2 and 12 were newly designed and synthesized in arylalkyl and alkenylamines series. Red sphere is nitrogen/positive ionizable feature while the cyan spheres are hydrophobic features. Source: Collina et al., 2007.

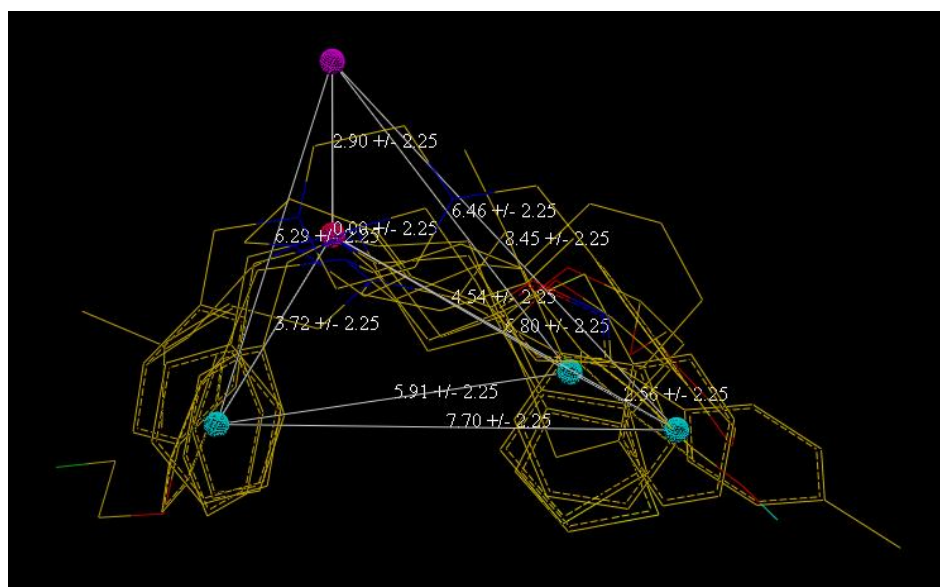


Figure 3.24 Alternate sigma 1 pharmacophore model with additional hydrophobic groups (green spheres) to compare with Laggner et al. model. Pink sphere is N atom and purple sphere is lone pair of electrons.

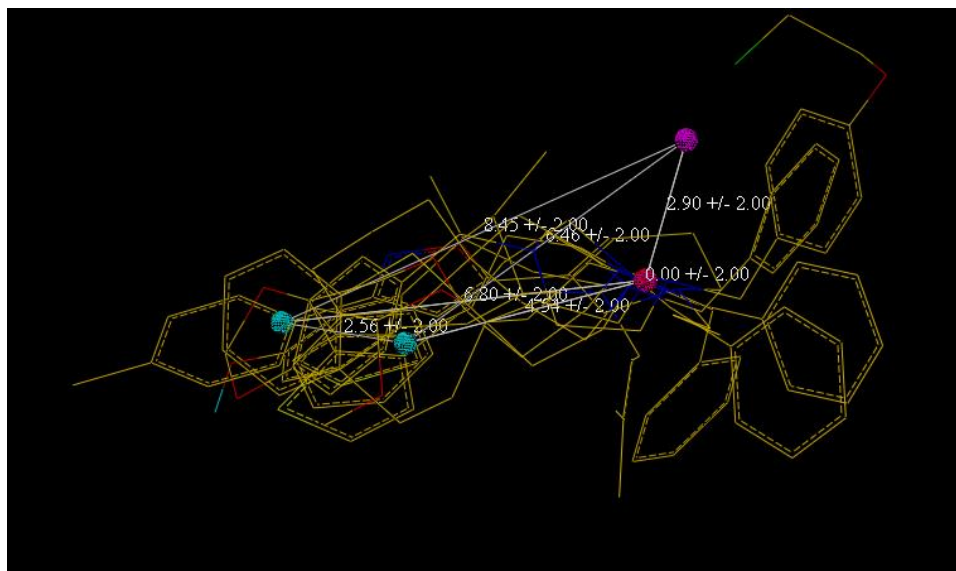


Figure 3.25 Additional alternate sigma 1 pharmacophore model with additional hydrophobic group (green sphere) to compare with Laggner et al. model. Pink sphere is N atom and purple sphere is lone pair of electrons.

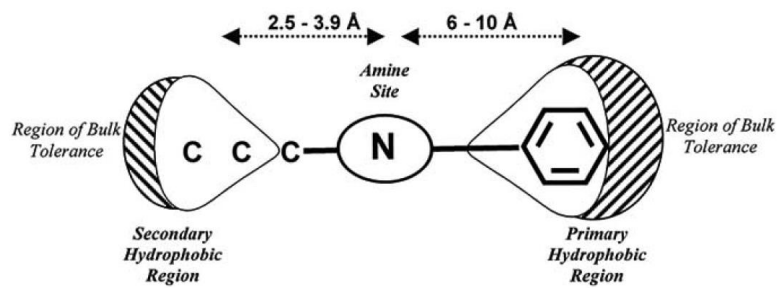


Figure 3.26 Sigma 1 pharmacophore model for Glennon.
Source: Glennon, 2005.

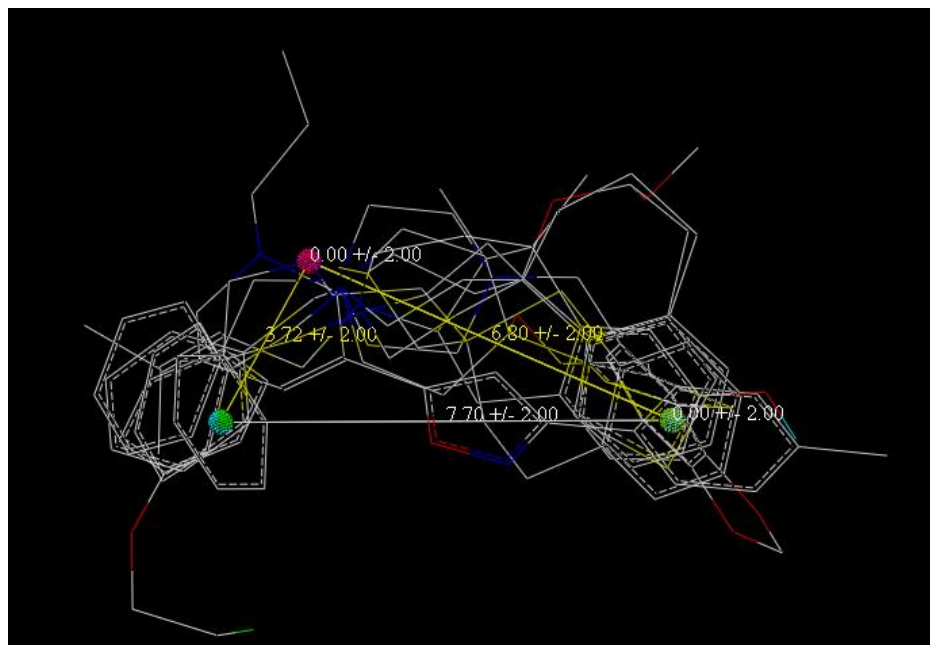


Figure 3.27 Additional alternate sigma 1 pharmacophore model without lone pair of electrons to compare with the Glennon model. Pink sphere is N atom and green spheres are hydrophobic groups

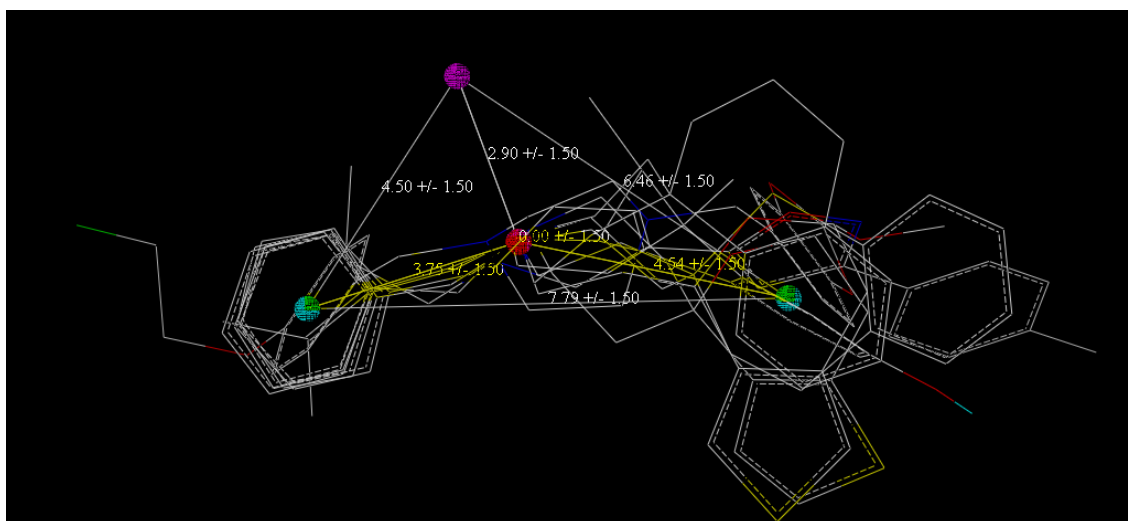


Figure 3.28 Additional alternate sigma 1 pharmacophore model with lone pair of electrons to compare with Glennon model. Pink sphere is N atom and green spheres are hydrophobic groups Lone pair is included as purple sphere.

The last pharmacophore model analyzed in this work was from Caballero et al. (2012). In this case, Cabellero and colleagues had modeled methyl 2-(aminomethyl)-1-

phenylcyclopropane-1-carboxylate (MAPCC) derivatives, resulting in a pharmacophore model as shown as “c” in Figure 3.29. Note the comparison between that model and the aforementioned Glennon and Laggner models shown as (a) and (b) in the Figure 3.29, respectively (Cabellero et al., 2012). Cabellero’s model differs from the Gund, Laggner and Glennon models due to additional acceptor sites; this can mainly be attributed to the fact that the structure is unique, particularly with the additional O atoms. The visual molecule overlay for their pharmacophore was presented in their paper as well, however, these molecules only had minor differences in terms of substituents and therefore the conformations in their GALAHAD pharmacophore model molecules did not appear to alter much as can be observed visually in Figure 3.30. Therefore, the researcher for this study assumed that this pharmacophore is very specific for the MAPCC derivatives class and does not represent a possible comprehensive sigma 1 pharmacophore.

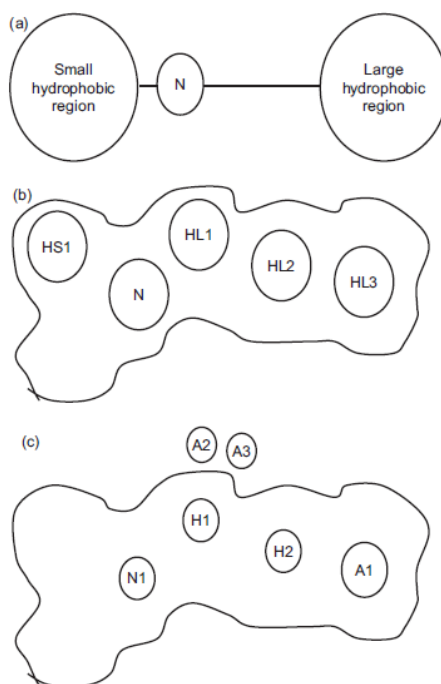


Figure 3.29 Caballero and coworkers' figure depicting comparisons between Glennon (a), Laggner (b) and their work (c). H1 and H2 are hydrophobic groups. N1 is Nitrogen. A1, A2 and A3 are all acceptor groups.
Source: Caballero et al., 2012.

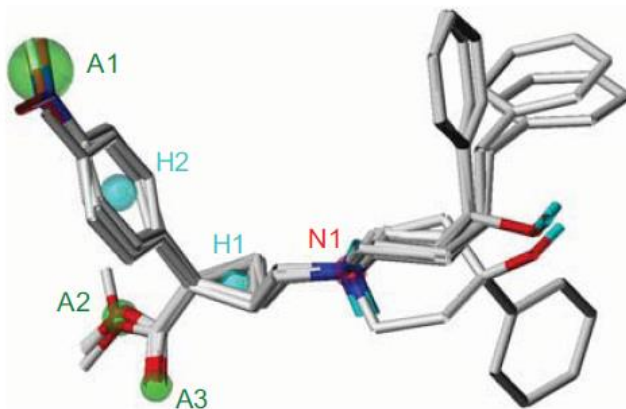


Figure 3.30 Caballero and coworkers' GALAHAD pharmacophore model of MAPCC derivatives and molecular alignment of the compounds. Cyan spheres are hydrophobic points; red is positive nitrogen and green spheres are acceptor points.
Source: Caballero et al., 2012.

In summary, pharmacophore models were derived by the researcher for the classes studied in this work. Additionally a representative pharmacophore was designed and applied in the alignment techniques discussed in the CoMFA in Section 3.5. Again, due to the success of the CoMFA using the pharmacophore in Figure 3.19 (which focuses on the lone pair, hydrophobic/aromatic group and the N atom) and also due to the aforementioned differences noted in the molecules and pharmacophore approaches chosen by the other researchers, the leading, comprehensive model proposed by this study remains to be the postulated model as depicted in Figures 3.19 – 3.21. As an additional key point, Spipethiane (compound 43) was used as the reference for all of the

representative pharmacophore models for sigma 1 and Spipethiane was consistently applied as the template/reference molecule in the alignments for the CoMFA studies in Section 3.5.

3.5 Comparative Molecular Field Analysis

3.5.1 Geometry Optimization and Electrostatic Studies

Each molecule in this study was optimized and saved at the *ab initio* HF/6-31G* and density functional B3LYP/6-31G* levels with electrostatic charges. Once each molecule was optimized, it was saved as a “.mol2” file with “electrostatic” to carry the corresponding geometry and calculated electrostatic charges into SYBYL-X 2.1.

3.5.2 Alignment

Alignment of the HF/6-31G* and B3LYP/6-31G* optimized geometries for the sigma 1 ligands was an essential step in generating a CoMFA model for each calculation level, respectively. A key point is that this was a rigid alignment approach with the intent to maintain the bound conformation of each molecule at the calculation level being studied. Many researchers, however, use flexible alignment approaches; as an example, Caballero and researchers state that their 3D-QSAR models rely on the arbitrary alignment of conformationally flexible ligands (2012). Since part of the objective of this study was to observe the results, comparing *ab initio* with density functional methods, and also since the conformation is unknown for each molecule when it binds to the sigma 1 receptor, the

assumption was made that the energy should be minimized. Therefore the *ab initio* and density functional methods calculated energy minimized geometries while also calculating the electrostatic charges. The resulting molecules were then rigidly aligned to each other.

The approach to alignment for the sigma 1 ligands consisted of matching up the N atom and surrounding items, particularly those of the cyclohexyl ring, and matching up the phenyl/thiophene (hydrophobic ring) moieties with the objective being to bind the molecules together at the pharmacophore binding groups as seen in Figures 3.19 – Figures 3.21. Spipethiane was the reference molecule used for the pharmacophore model and therefore was the template molecule used to drive the alignment process. Since 28 of the molecules in the data set that had similar geometry (cyclohexane ring), they were initially matched to Spipethiane as the template using the “DISTILL RIGID” alignment tool. The remaining molecules in the various classes were then manually aligned using the “match atoms” feature; Spipethiane was first used as the template to match with the lead compounds for the remaining series. Then the remaining molecules of those classes were aligned to the lead compounds. Finally, the spirocyclic thiophene series was removed from the whole database and was manually aligned at the thiophene moieties and at the N and surrounding atoms to ensure a tighter alignment; then it was reintroduced back to the database. Note that the researcher determined it was appropriate to leave out the fluoro-oligo-ethoxylated 4-benzylpiperazine derivatives. Though the most active ligand from that series remains in the pharmacophore, the series, perhaps due to extremely different geometry/length and very varied activities (1.85 to 505 nM) challenged the CoMFA models in robustness. Therefore, it was determined that this

series could perhaps instead be studied separately in the future and should be left out of the CoMFA model; this is not uncommon in the area of QSAR, as other researchers have similarly left out compounds when approaching rigorous modeling as seen by Dessalew and colleagues for aminothiazole derivatives (Dessalew et al., 2007). The resulting alignment for the sigma 1 ligands therefore consisted of 41 total sigma 1 molecules from all of the other classes and reference molecules described. Consistent with the robust criteria described in Section 2.2, 5 molecules were chosen as the test set with the remaining 36 molecules acting as the training set. Additional details are provided in Section 3.5.3. The final alignment of all 41 molecules can be viewed in Figure 3.31 for HF/6-31G* and Figure 3.32 for B3LYP/6-31G*. The resulting alignments led to robust models as described in Section 2.2.2. Additional details about the CoMFA models are described in Section 3.5.3.

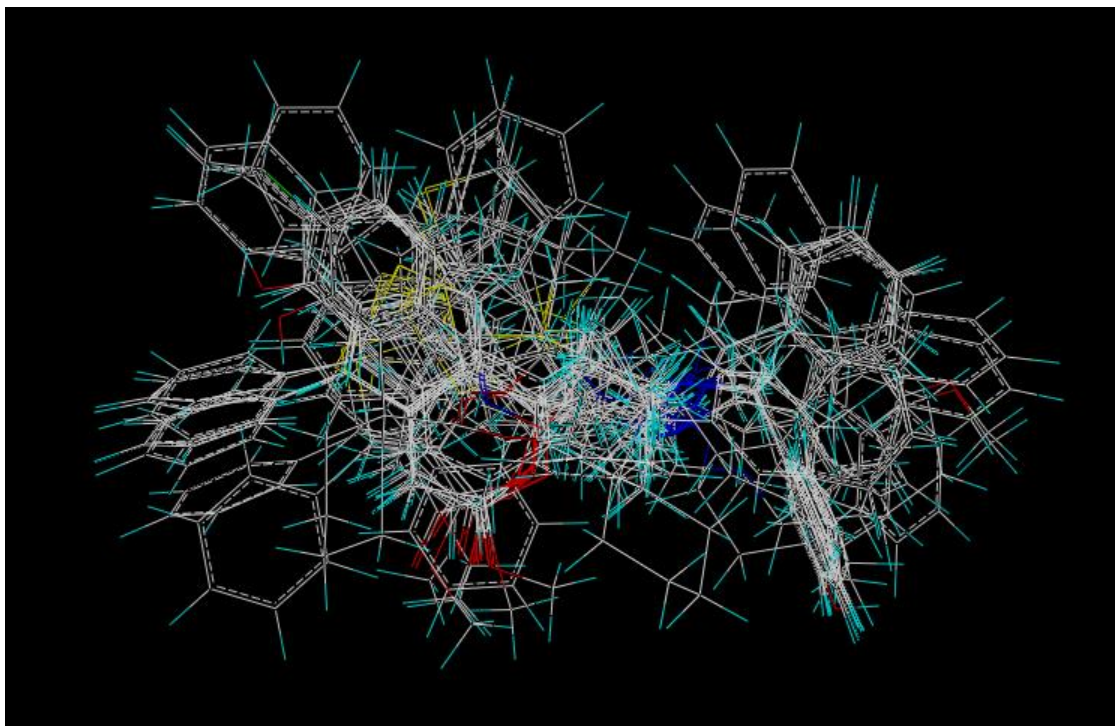


Figure 3.31 Alignment of all 41 sigma 1 ligands at the HF/6-31G* calculation level.

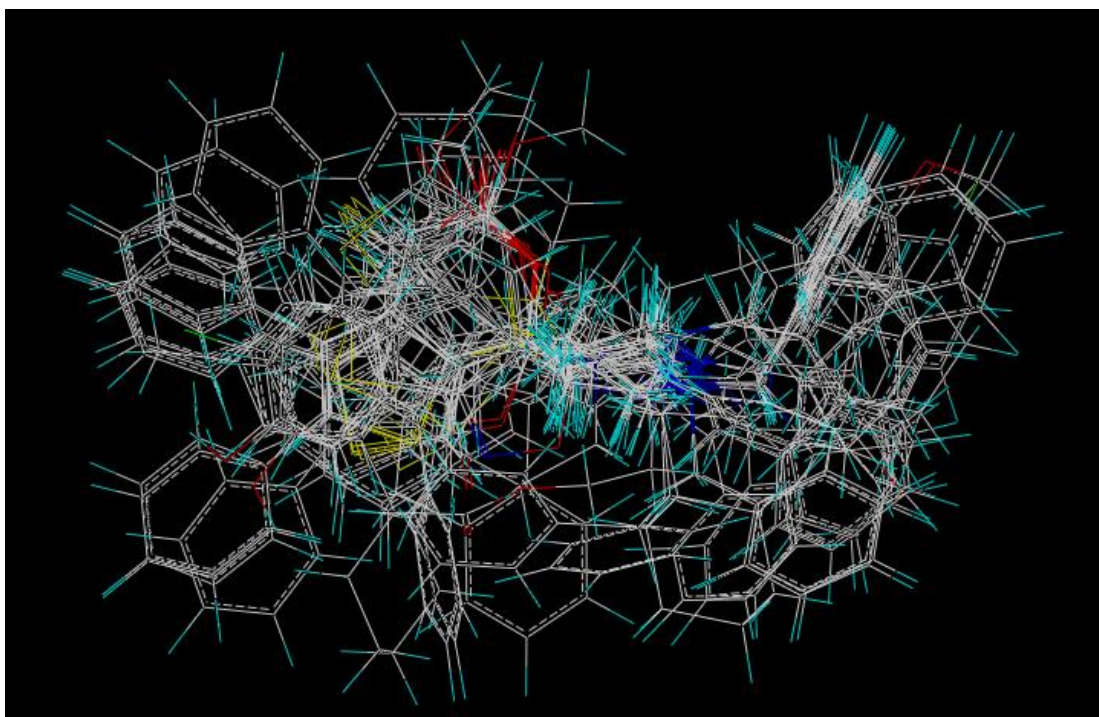


Figure 3.32 Alignment of all 41 sigma 1 ligands at the B3LYP/6-31G* calculation level.

3.5.3 Quantitative Structure Activity Data Analysis

The CoMFA models were initiated by first conducting the molecular alignment as described in Section 3.5.2. Each activity (K_i) value was converted to a pK_i value using Equation 2.4. The training set for the CoMFA ensured a range of at least 3 log units in terms of pK_i , as is suggested in the field and demonstrated by other researchers (Bolden et al., 2013). The training set ranged from -2.6839 to 1.0969 whereas the test set ranged from -1.6021 to 0.1805 log units. The histograms of the pK_i vs number of molecules are shown in Figures 3.33A and 3.33B.

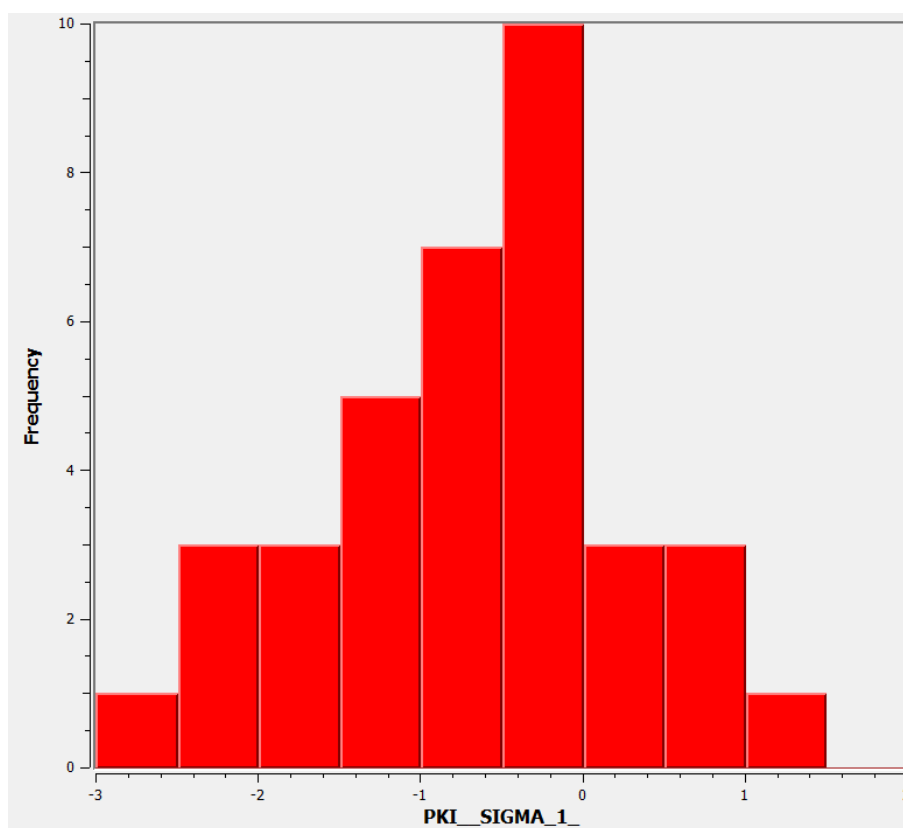


Figure 3.33A Histogram of frequency vs pK_i for sigma 1 ligands in training set.

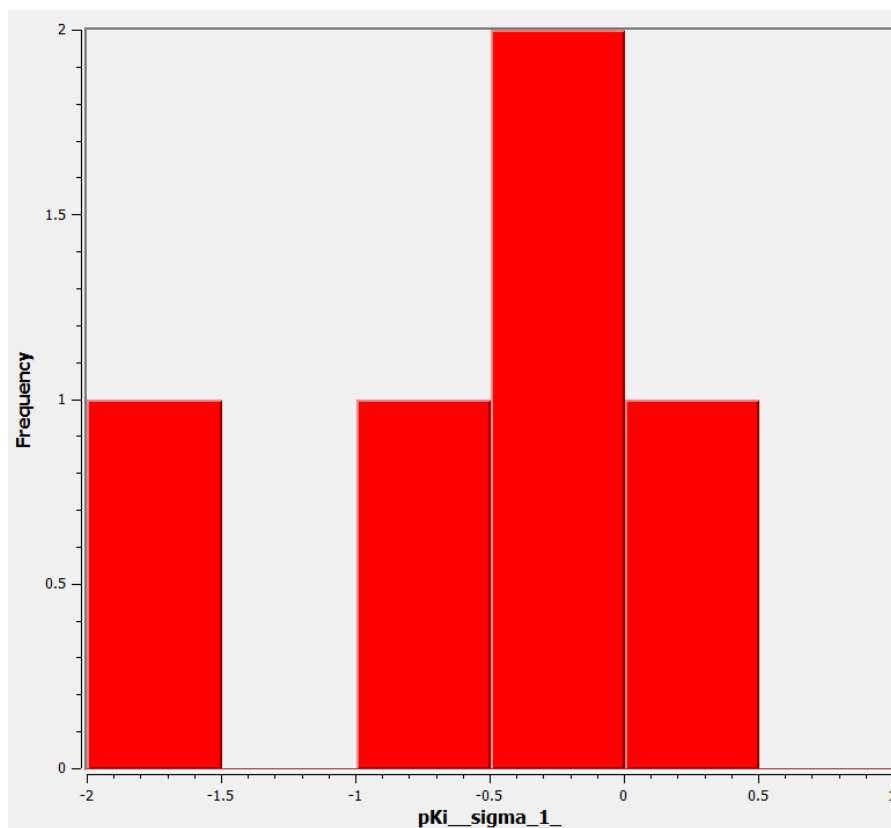


Figure 3.33B Histogram of frequency vs pK_i for sigma 1 ligands in test set.

The CoMFA models were constructed using the default settings in SYBYL-X 2.1. Therefore, an sp^3 hybridized carbon atom was probed with a +1.0 unit charge which extended at least 4 Å beyond each molecule, 2.0 Å grid spacing and the default 30 kcal/mol energy cutoff for steric and electrostatic fields. The CoMFA column, combined with the literature pK_i values, generated the Partial Least Squares cross-validated q^2 for each set, resulting in a predicted bioactivity (pK_i) value for each training set molecule. The test set, molecules which were not used to create the model, was used to validate the model by comparing predicted bioactivities generated with the experimental results. The resulting sigma 1 dataset at HF/6-31G* with 36 molecules in the training set resulted in a q^2 value of 0.505; the predicted bioactivity values for that set is in Table 3.8. The

resulting sigma 1 dataset at B3LYP/6-31G* with 36 molecules in the training set resulted in a q^2 value of 0.575; the predicted bioactivity values for that set is in Table 3.8. The results for the test set are in Table 3.9.

Table 3.8 Experimental and Predicted Bioactivities (pK_i) by the Training Set of Sigma 1 Compounds using *ab initio* and Density Functional Calculation Methods

Compounds	Lit. pK _i	HF/6-31G*	B3LYP/6-31G*
			Predicted pK _i
1	-0.301	-0.2581	-0.1822
2	-0.5798	-0.6452	-0.6272
3	-0.9031	-0.9516	-0.6721
4	-0.2553	-0.0579	-0.0921
5	-0.0414	0.0237	0.2759
6	-0.4314	-0.428	-0.3173
8	0.5229	0.3211	0.1738
9	0.5086	0.4623	0.5991
11	-1.6902	-1.5966	-1.3458
12	-2.1004	-1.9396	-1.7909
13	-2.1206	-2.0014	-2.09
14	-0.699	-1.0236	-1.0851
18	0	-0.332	-0.3653
19	-0.2788	-0.3033	-0.1645
20	-2.4065	-2.2125	-1.8888
21	0.4559	0.667	0.4532
22	0.6576	0.6577	0.5779
24	0.4949	0.5553	0.4325
25	-0.2041	-0.1467	-0.2289
26	-0.7324	-0.5731	-0.8959
27	-0.7243	-0.8645	-0.8959
28	-0.3802	-0.562	-0.7165
29	-1.2041	-0.9826	-1.0873
30	-1.3617	-1.4219	-1.3089
31	-0.6532	0.0019	-0.3292
32	0	-0.2851	-0.4657
33	-0.3979	-0.5994	-0.5278
35	-1.2041	-1.2222	-1.3218
36	-1.0414	-1.0603	-0.8683
37	-2.6839	-2.6033	-2.7247
38	-1.9395	-1.7999	-2.2428
39	-1.3747	-1.6467	-1.4024
41	1.0969	1.096	1.2858
42	-1.6435	-1.7795	-1.7619
43	0.301	0.2767	0.1636
44	-0.7634	-0.8428	-0.9157

Table 3.9 Experimental and Predicted Bioactivities (pK_i) by the Test Set of Five Sigma 1 Compounds using *ab initio* and Density Functional Calculation Methods

Compounds	Lit. pK_i	HF/6-31G*	B3LYP/6-31G*
			Predicted pK_i
3	-0.4624	-0.5672	-0.3821
10	0.1805	0.2109	-0.3535
23	-1.6021	-1.6747	-1.5586
34	-0.7404	-0.7629	-0.9589
40	-0.0792	0.6129	0.2104

The Partial Least Squares Analysis (PLS), as described in Section 2.2.1, was used by applying the SAMPLS algorithm in SYBYL-X 2.1 developed by Bruce Bush. The optimum number of components was determined by the SYBYL-X 2.1 in the output report from the SAMPLS algorithm and is shown in **bold** in Table 3.10. The number of optimal components identified in the report was then applied without cross-validation yielding the results in Table 3.11. The R^2 values for HF/6-31G* and B3LYP/6-31G* without cross-validation, using the optimal number of components for each, respectively, at 5 and 4 yielded 0.959 and 0.938. Note that Table 3.11 also presents the electrostatic and steric contributions to the CoMFA field.

Table 3.10 Optimal Component Number and q^2 by “Leave-One-Out” using SAMPLS by the Training Set of 36 Molecules

Lev.	Term	C. 1	C. 2	C. 3	C. 4	C. 5	C. 6	C. 7	C. 8	C. 9	C. 10
HF	s.e.e.	0.765	0.715	0.702	0.707	0.704	0.717	0.733	0.746	0.768	0.805
	q^2	0.338	0.438	0.474	0.484	0.505	0.504	0.499	0.499	0.489	0.461
B3	s.e.e.	0.713	0.660	0.641	0.642	0.658	0.690	0.701	0.723	0.749	0.763
	q^2	0.425	0.522	0.563	0.575	0.568	0.541	0.542	0.530	0.515	0.515

s.e.e. is standard error of estimates.

Table 3.11 QSAR Reports by Non-Crossvalidation Using SAMPLS by the Training Set of 36 Molecules

Calculation Level	S.E.E.	R ²	F Values	Steric.	Electro.
HF/6-31G*	0.203	0.959	(n1 = 5, n2 = 30) 139.468	0.381	0.619
B3LYP/6-31G*	0.246	0.938	(n1 = 4, n2 = 31) 116.722	0.392	0.608

s.e.e. is standard error of estimates.

The application of the robust criteria as described in Section 2.2.3 is shown in Figures 3.34 and 3.35 for HF/6-31G* in the graphs of predicted pK_i values vs experimental pK_i values. The training set and tests were subject to Equations 2.5 – 2.9; those equations were used to calculate and confirm that the HF/6-31G* CoMFA model meets the robust criteria as defined by Golbraikh and colleagues in Table 3.12A (2002, 2003).

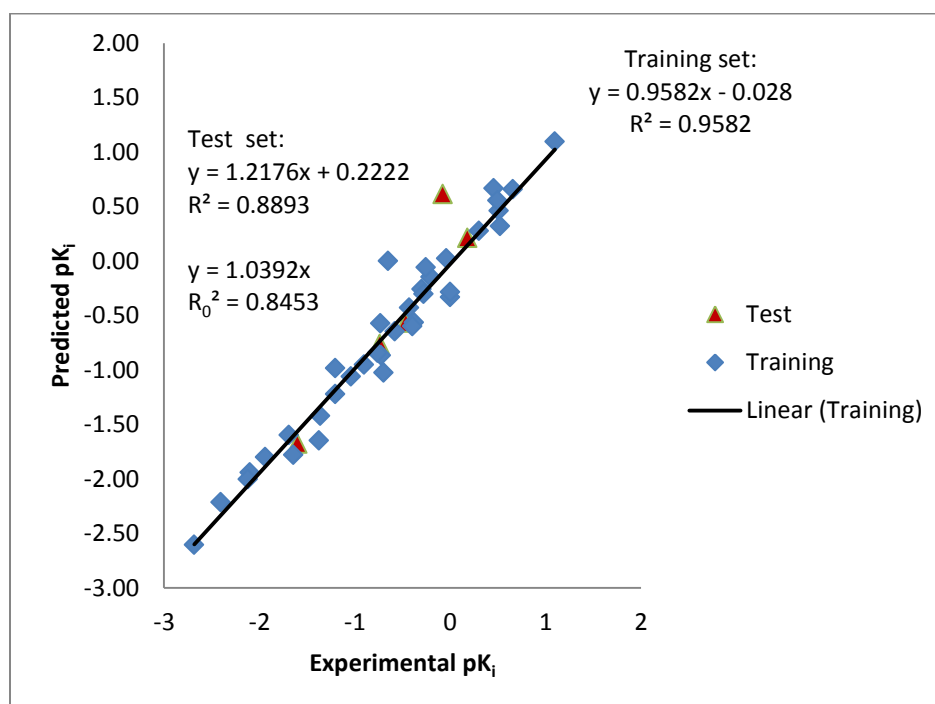


Figure 3.34 Graph of Predicted pK_i vs Experimental pK_i by the CoMFA model at HF/6-31G*.

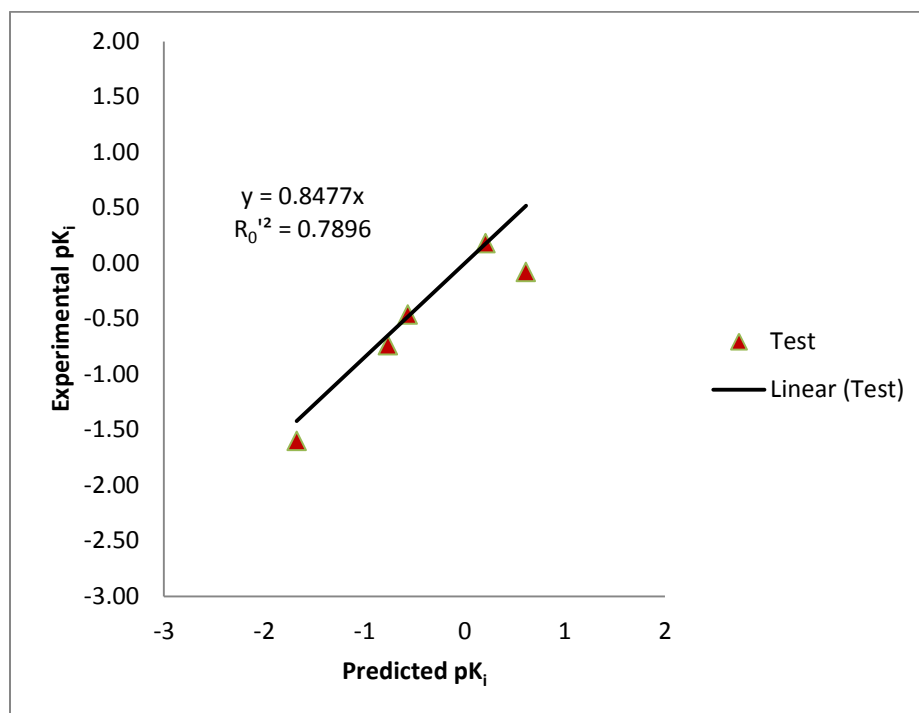


Figure 3.35 Graph of Experimental pK_i vs Predicted pK_i for Test Set by the CoMFA model at HF/6-31G*.

Table 3.12A Results for QSAR Robust Criteria Equations 2.5 – 2.9 for HF/6-31G* (Sigma 1)

Equations (2.5 – 2.9)	Value
$q^2 > 0.5$	$q^2 = 0.505$
$R^2 > 0.6$	$R^2 = 0.89$
$\frac{(R^2 - R_0'^2)}{R^2} < 0.1$ and $0.85 \leq k \leq 1.15$	$\frac{(R^2 - R_0'^2)}{R^2} = 0.05$ and $k = 1.04$
$ R_0'^2 - R_0''^2 < 0.3$	$ R_0'^2 - R_0''^2 = 0.06$

The application of the robust criteria as described in Section 2.2.3 is shown in Figures 3.36 and 3.37 for B3LYP/6-31G* in the graphs of predicted pK_i values vs experimental

pK_i values. The training set and tests were subject to Equations 2.5 – 2.9; those equations were used to calculate and confirm that the B3LYP/6-31G* CoMFA model meets the robust criteria as defined by Golbraikh and colleagues in Table 3.12B (2002, 2003).

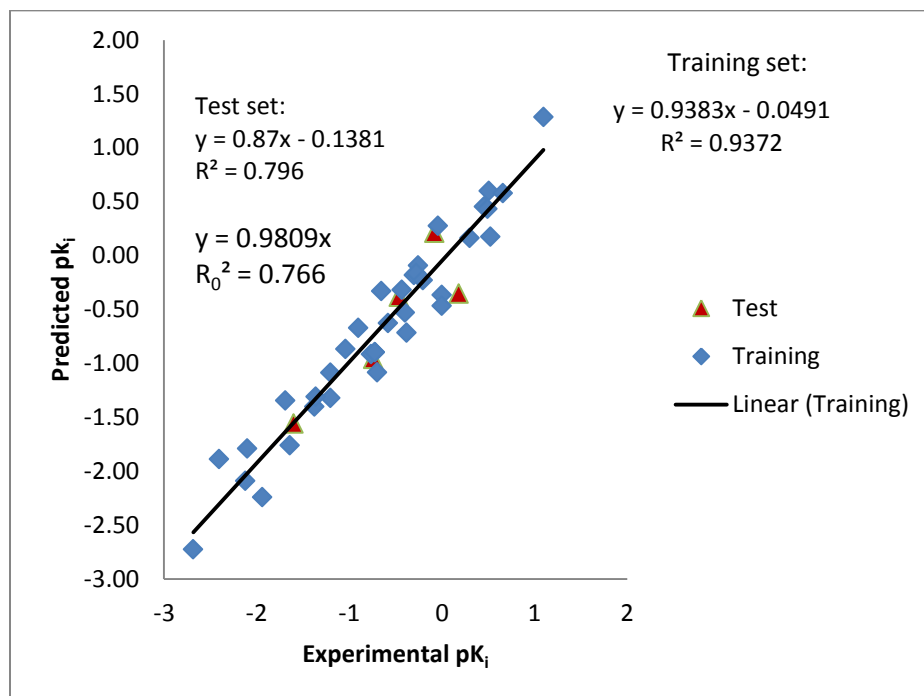


Figure 3.36 Graph of Predicted pK_i vs Experimental pK_i by the CoMFA model at B3LYP/6-31G*.

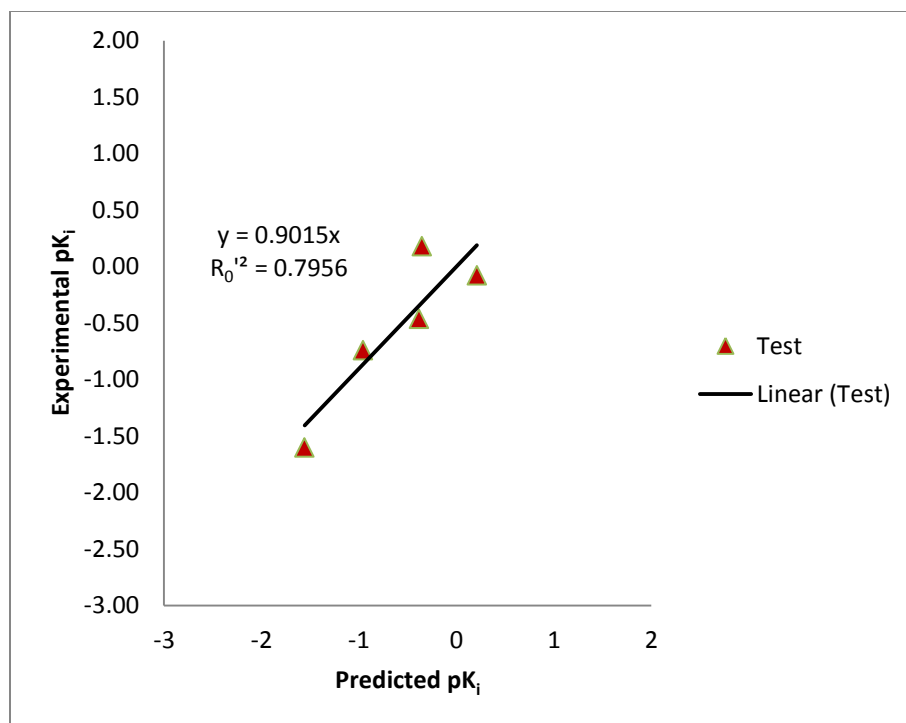


Figure 3.37 Graph of Experimental pK_i vs Predicted pK_i for Test Set by the CoMFA model at B3LYP/6-31G*.

Table 3.12B Results for QSAR Robust Criteria Equations 2.5 – 2.9 for B3LYP/6-31G* (Sigma 1)

Equations (2.5 – 2.9)	Value
$q^2 > 0.5$	$q^2 = 0.575$
$R^2 > 0.6$	$R^2 = 0.80$
$\frac{(R^2 - R_0^2)}{R^2} < 0.1$ and $0.85 \leq k \leq 1.15$	$\frac{(R^2 - R_0^2)}{R^2} = 0.04$ and $k = 0.981$
$ R_0^2 - R_0'^2 < 0.3$	$ R_0^2 - R_0'^2 = 0.03$

In summary, the bioactivity prediction for both models at HF/6-31G* and B3LYP/6-31G* were considered robust via PLS and the criteria set by Golbraikh and colleagues (2002, 2003). Therefore, the model can serve as a means to predict other compounds for

sigma 1 activity.

3.5.4 Contour Maps of CoMFA Models

Contour maps from the CoMFA models were explored with the objective to understand the desired sterics and electrostatics that could enhance the activity of a molecule, enabling the design of new ligands. In the maps, green represents steric bulk desirable whereas yellow represents steric bulk undesirable. In terms of electrostatics, the maps depict red for negative charge desirable whereas blue represents positive charge as desirable. The differences observed in the CoMFA contour maps between HF/6-31G* and B3LYP/6-31G* were also explored.

Figure 3.38 and Figure 3.39 show the contour maps for compound 43, Spipethiane, which served as the reference molecule for pharmacophore generation as well as the template molecule for the CoMFA alignment. Note that the steric bulk desirable is consistent for the phenyl ring on the right and the left for both calculation levels, however, there is some difference regarding bulk above and below the center of the molecule. In terms of electrostatics, negative charge was consistently desirable over the left phenyl ring, however positive charge did not display consistently between the two calculation levels for the maps.

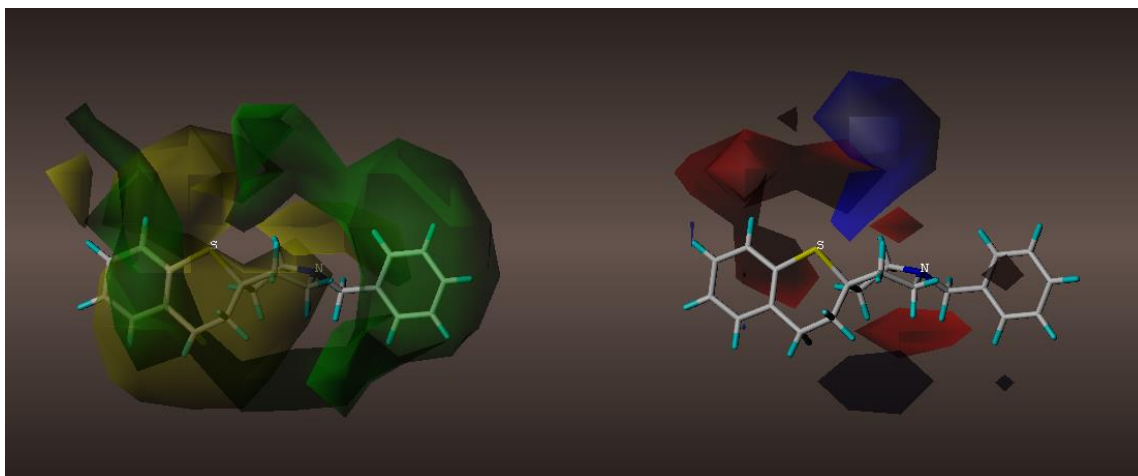


Figure 3.38 Contour map of compound 43 (Spipethiane) at HF/6-31G*.

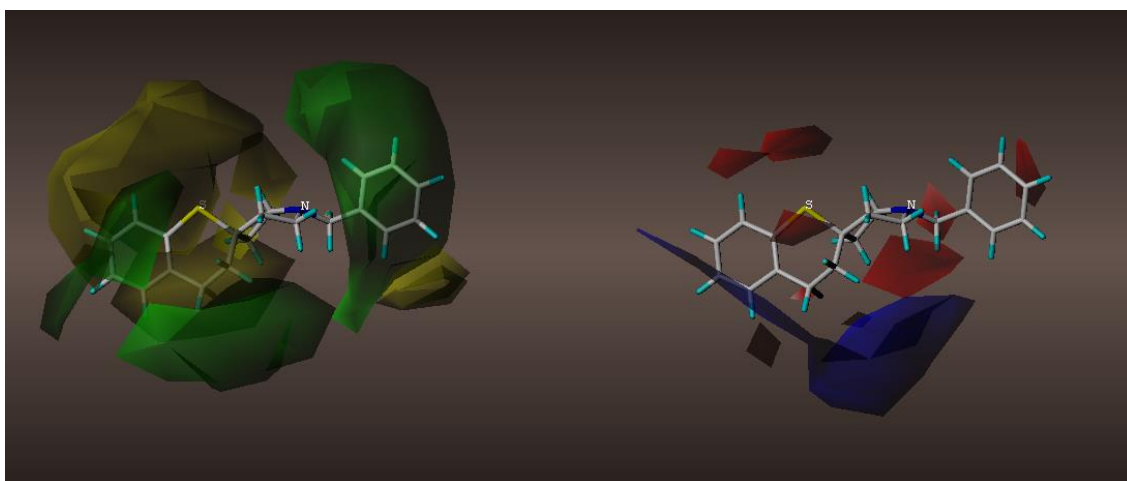


Figure 3.39 Contour map of compound 43 (Spipethiane) at B3LYP/6-31G*.

Figure 3.40 and Figure 3.41 show the contour maps for compound 41, PD144418, the most active sigma 1 ligand in this study. Similar to the contour maps for Spipethiane, the steric bulk desirable is consistent for the phenyl ring on the left for both calculation levels; it is also consistent on the right side with the CH₂ groups. There is some difference regarding bulk above and below the center of the molecule. In terms of electrostatics, negative charge was consistently desirable over the left phenyl ring,

however, positive charge did not display consistently between the two calculation levels for the maps.

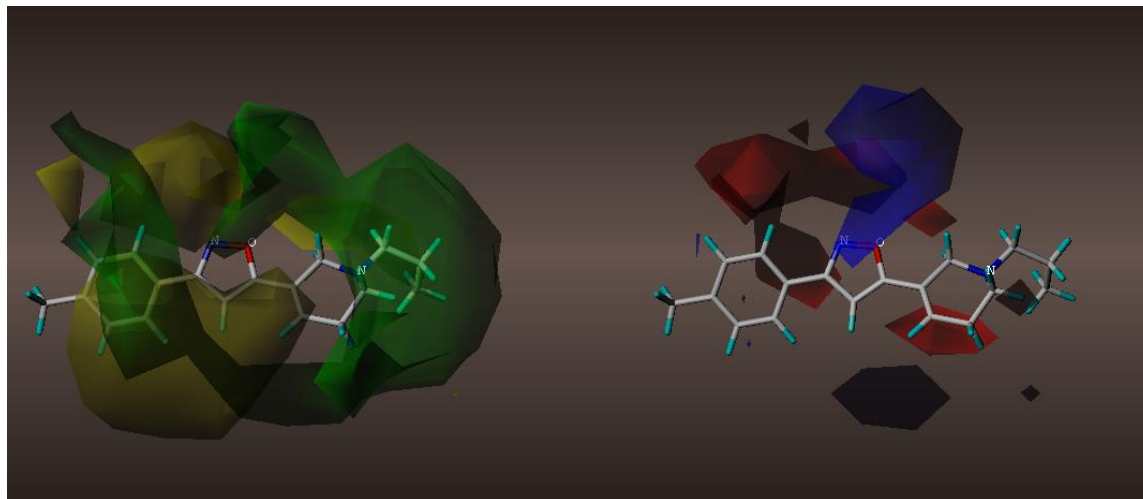


Figure 3.40 Contour map of compound 41 (PD144418) at HF/6-31G*.

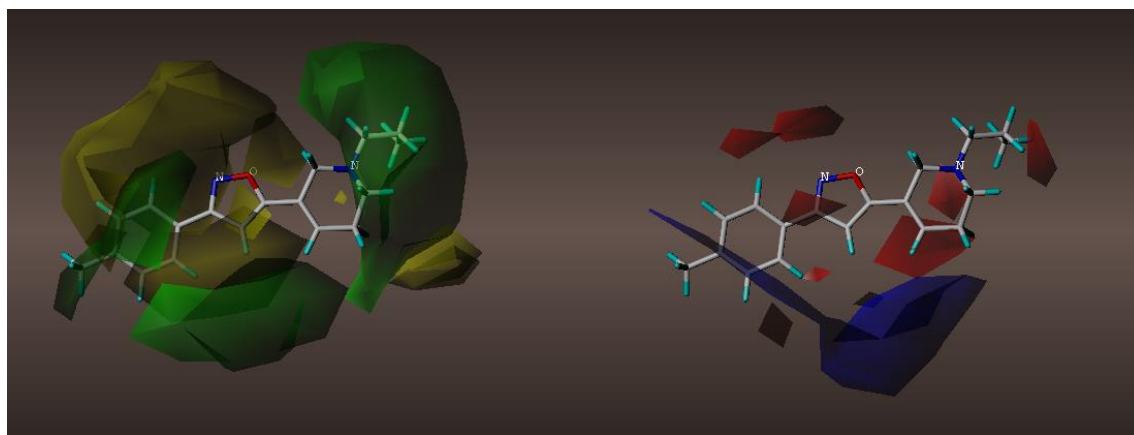
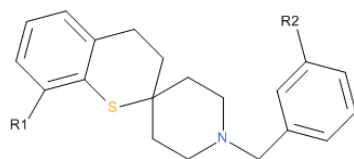


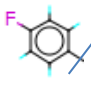
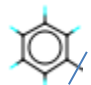
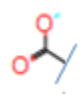
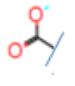
Figure 3.41 Contour map of compound 41 (PD144418) at B3LYP/6-31G*.

Additional contour maps showing the contour maps of the lead compounds can be found in the APPENDIX.

3.6 Design of New Sigma 1 Ligands

Utilizing the analysis conducted in Section 3.5.4, the design of new ligands was conducted on compound 43, Spipethiane and compound 41, PD144418. The contour maps showed that the area over the phenyl ring (left of the area with the S atom as seen in Figures 3.38 and 3.39 – considered to be R1) had more bulk desirable, however it depicts a slim profile for bulk. It also shows that the same area had negative charge desirable. Therefore, various combinations were tried to meet the profile for bulk over the phenyl ring while altering the electronegativity. Additionally, the phenyl ring on the right side in Figures 3.38 and 3.39 showed a clear bulk desirable area – considered to be R2 - and therefore, a tertiary butyl group was also tried for that area. The predicted activities are shown in Table 3.13. The highest predicted activity increase consisted of: 0.2767 to 0.9242 at HF/6-31G* and 0.1636 to 0.7971 at B3LYP/6-31G* (literature value at 0.301). Additionally, electronegative groups added in the R1 position such as COOH, F and Cl, with H as the R2, improved bioactivity. A tertiary butyl group as the R2 with H as the R1 also improved bioactivity. Note that low K_i values are desirable as they represent high bioactivity (less compound to create an effect), however when the K_i values are converted to pK_i values then high pK_i values are most desirable as they mean high bioactivity (low pK_i values represent low activity). The contour maps related to the combinations of R groups shown in Table 3.13 are in Figures 3.42 – 3.59.

Table 3.13: Spipethiane-based New Ligands

Compounds	R1	R2	Lit. pKi	HF/6-31G*	B3LYP/6-31G*
				Predicted pKi	
43	H	H	0.301	0.2767	0.1636
45		H	N/A	-0.2077	-0.1841
46		H	N/A	-0.0808	-0.2361
47	CH ₃	H	N/A	-0.0682	-0.1227
48	Cl	H	N/A	0.4989	0.303
49		H	N/A	0.7345	0.6057
50	F	H	N/A	0.6274	0.4738
51	I	H	N/A	0.2085	0.0463
52		tbutyl	N/A	0.9242	0.7971
53	H	tbutyl	N/A	0.4608	0.3224

In Figures 3.42 and 3.43 a phenyl ring with a fluorine attached (to help the electronegativity) was added as the R1 group. The R1 group overlapped into the yellow undesirable area, perhaps the reason the bioactivity did not improve for this case.

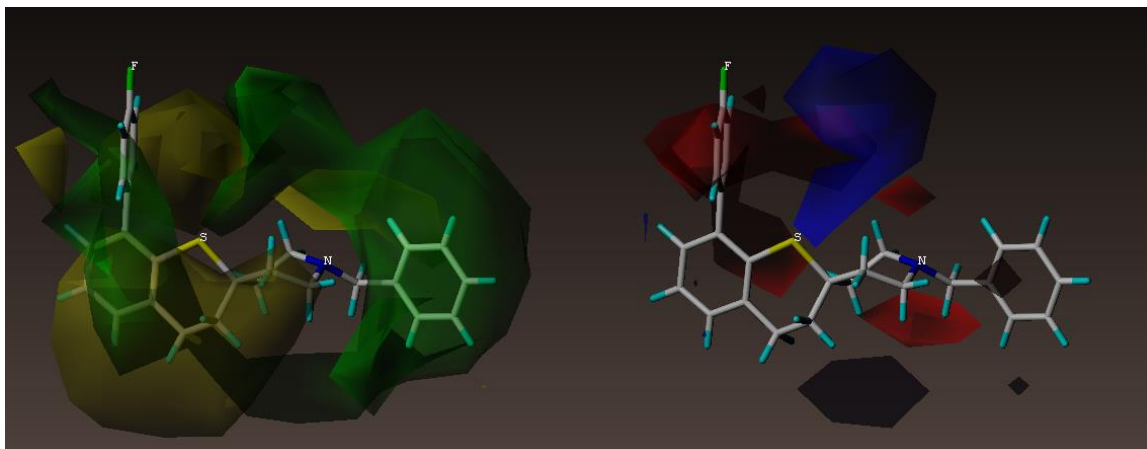


Figure 3.42 Contour map of compound 45 at HF/6-31G*.

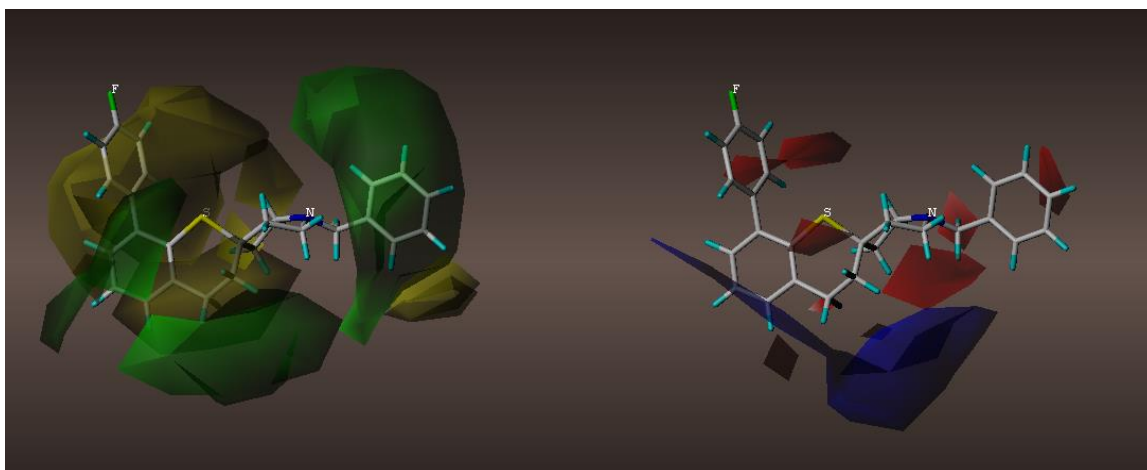


Figure 3.43 Contour map of compound 45 at B3LYP/6-31G*.

In Figures 3.44 and 3.45 a phenyl ring was added to explore adding bulk as R1 without the influence of fluorine; the activity did not improve, perhaps because the R1 group overlapped into the undesirable bulk area of the contour map.

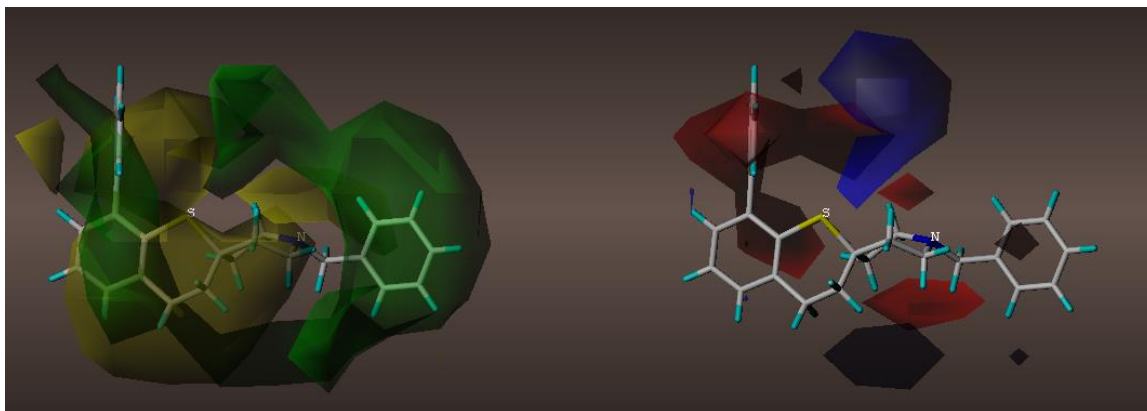


Figure 3.44 Contour map of compound 46 at HF/6-31G*.

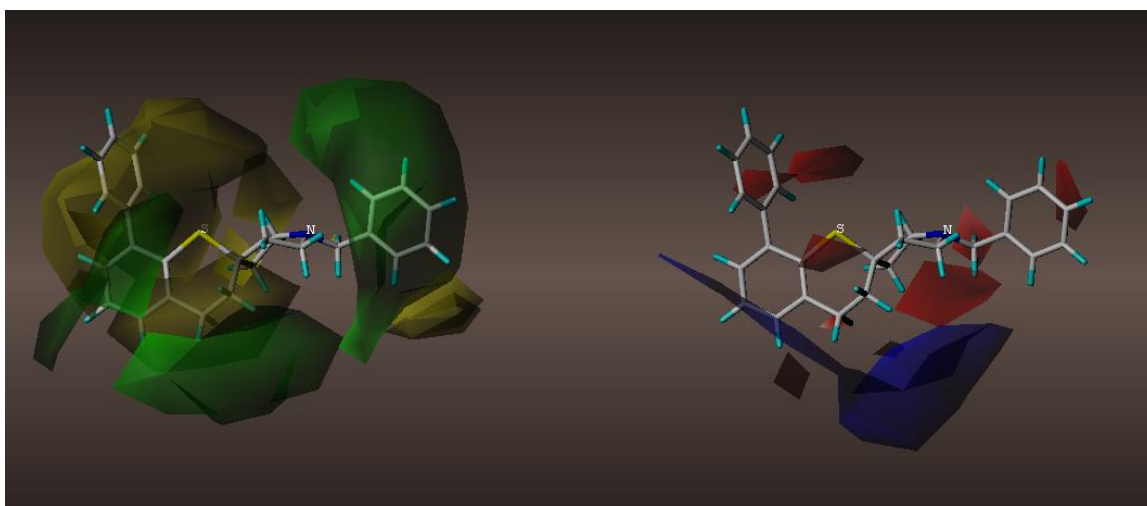


Figure 3.45 Contour map of compound 46 at B3LYP/6-31G*.

In Figures 3.46 and 3.47 a methyl group was added as R1 with the intent to better fit the desirable bulk profile; even though the methyl group did not overlap into the undesirable bulk area of the contour map in the HF/6-31G*, there was no benefit to adding it in terms of bioactivity.

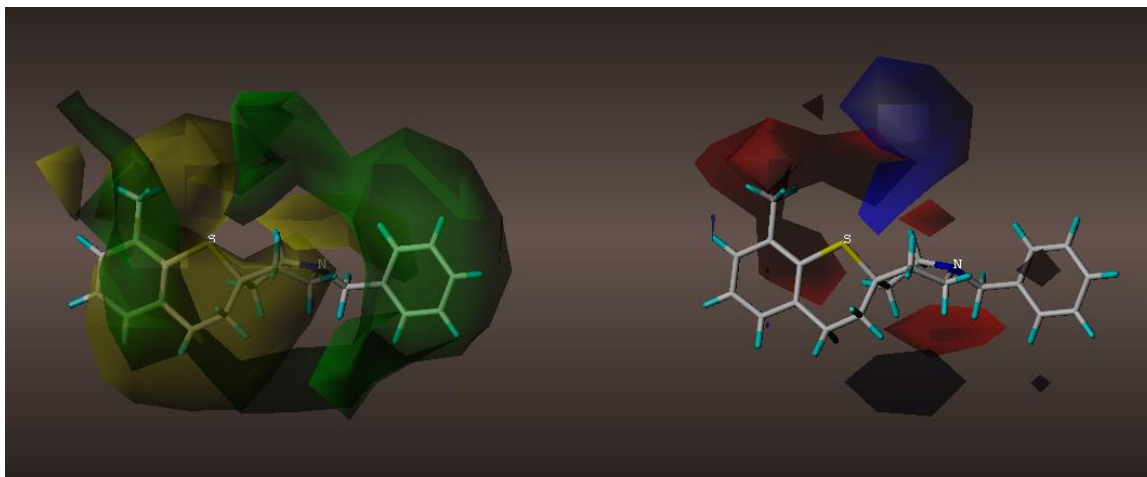


Figure 3.46 Contour map of compound 47 at HF/6-31G*.

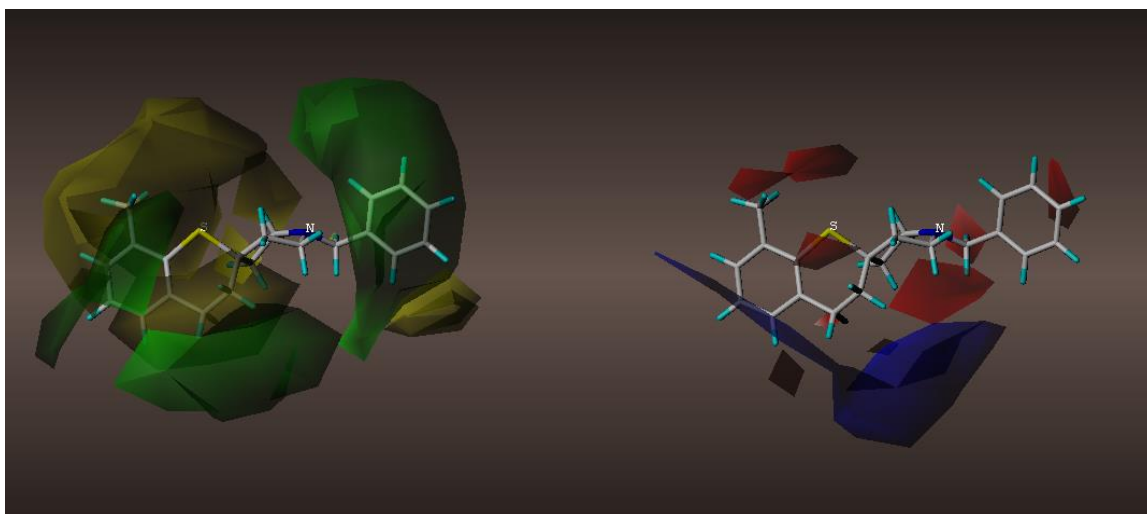


Figure 3.47 Contour map of compound 47 at B3LYP/6-31G*.

In Figures 3.48 and 3.49, chlorine was added as the R1 substituent. The overlap into the desirable negative charge area can be observed on the map and perhaps explains the improved bioactivity values of 0.4989 and 0.303 (from 0.2767 and 0.1636) at HF/6-31G* and B3LYP/6-31G*, respectively.

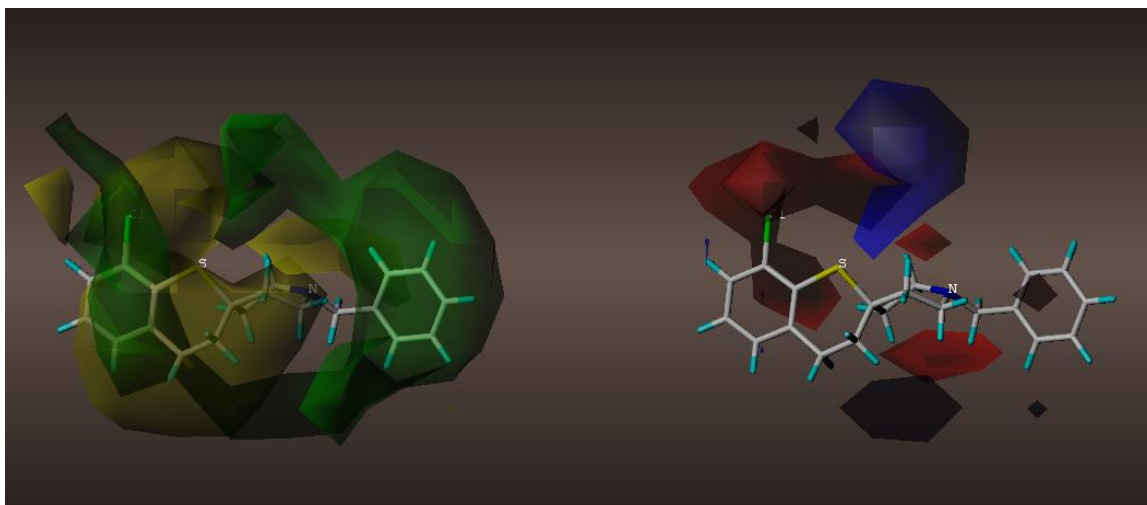


Figure 3.48 Contour map of compound 48 at HF/6-31G*.

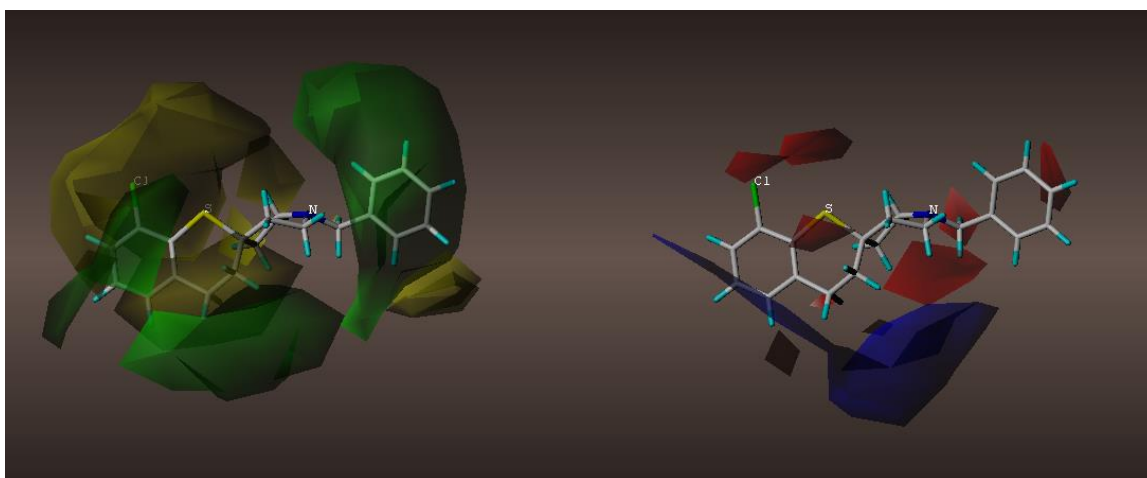


Figure 3.49 Contour map of compound 48 at B3LYP/6-31G*.

In Figures 3.50 and 3.51, COOH was added as the R1 substituent. The overlap into the desirable negative charge area can be observed on the map and perhaps explains the improved bioactivity values of 0.7345 and 0.6057 (from 0.2767 and 0.1636) at HF/6-31G* and B3LYP/6-31G*, respectively.

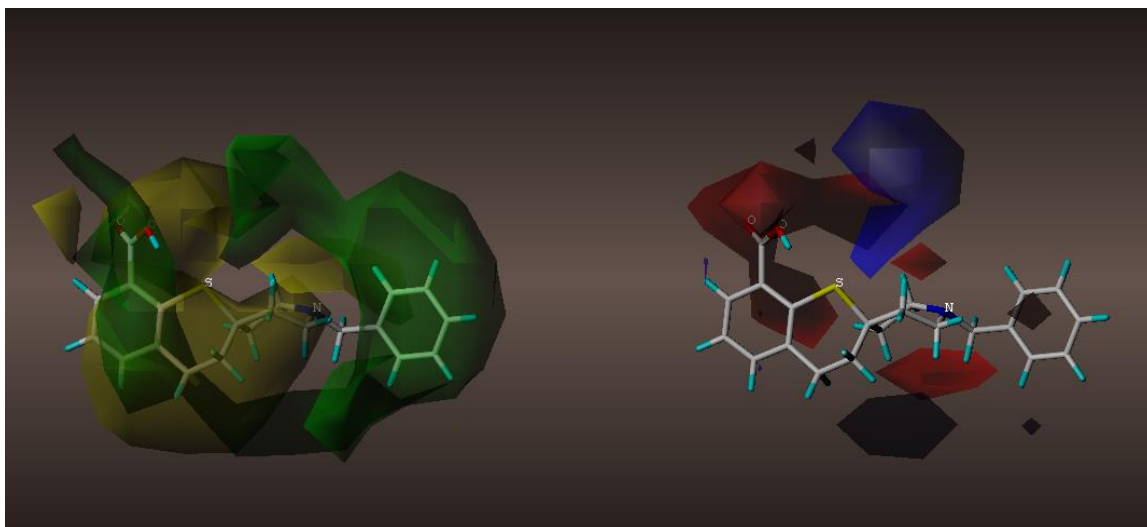


Figure 3.50 Contour map of compound 49 at HF/6-31G*.

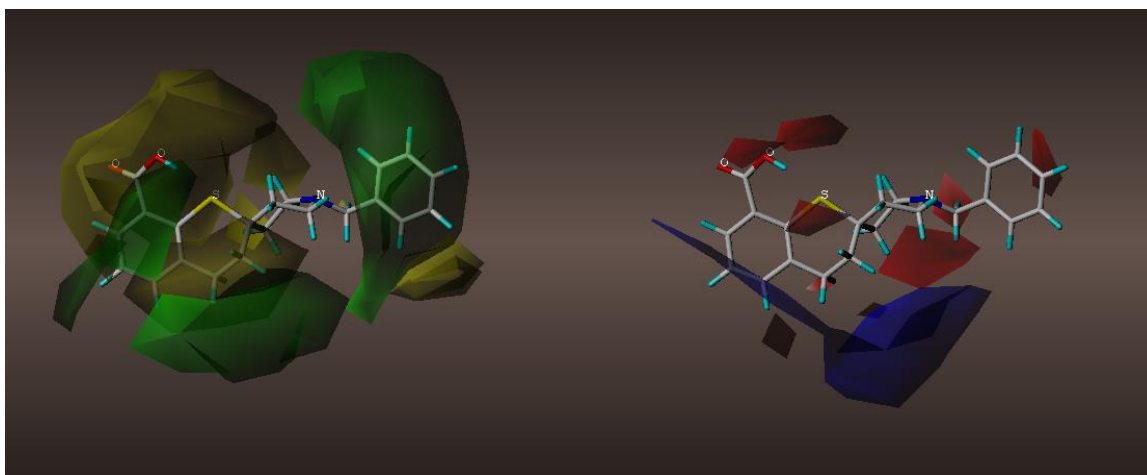


Figure 3.51 Contour map of compound 49 at B3LYP/6-31G*.

In Figures 3.52 and 3.53, F was added as the R1 substituent. The overlap into the desirable negative charge area can be observed on the map and perhaps explains the improved bioactivity values of 0.6274 and 0.4738 (from 0.2767 and 0.1636) at HF/6-31G* and B3LYP/6-31G*, respectively.

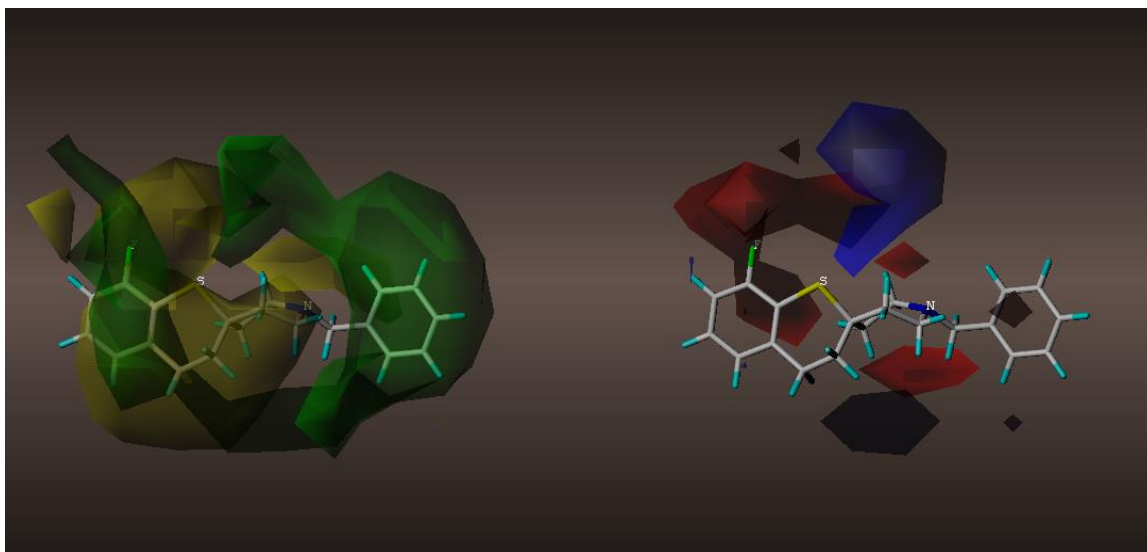


Figure 3.52 Contour map of compound 50 at HF/6-31G*.

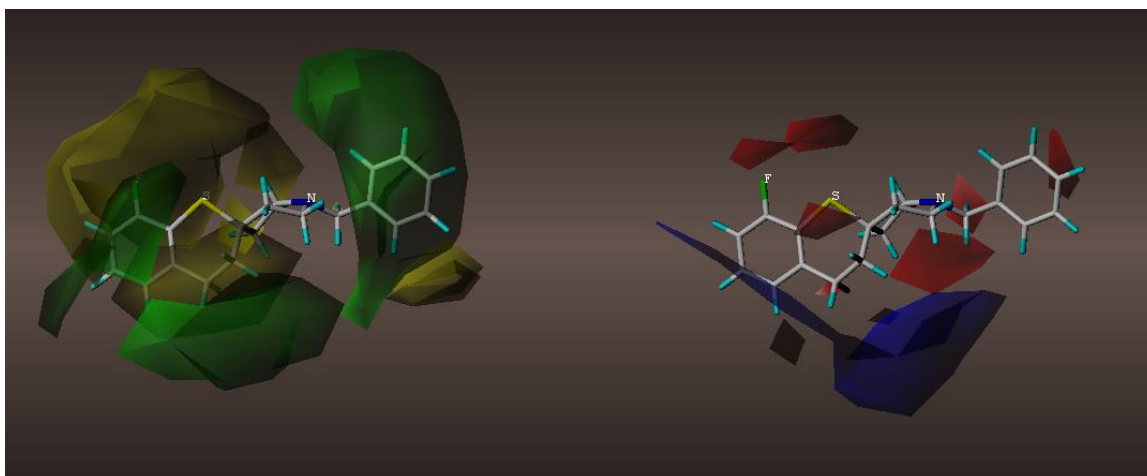


Figure 3.53 Contour map of compound 50 at B3LYP/6-31G*.

In Figures 3.54 and 3.55, I was added as the R1 substituent. The bioactivity did not improve for this case at either calculation level.

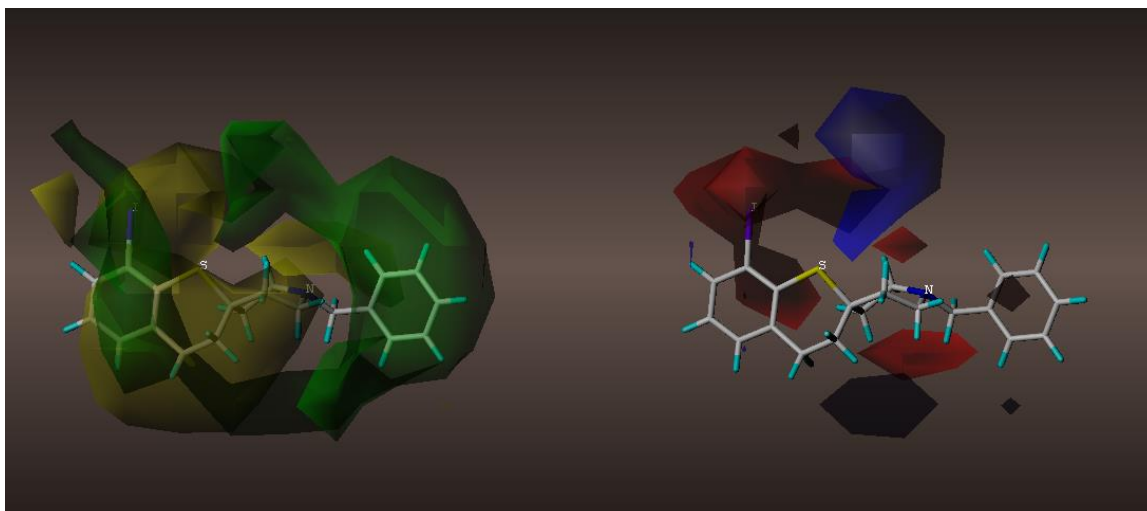


Figure 3.54 Contour map of compound 51 at HF/6-31G*.

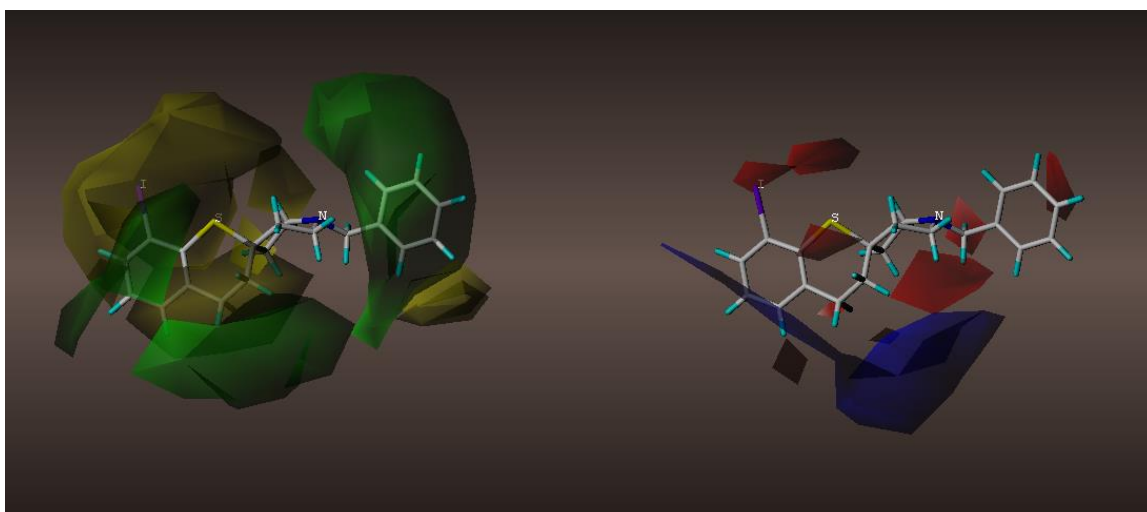


Figure 3.55 Contour map of compound 51 at B3LYP/6-31G*.

As aforementioned, there was successful minimization with increased activity by adding electronegative substituents or groups such as COOH at the R1 spot and adding a tertiary butyl (tbutyl) group to the R2 spot. In fact, for Spipethiane, this combination, shown in Figures 3.56 and 3.57, resulted in the most highly active new ligand according to both the HF/6-31G* and B3LYP/6-31G* CoMFA models at 0.9242 and 0.7971 pK_i values, respectively, essentially meaning a possible value of 0.119 nM when the 0.9242 value is

converted. This data is useful as it shows that Spipethiane, which is more rigid than the most active sigma 1 ligand identified, PD144418 could potentially have close to the same activity, where PD144418 currently measures at 0.08 nM. PD144418 as a basis for new ligands was also explored to determine if there are possibilities to increase the value of 0.08nM (1.0969 pK_i) as seen in Table 3.14.

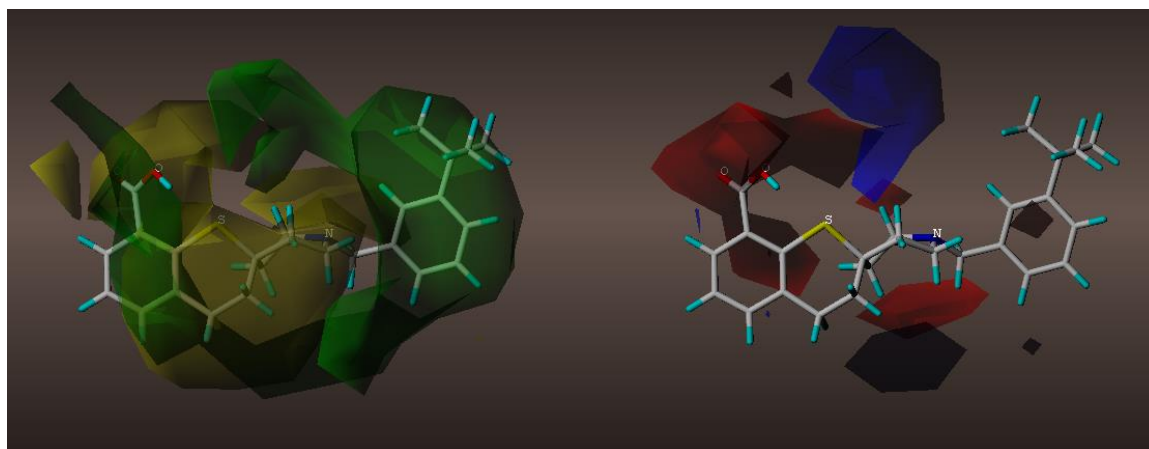


Figure 3.56 Contour map of compound 52 at HF/6-31G*.

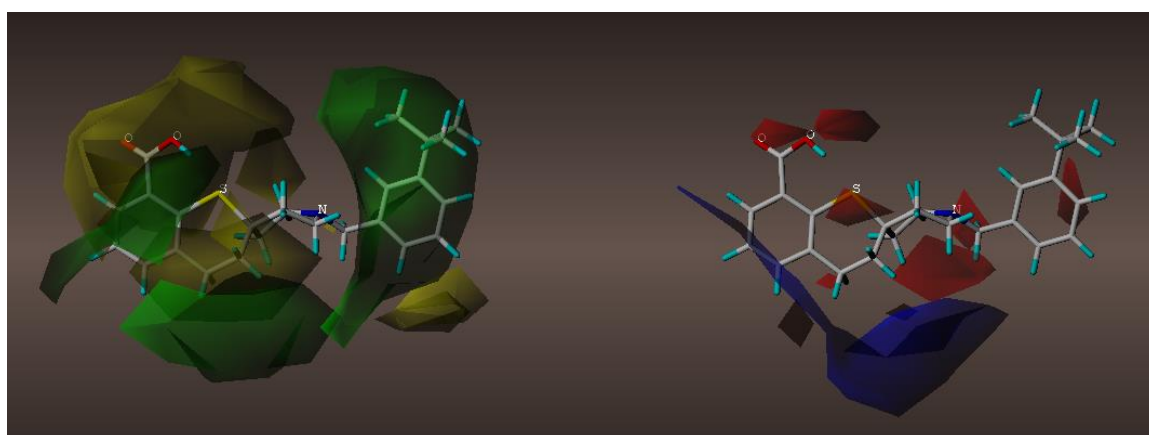


Figure 3.57 Contour map of compound 52 at B3LYP/6-31G*.

Continuing to apply tbutyl as an R2 group, but without an R1 group (using hydrogen instead), the activity is still higher than predicted for the original molecule by both

models but is not as effective as when having an R1 group such as COOH. Consequently the pKi values were 0.4608 and 0.3224 for HF/6-31G* and B3LYP/6-31G*, respectively. The corresponding contour maps for tbutyl as an R2 group only are in Figures 3.58 and 3.59.

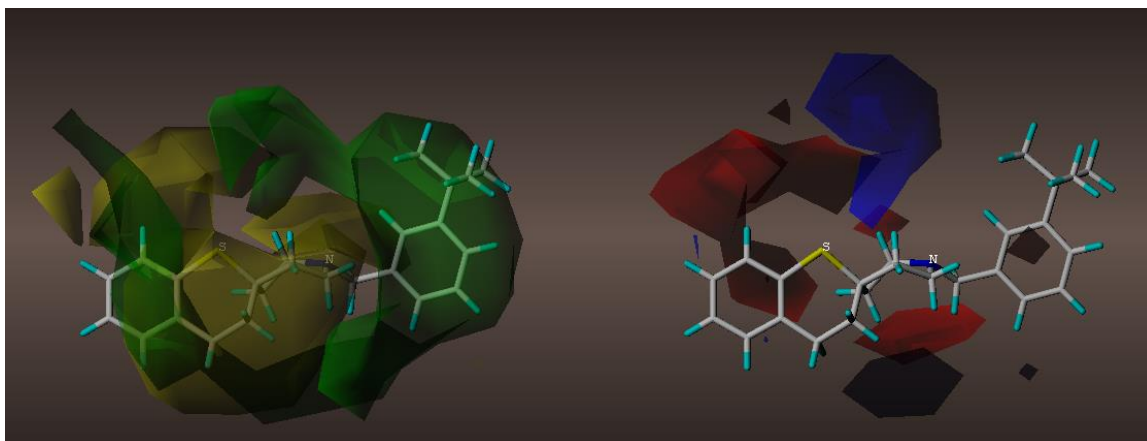


Figure 3.58 Contour map of compound 53 at HF/6-31G*.

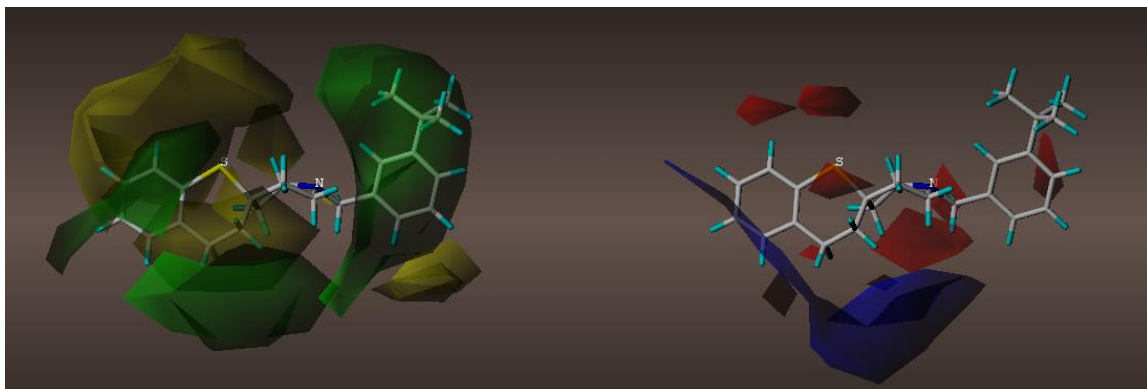
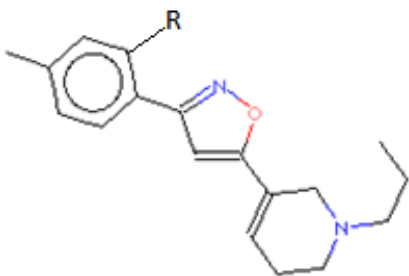


Figure 3.59 Contour map of compound 53 at B3LYP/6-31G*.

The design of new ligands around Spipethiane led to findings mentioned above; therefore, design of new ligands also occurred with PD144418, the most highly active sigma 1 ligand, to determine if there is the possibility that it could be even more active. Table 3.14 demonstrates that the addition of electronegative substituents or groups such

as F, Cl and COOH can help improve the bioactivity of PD144418 but that the addition of bulk, in either R, R1 or R2 (Table 3.14 and Table 3.15), did not help. Part of this could be due to the fact that since PD144418 is more flexible than Spipethiane; when the molecule would minimize at the calculation levels the substituents would not always appear in the expected location from the way it was designed. The highest predicted bioactivity consisted of adding COOH on the R position (similar to R1 on Spipethiane earlier) to yield a pK_i of 1.5842 vs 1.2858 (literature pK_i as 1.0969); this could potentially mean a K_i value of 0.03 nM (literature value is 0.08 nM).

Table 3.14: PD144418-based Ligands

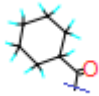
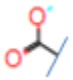
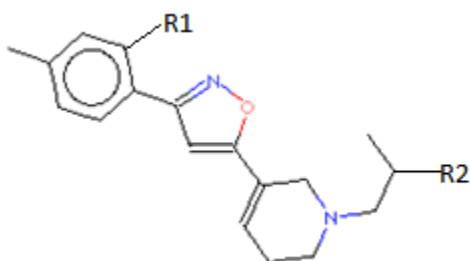
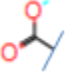
Compounds	R	Lit. pKi	HF/6-31G*	B3LYP/6-31G*
				Predicted pKi
41	H	1.0969	1.096	1.2858
54	Cl	N/A	1.0975	1.425
55		N/A	0.5144	1.1845
56	(diamantane)	N/A	0.1275	0.2823
57		N/A	1.0129	1.5842
58	F	N/A	1.4306	1.4538

Table 3.15: Additional PD144418-based Ligands (Comparison With Second R Group)



Compounds	R1	R2	HF/6-31G*	B3LYP/6-31G*
				Predicted pKi
59		tbutyl	0.6897	1.0166
60	H	tbutyl	1.0846	1.2685

Figures 3.60 and 3.61 demonstrate a situation where the molecule minimized in a way that the Cl added as the R group could not reach the red area of electronegativity desirable as well as expected, however the bioactivity did improve, minimally for HF/6-31G*. B3LYP/6-31G* had slightly better improvement yielding a bioactivity of 1.425 vs 1.2858.

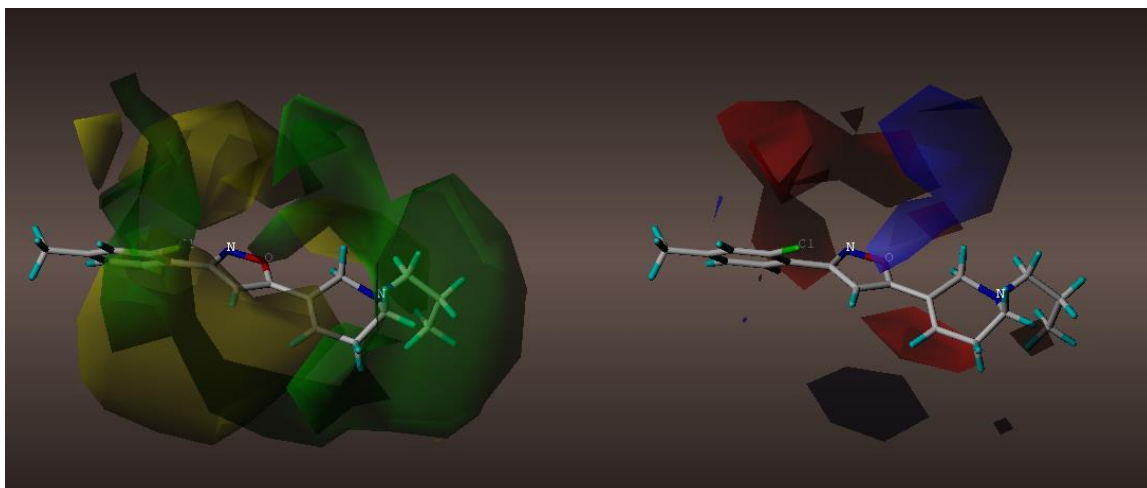


Figure 3.60 Contour map of compound 54 at HF/6-31G*.

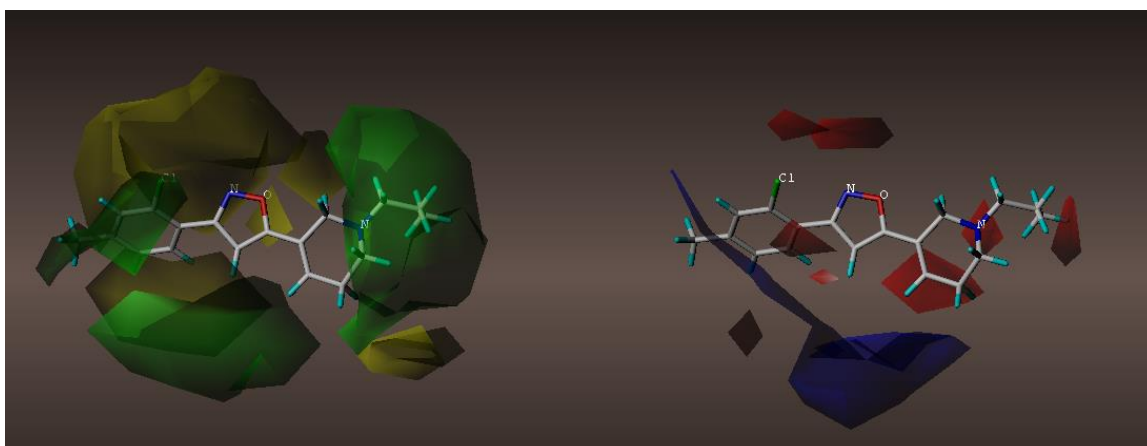


Figure 3.61 Contour map of compound 54 at B3LYP/6-31G*.

Figures 3.62 and 3.63 demonstrate a situation where the molecule minimized in a way that the cyclohexyl with CO added as the R group overlapped to the yellow undesirable area. Also the O atom did not overlap into the desirable red electronegative area. Therefore, the bioactivity did not improve for compound 55.

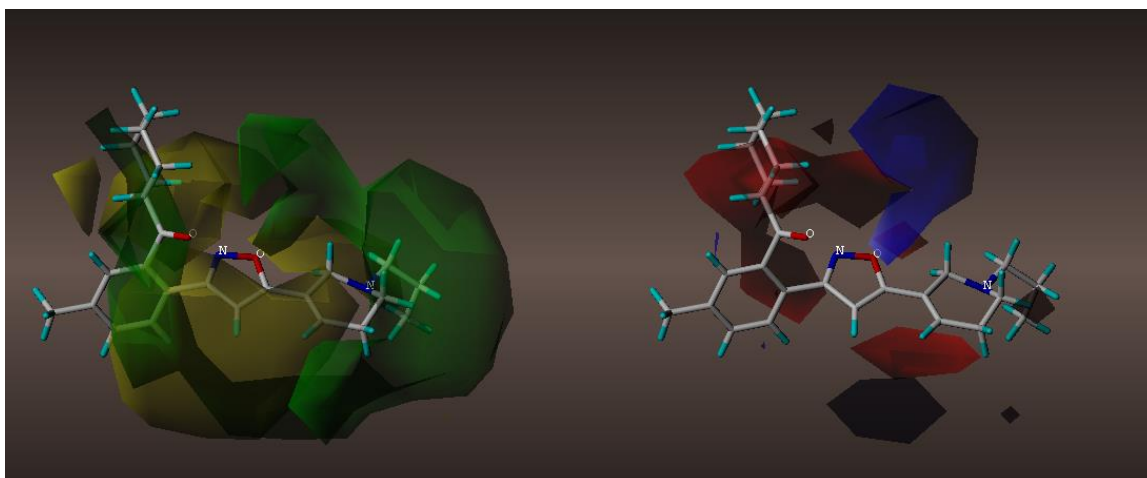


Figure 3.62 Contour map of compound 55 at HF/6-31G*.

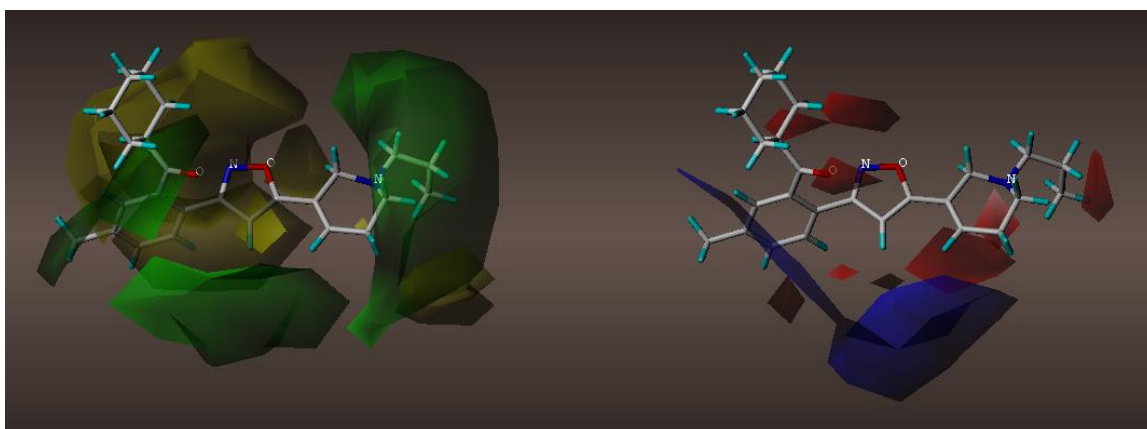


Figure 3.63 Contour map of compound 55 at B3LYP/6-31G*.

In an attempt to overlap the bulk desirable areas of the contour maps in Figures 3.64 and 3.65, diamantane was added as the R group for compound 56. The bioactivity did not improve, however, even though part of diamantane overlapped the green areas.

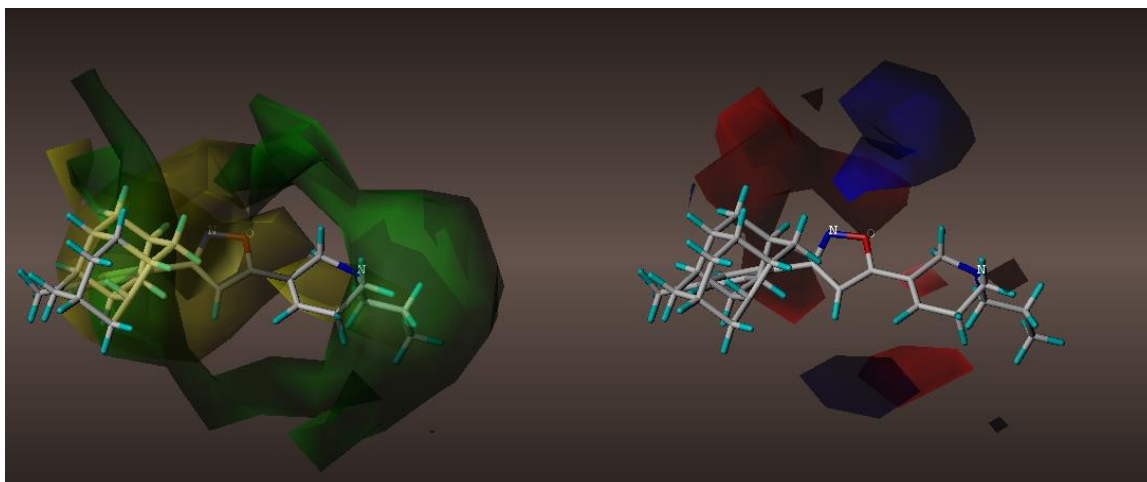


Figure 3.64 Contour map of compound 56 at HF/6-31G*.

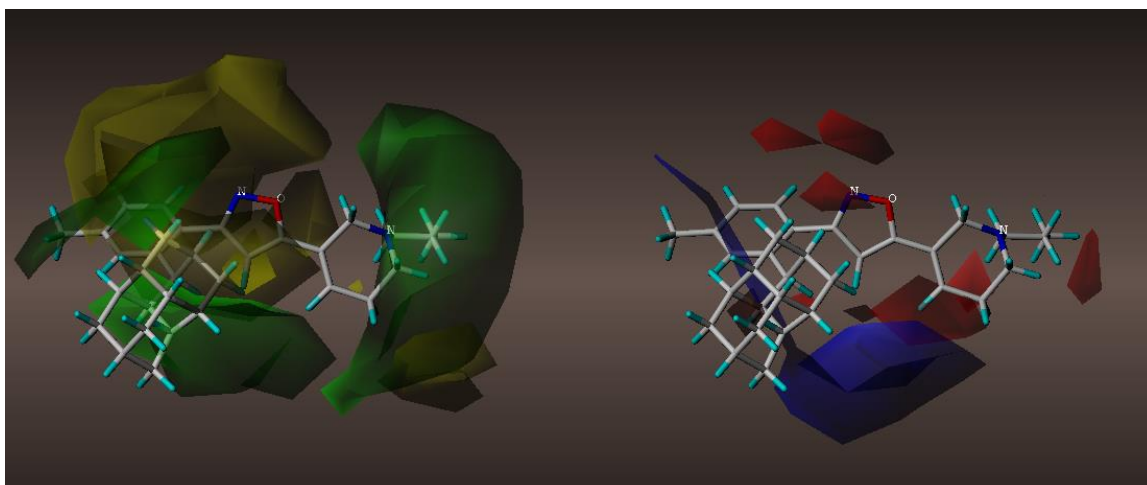


Figure 3.65 Contour map of compound 56 at B3LYP/6-31G*.

COOH was added as the R group for Figures 3.66 and 3.67 in compound 57. Though the minimization of the molecule appears to present another case where the R group could not overlap well with the red desirable electronegative areas, the bioactivity improved for the B3LYP/6-31G* CoMFA model, yielding the aforementioned 1.5842 value.

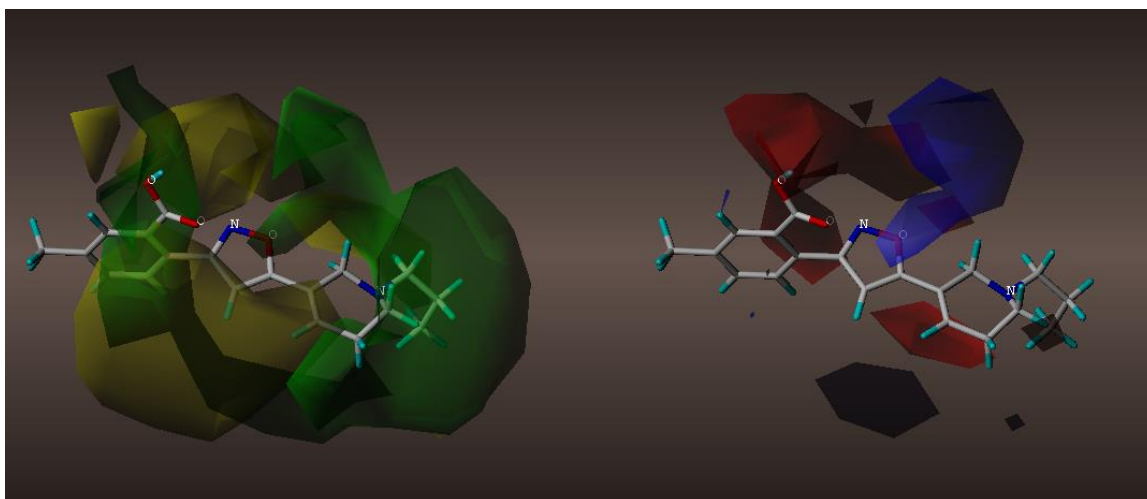


Figure 3.66 Contour map of compound 57 at HF/6-31G*.

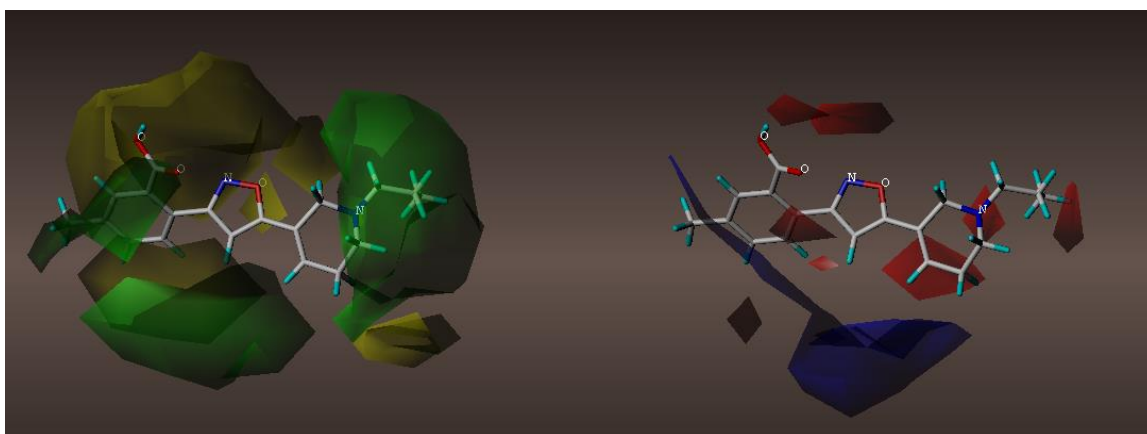


Figure 3.67 Contour map of compound 57 at B3LYP/6-31G*.

F was added as the R group for Figures 3.68 and 3.69 in compound 58. In this case the F consistently overlapped the red electronegative areas and improved the bioactivity on both HF/6-31G* and B3LYP/6-31G* levels at 1.4306 and 1.4538, respectively (vs 1.096 and 1.2858).

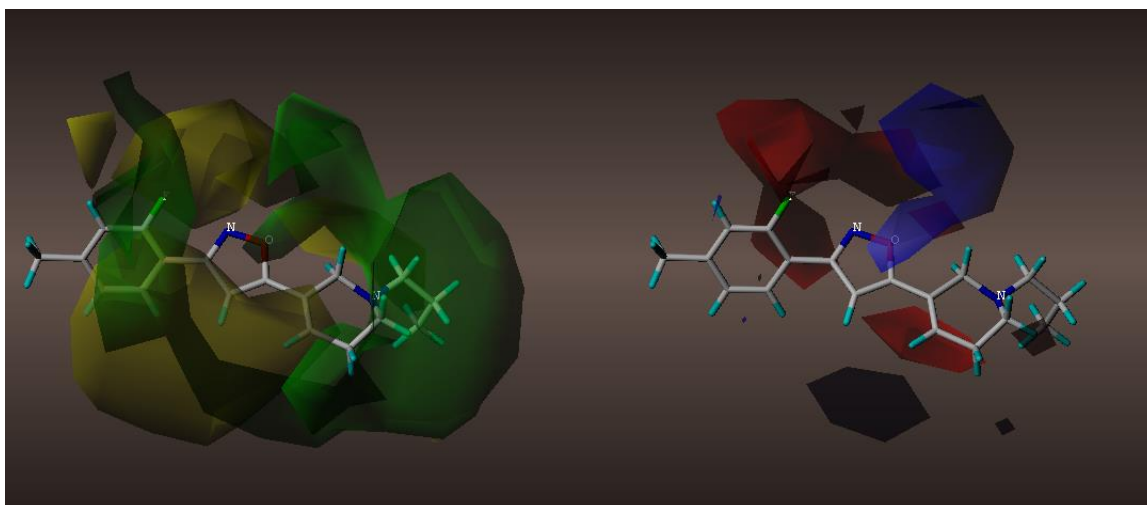


Figure 3.68 Contour map of compound 58 at HF/6-31G*.

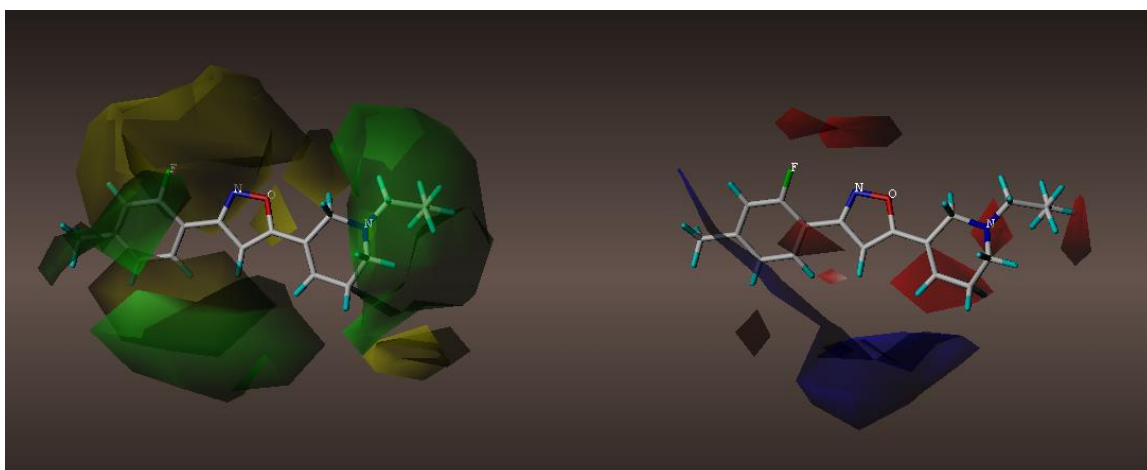


Figure 3.69 Contour map of compound 58 at B3LYP/6-31G*.

There was an additional combination considered based on the successful results from the newly designed ligands based on Spipethiane. Therefore, for Table 3.15, R2 used a tertiary butyl group and the consideration of H or COOH was used for R1. The results show that there is no improvement in bioactivity even though the tbutyl group overlaps well with the green desirable bulk area in Figures 3.70 – 3.73. Further, due to the

minimization of the molecule, the added COOH did not overlap with the red electronegative desirable area.

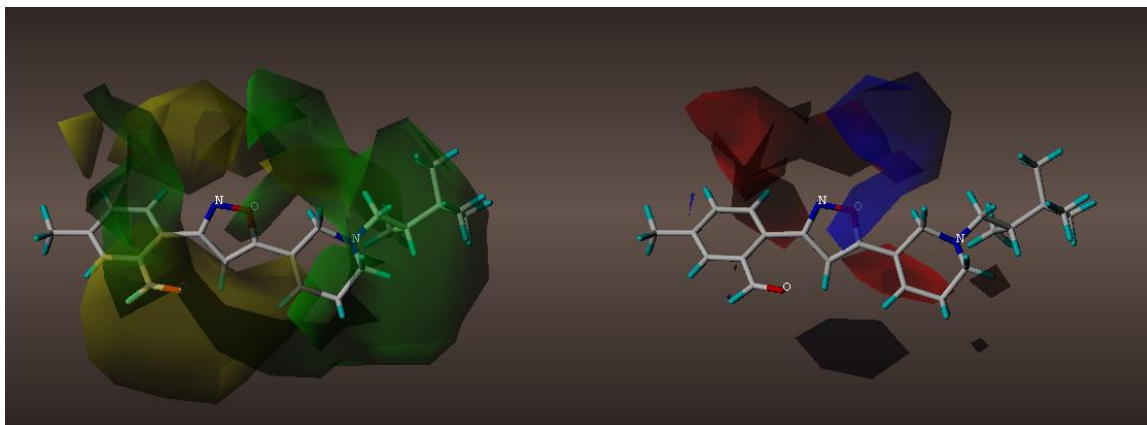


Figure 3.70 Contour map of compound 59 at HF/6-31G*.

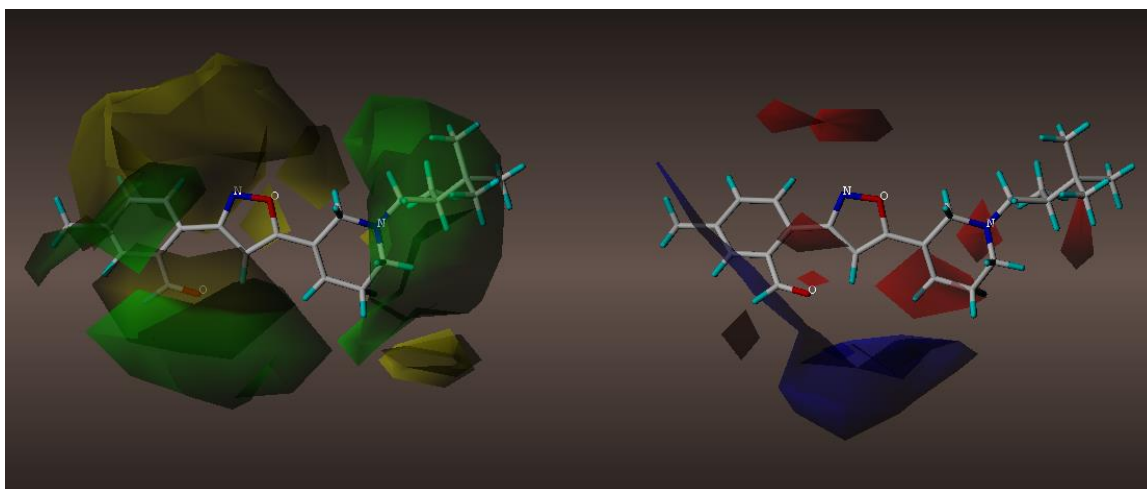


Figure 3.71 Contour map of compound 59 at B3LYP/6-31G*.

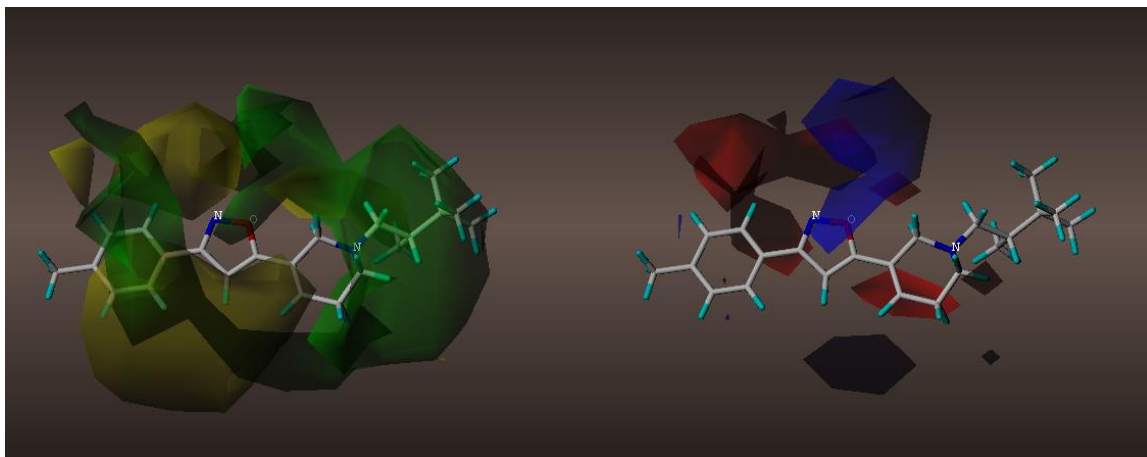


Figure 3.72 Contour map of compound 60 at HF/6-31G*.

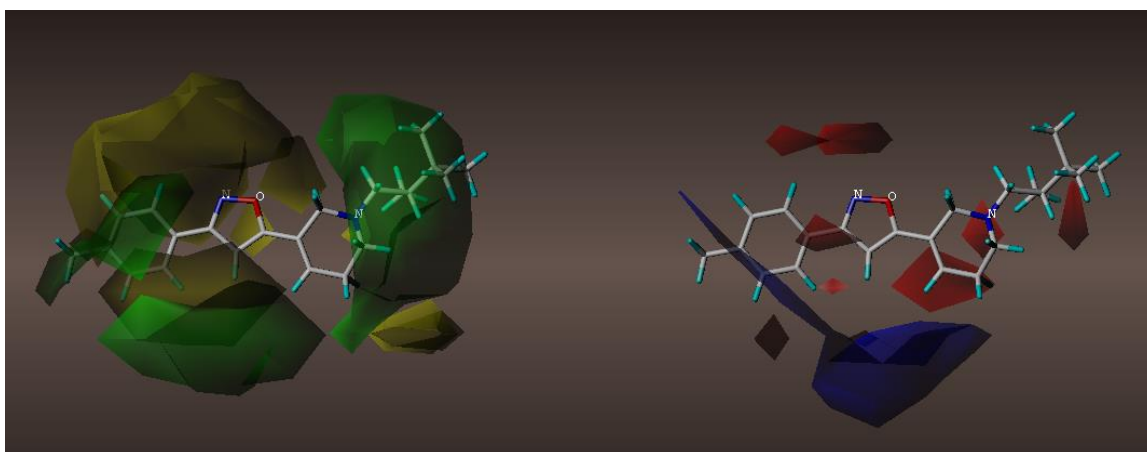


Figure 3.73 Contour map of compound 60 at B3LYP/6-31G*.

Note that there were attempts to add diamantane as an R1 group to explore adding bulk further to compound 43, spipethiane (as it was done for PD144418), however the resulting molecules did not minimize successfully and were therefore aborted. Similarly, adding a cyclohexane ring attached to a C=O group at the R1 location also did not minimize successfully for Spipethiane; this particular combination was aimed at exploring bulk combined with electronegativity.

Therefore, for both compound 41, PD144418, and compound 43, Spipethiane, the

best cases of completed optimizations at both calculation levels with increases in activity were due to the addition of electronegative substituents or groups such as fluorine, chlorine and COOH. It was also observed that adding the tbutyl group in the R2 position, while having an electronegative group such as COOH at R1, for Spipethiane increased the activity. Certainly these are promising results, leading to the possibility that the newly predicted highly active ligands could be synthesized and potentially used in the future as drug candidates.

CHAPTER 4

MOLECULAR MODELING OF SIGMA 2 RECEPTOR LIGANDS

4.1 Introduction

It is generally acknowledged that there is less knowledge about the sigma 2 receptor as opposed to the sigma 1 receptor due to the lack of high-affinity, selective ligands (Berardi et al., 2004). The sigma 2 receptor has not been cloned as the sigma 1 receptor has (Abate et al., 2011). Lack of knowledge surrounding sigma 2 receptors, however, does not bear any relationship to the importance of the sigma 2 receptors. In fact, sigma 2 receptor ligands have been studied for treatment of pancreatic cancer because they are preferentially internalized by proliferating cells and induce apoptosis; multiple sigma 2 receptor ligands, even up to 10 nM affinity, are shown to decrease tumor burden in preclinical models of human pancreatic cancer (Hornick et al., 2012). Interest in sigma 2 receptors has been increasing especially since sigma 2 receptors are overexpressed in a wide variety of human tumor cell lines, representing biomarkers for the diagnosis of tumors with non-invasive techniques such as Positron Emission Tomography (PET) or Single Photon Emission Computed Tomography (SPECT) (Abate et al., 2011). Therefore, finding high-affinity, selective sigma 2 ligands is on the rise, however known sigma 2 receptor ligands generally exhibit a poor selectivity profile, particularly over the sigma 1 receptor (Berardi et al., 2003). Many of the researchers in the literature have synthesized and studied sigma 2 receptor ligands; comparatively, the affinity values to the sigma 1 receptor ligands are much higher. There is a focus on increased selectivity, however. Even if the affinity values do not appear as strong as what is displayed for

sigma 1 ligands, there seems to be increased emphasis on the concept of selectivity to ensure there is not competition from sigma 1 ligands in the radioligand studies (Berardi et al., 2004; Fan et al., 2011; Hajilour et al., 2011;).

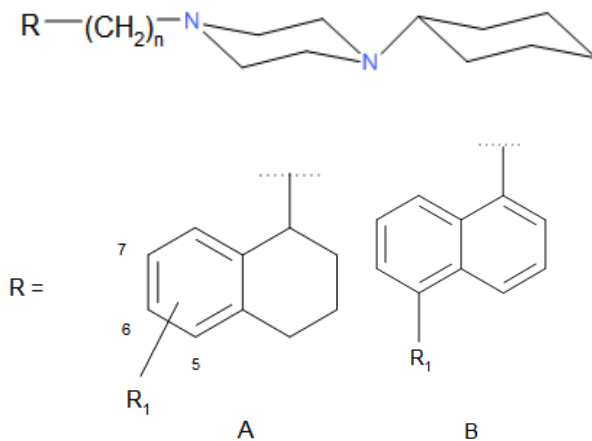
Though the Gund group has done some pharmacophore and CoMFA studies on sigma 2 receptor ligands through theses, published models in scholarly journals do not exist as they do for the sigma 1 receptor ligands at this time. Some comparison to the theses' models exist in Section 4.4.1 as well as to a representative external model.

4.2 Selection of Ligands

Overall sigma 2 receptor ligands in the present study were selected based on compounds that were shown to be active for sigma 2 while also being selective for sigma 2. Naturally all of the studies used radioligand competitive binding assays with [³H]-DTG along with (+)-pentazocine to block sigma binding sites (Berardi et al., 2004; Fan et al., 2011; Hajilour et al., 2011;).

Compounds 1-18 for sigma 2 receptor ligands were selected especially due to the fact that PB28, a sigma 2 receptor ligand with very high affinity (0.34 nM, compound 5), is a member of this class; therefore it is quite fitting to study derivatives of 1-Cyclohexylpiperazine to determine if those compounds will yield similar binding affinities or selectivities (Berardi et al., 2004). Additionally, Wirpsza and Patel had used several of these molecules in their modeling studies as part of the earlier work on sigma 2 receptor ligands with the Gund group (Wirpsza, 2008; Patel, 2010) The series studied in the current work are displayed in Table 4.1.

Table 4.1 Binding and Functional Data of 4-(Tetralin-1-yl) and 4-(Naphthalen-1-yl)alkyl Derivatives of 1-Cyclohexylpiperazine



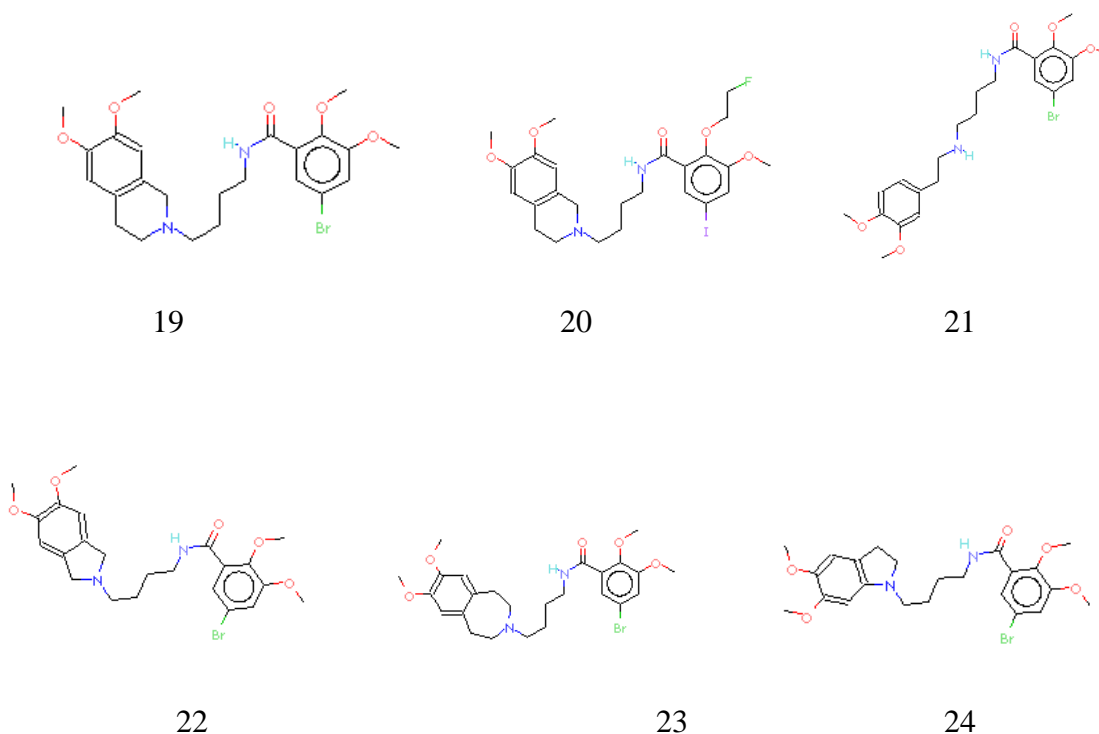
Compound	R	R ₁	n	$\sigma_1 K_i$ (nM)	$\sigma_2 K_i$ (nM)	σ_1 / σ_2	σ_2 / σ_1
1	A	5-OCH ₃	0	0.40 ± 0.02	7.90 ± 1.60		20
2	A	5-OCH ₃	1	0.31 ± 0.10	16.4 ± 4.2		53
3	A	5-OCH ₃	2	1.57 ± 0.41	21.1 ± 3.4		13
4	A	H	3	0.61 ± 0.08	0.68 ± 0.03		1.1
5*	A	5-OCH ₃	3	13.6 ± 1.9	0.34 ± 0.02	40	
6	A	6-OCH ₃	3	0.36 ± 0.12	5.42 ± 0.64		15
7	A	7-OCH ₃	3	9.04 ± 1.02	1.22 ± 0.17	7.4	
8	A	H	4	0.036 ± 0.015	14.6 ± 3.7		406
9	A	5-OCH ₃	4	1.54 ± 0.36	3.58 ± 0.55		2.3
10	A	H	5	1.45 ± 0.35	7.85 ± 0.49		5.4
11	A	5-OCH ₃	5	1.52 ± 0.63	0.35 ± 0.09	4.3	
12	A	5-OCH ₃	6	3.07 ± 0.70	103 ± 23		34
13	A	5-OH	3	5.40 ± 0.40	2.66 ± 0.66	2	
14	A	6-OH	3	0.69 ± 0.05	1.12 ± 0.17		1.6
15	B	H	3	2.16 ± 0.63	0.69 ± 0.08	3.1	
16	B	OCH ₃	3	1.57 ± 0.15	9.24 ± 1.37		5.9
17	B	H	4	0.22 ± 0.03	30.5 ± 8.7		139
18	B	H	5	2.40 ± 0.47	0.57 ± 0.08	4.2	

*Indicates included in the comprehensive sigma 2 pharmacophore derivation.

Source: Berardi et al., 2004.

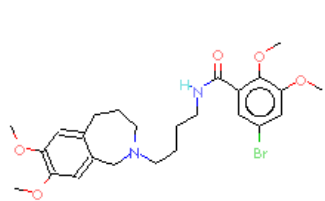
5-Bromo-N-[4-(6,7-dimethoxy-3,4-dihydro-1H-isoquinolin-2-yl)-butyl]-2,3-dimethoxy-benzamide (compound 19) is one of the most potent and selective sigma 2 receptor ligands reported with 8.2 nM affinity accompanied by 1573-fold selectivity over sigma 1 sites (Fan et al., 2011). Therefore, it is important to conduct molecular modeling on this molecule, compound 19, along with a series of new analogs where the amine ring fused to the aromatic ring was varied in size (Fan et al., 2011). These molecules, compounds 19 – 28, are located in Table 4.2.

Table 4.2 Binding and Functional Data of Substituted Aminobutyl-benzamides

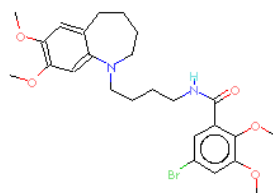


Source: Fan et al., 2011.

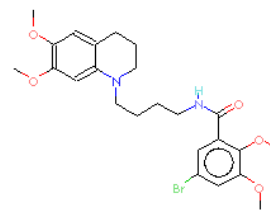
Table 4.2 (continued) Binding and Functional Data of Substituted Aminobutylbenzamides



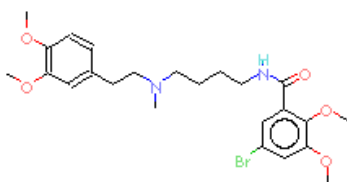
25



26



27



28

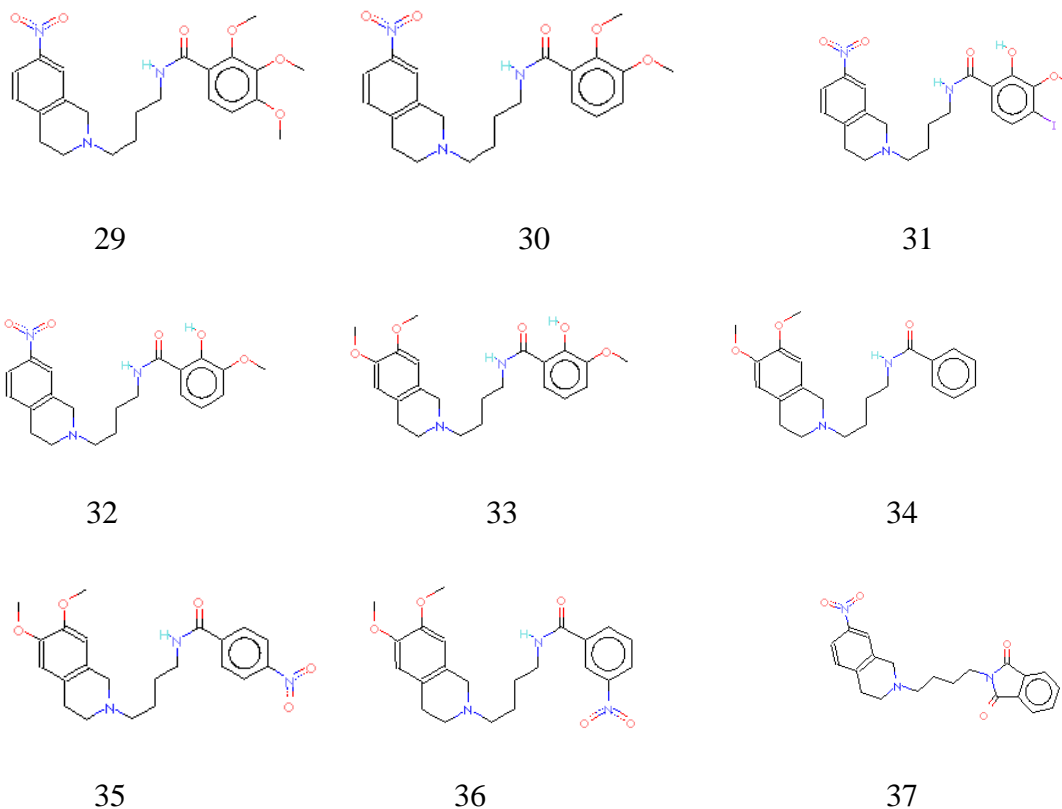
Compound	$\sigma_1 K_i$ (nM)	$\sigma_2 K_i$ (nM)	σ_1 / σ_2
19*	12,900	8.2	1573
20	881 ± 15	2.7 ± 0.1	326
21	880 ± 60	4616 ± 247	0.2
22	1442 ± 88	0.82 ± 0.06	1758
23	5073 ± 82	734 ± 50	8.5
24	4521 ± 45	9681 ± 522	0.47
25	2068 ± 60	315 ± 15	6.58
26	2564 ± 175	8957 ± 335	0.29
27	4499 ± 182	5823 ± 224	0.77
28	583 ± 28	2126 ± 240	0.27

*Indicates included in the comprehensive sigma 2 pharmacophore derivation.

Source: Fan et al., 2011.

Compounds 29-37 represent molecules where the contribution of electron-donating and electron-withdrawing groups were explored through synthesis and characterization of new compounds featuring a benzamide moiety and an isoquinoline moiety linked by an alkyl chain (Hajipour et al., 2011). Hajipour and coworkers focused on the concept of improving selectivity for the sigma 2 receptor (2011). These molecules are in Table 4.3.

Table 4.3 Binding and Functional Data of Benzamide-isoquinoline Derivatives



Source: Hajipour et al., 2011.

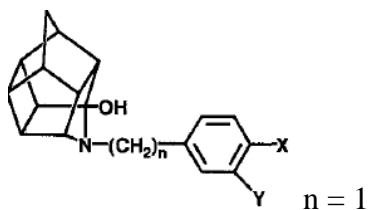
Table 4.3 (continued) Binding and Functional Data of Benzamide-isoquinoline Derivatives

Compound	$\sigma_2 K_i$ (nM)	$\sigma_1 K_i$ (nM)	σ_1 / σ_2
29	26.78 ± 2.92	10,320 ± 363	385
30	12,930 ± 55.77	7,870 ± 264	0.61
31	866.70 ± 138.6	74,680 ± 305	86.17
32	4,000 ± 177.9	11,200 ± 469	2.80
33	1,400 ± 286	67,800 ± 4.155	48.40
34	5,290 ± 408	>10 ⁷	
35	152,000 ± 4,106	14,690 ± 1,121	0.096
36	>10 ⁷	1.21 × 10 ⁶	0.29
37*	21.26 ± 2.41	87.5 ± 3.07	4.12

*Indicates included in the comprehensive sigma 2 pharmacophore derivation.

Source: Hajipour et al., 2011.

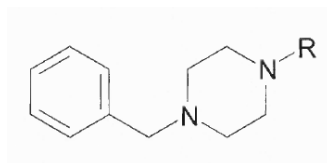
Some of the work in the 1990s included comparison of binding parameters for sigma 1 and sigma 2 in rat and guinea pig brain membranes using a trishomocubane series by Nguyen and colleagues (Nguyen et al., 1996). Some molecules from this series were included in this work so that an additional sigma 2 class could be included, especially since the series was studied by Jung during the earlier work on sigma 2 for the Gund group (Jung, 2004). Also, reference compound 57 discussed later in this section is a trishomocubane derivative compound which is another reason why it is fitting to include several other molecules from the series. Table 4.4 summarizes the subset of trishomocubanes used in the current study for pharmacophore and CoMFA model development.

Table 4.4: Trishomocubane Subset of Compounds

Compound	X	Y	$\sigma_2 K_i$ (nM)	$\sigma_1 K_i$ (nM)	σ_1 / σ_2
38	OCH ₃	H	136 ± 19	103 ± 1	0.76
39	H	Cl	30 ± 1	186 ± 8	6.2
40	H	Br	40 ± 22	208 ± 13	5.20
41	H	I	54 ± 18	169 ± 10	3.13
42	H	CH ₃	108 ± 6	97 ± 6	0.90

Source: Nguyen et al., 1996.

In previous work by the Gund group, a large series of 1-alkyl-4-benzylpiperazine derivatives was studied by both Wirpsza and Patel based on Costantino and coworkers' research (Costantino, 2004; Wirpsza, 2008; Patel, 2010). A subset of seven molecules, presented in Table 4.5, were chosen to include from the previous Gund work in order to build on the foundation of the sigma 2 studies, expanding the sigma 2 class type for the pharmacophore representative model as well as the CoMFA models for this work.

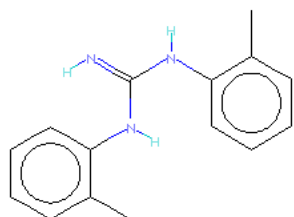
Table 4.5 : 1-aralkyl-4-benzylpiperazine Derivatives Subset

Compound	R	$\sigma_2 K_i$ (nM)	$\sigma_1 K_i$ (nM)	σ_1 / σ_2
43		1.70	0.80	0.47
44		1.48	0.30	0.20
45*		1.59	0.30	0.19
46		3.02	0.30	0.10
47		25.6	15.4	0.60
48		4.75	1.20	0.25
49		5.35	2.66	0.50

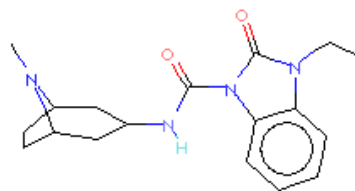
Sources: Costantino et al., 2005 and Patel, 2010.

Several reference molecules were included in the pharmacophore derivation for the sigma 1 representative pharmacophore and CoMFA studies as explained in Chapter 3. Similarly, three rigid references were added to the dataset for the sigma 2 ligand models. The references previously used by the Gund group for sigma 2, also used in the current study, are shown in Table 4.6. Also note that Haloperidol, compound 53, was included as an additional flexible molecule as a means to later (in Chapter 5) compare the differences between sigma 1 and sigma 2 since it is active for both; it was included in the sigma 1 set in Chapter 3. Therefore, Haloperidol was used in the test set for both sigma 1 and sigma 2 and was not used as a molecule in the construction of the CoMFA model. This is a key point because the activity data varied for this molecule in various studies by researchers. The data included in Table 4.6 for Haloperidol is not from Gund (2003) as in the sigma 1 analysis for Chapter 3; instead more recent data was used for sigma 2 ligand studies by Fan et al., especially because the aminobutyl-benzamide series, studied in this work and included in the models, came from the same study (2011). The activity data served as a means to compare the test set data primarily for each CoMFA model.

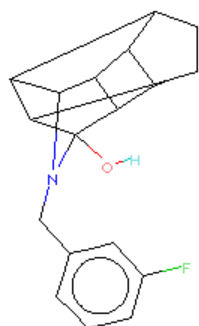
Table 4.6: Binding and Functional Data of Reference and Other Compounds



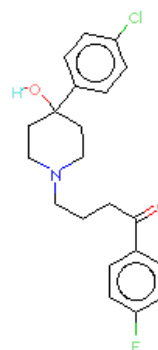
50 1,3-di (2-tolyl) guanidine (DTG)



51 BIMU-1



52 ANSTO-19 (Trishomocubane Derivative)



53 Haloperidol

Compound	$\sigma_2 K_i$ (nM)	$\sigma_1 K_i$ (nM)	σ_1 / σ_2
50*	13.4 ± 2.0	7436 ± 308	554.93 (Berardi et al., 2004)
51*	32 ± 15.2	6300	- (Bonhaus et al., 1993)
52*	20 ± 4	152 ± 1	7.60 (Nguyen et al., 1996)
53	9.58 ± 0.98	0.83 ± 0.03	11.5 (Fan et al., 2011)

*Indicates included in the comprehensive sigma 2 pharmacophore derivation.

Sources: Wirpsza, 2010 (original data sources listed above as specified by Wirpsza for compounds 55-57).

4.3 Materials and Methods

All molecules were initially drawn in Spartan '14 and then optimized at the HF/6-31G* and B3LYP/6-31G* levels prior to being imported into the SYBYL-X 2.1 program. Molecular databases were created within SYBYL-X 2.1 to represent each class of compounds for the sigma 2 receptor ligands. DISCOtech, a tool within SYBYL-X 2.1, was then used to generate pharmacophores for each of the classes. Pharmacophore development for each set of selected molecules was conducted by utilizing the options within DISCOtech for feature selection (binding site), conformer searches, etc. to yield potential pharmacophore models. Following the development of pharmacophore models for each class, a database was created to include the most active/lead compounds with some rigid references and active references from the previous work by Gund and colleagues. This database was then utilized to develop a comprehensive pharmacophore to represent all of the sigma 2 ligand classes studied in this work. Once pharmacophore models were completed, the Comparative Molecular Field Analysis models were created for the sigma 2 molecules calculated at HF/6-31G* and B3LYP/6-31G* levels, respectively. Note that that the approach described in Chapter 3 for the sigma 1 ligands utilized in the CoMFA models was slightly different for sigma 2 ligands since the bioactivities varied so much; therefore the most active compounds from each of the classes were selected to yield a training set range between 3 and 4 log units (similar to the range for sigma 1 ligands in Chapter 3) since some of the activities for the molecules for sigma 2 were extremely poor. New ligands were designed once the CoMFA models were determined to meet robust criteria; contour maps generated from the CoMFA models were studied during the new ligand design process. Additional information about the

pharmacophore derivation, CoMFA and design of new ligands are in Sections 4.4, 4.5, and 4.6, respectively.

4.4 Pharmacophore Derivation

DISCOtech allows the researcher to manually select the binding features of each molecule to be considered for pharmacophore generation. For these classes, hydrophobic groups, positive nitrogen and lone pair were used. This was done via an iterative process. First, models were explored without constraints or features selected, and gradually various combinations of binding groups were included. Specifics regarding each class and the derivations are discussed in Section 4.4.1.

4.4.1 Pharmacophore Models

Pharmacophores were generated using DISCOtech in SYBYL-X 2.1 for each class of compounds and are shown as labelled in Figures 4.1 through 4.15. Similar to sigma 1, the main binding sites are the nitrogen site, the lone pair of electrons and a hydrophobic group, however an additional hydrophobic group was also used as a binding site on the opposite side of the N atom, producing a modified “pyramid” type pharmacophore with the exception of one class; the substituted benzamide-isoquinolines had a “triangle” type pharmacophore, however with different distances than observed in the sigma 1 work. The comprehensive pharmacophore to represent all of the sigma 2 classes studied in this work are in Figures 3.16 through 4.18. The distances for the 4-point pharmacophore are noted in the figures with more discussion around the comprehensive pharmacophore.

Figures 4.1 – 4.3 depict the pharmacophore development for the 18 molecules of the 1-cyclohexylpiperazine series. The length of the molecules in this series varied

greatly and therefore the hydrophobic point for the phenyl groups, on the side with the additional CH₂ groups in-between, is seen among the chains/phenyl rings on the side of the phenyl rings.

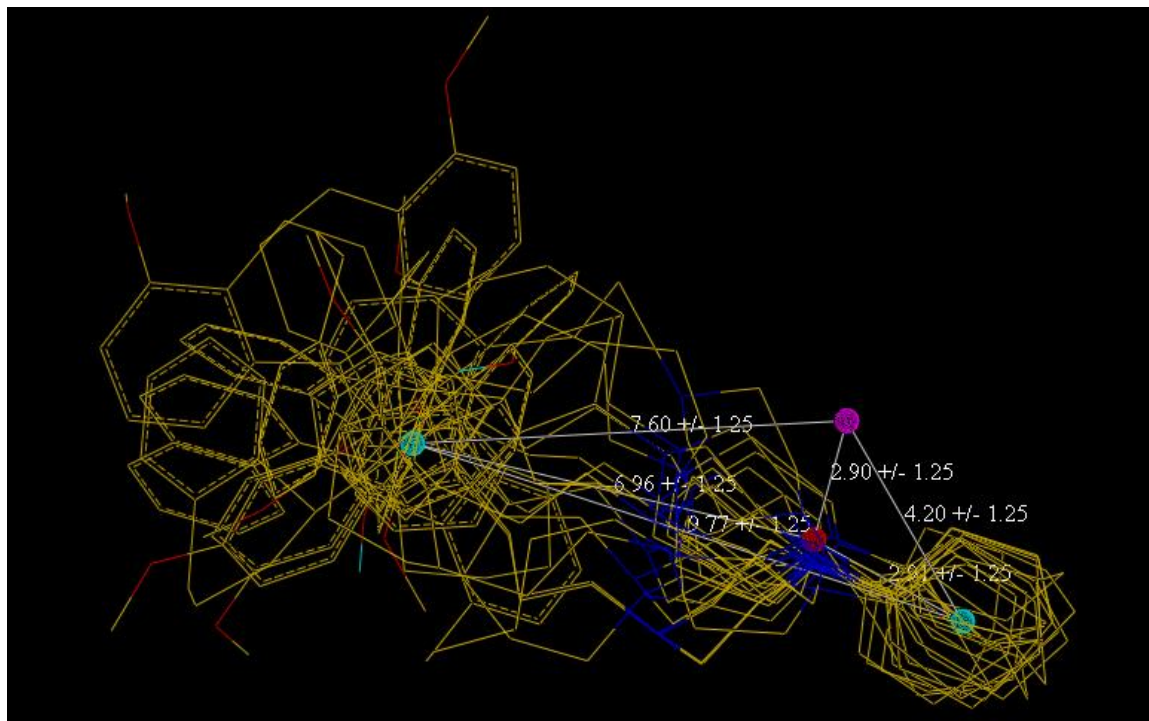


Figure 4.1 DISCOtech pharmacophore derivation of 1-cyclohexylpiperazines (compounds 1-18, hydrogen atoms hidden). Purple sphere = lone pair, red sphere = N atom and green spheres = hydrophobic points.

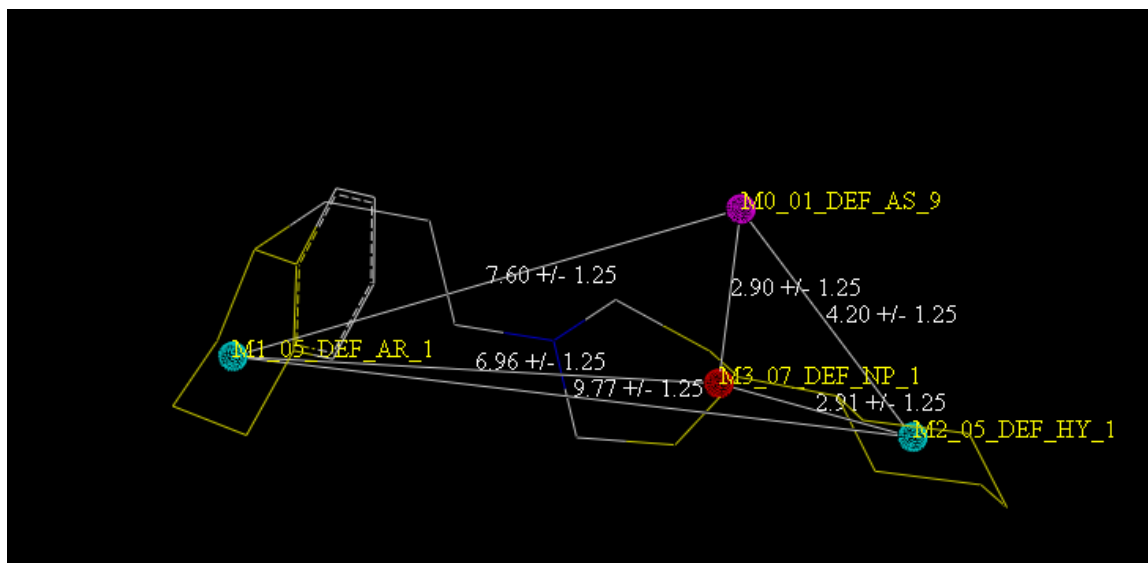


Figure 4.2 DISCOtech pharmacophore derivation of 1-cyclohexylpiperazines (compounds 1-18), overlay with compound 5, PB 28 (hydrogen atoms hidden). Purple sphere = lone pair, red sphere = N atom and green spheres = hydrophobic points.

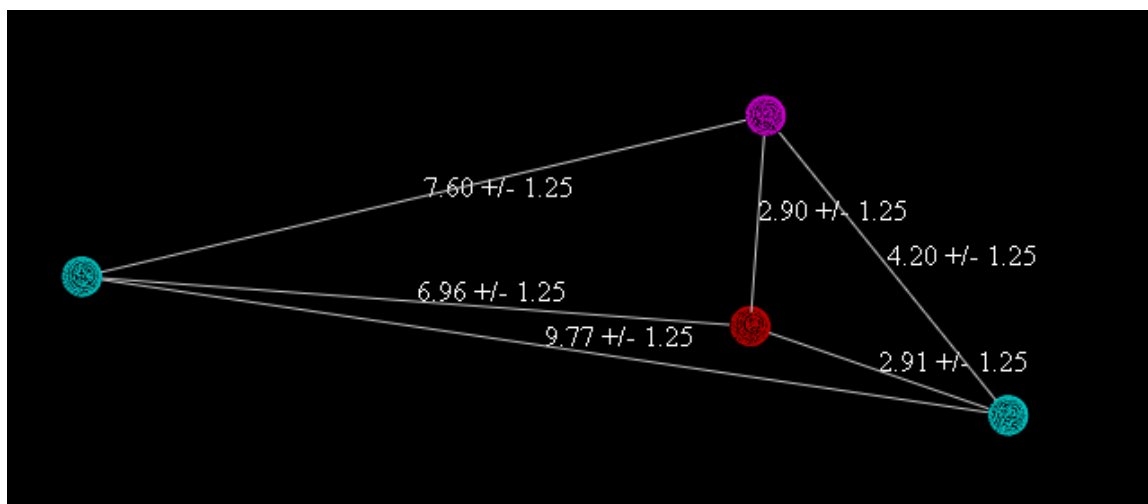


Figure 4.3 DISCOtech pharmacophore derivation of 1-cyclohexylpiperazines (compounds 1-18). Purple sphere = lone pair, red sphere = N atom and green spheres = hydrophobic points.

The aminobutyl-benzamide pharmacophore development is shown in Figures 4.4 - 4.6. These molecules have a similar pharmacophore to the previous class with the 1-cyclohexylpiperazines, however the lengths between the binding groups (hydrophobic/N atoms) are generally longer due to the fact that the molecules are a long series. The 6 molecules with highest bioactivity values were used for this series, as some of the activity values were extremely poor.

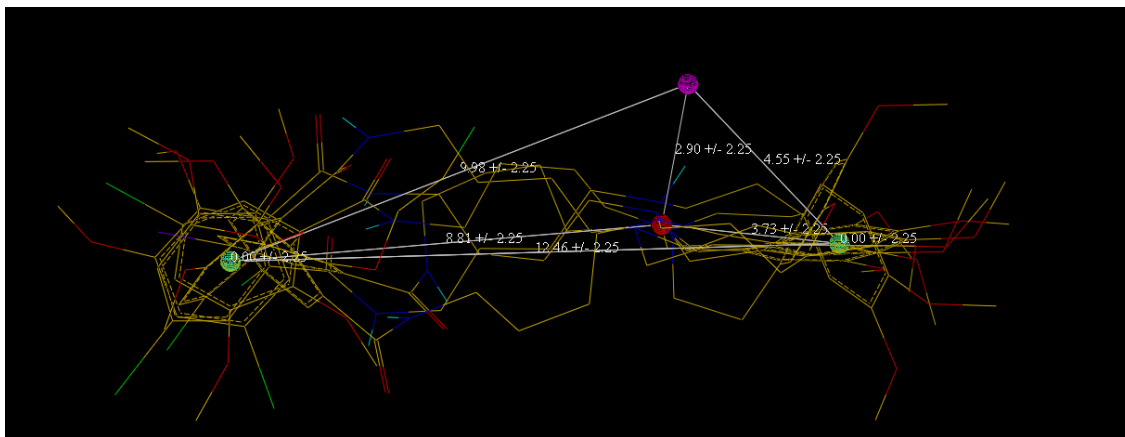


Figure 4.4 DISCOtech pharmacophore derivation of substituted aminobutyl-benzamides (compounds 19, 20, 22, 23, 25, and 28, hydrogen atoms hidden). Purple sphere = lone pair, red sphere = N atom and green spheres = hydrophobic points.

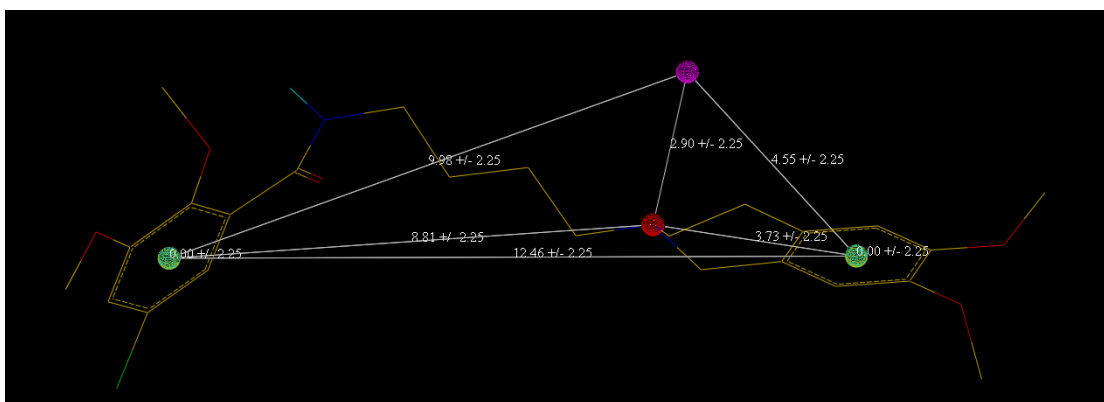


Figure 4.5 DISCOtech pharmacophore derivation of substituted aminobutyl-benzamides, overlay with compound 20 – hydrogen atoms hidden . Purple sphere = lone pair, red sphere = N atom and green spheres = hydrophobic points.

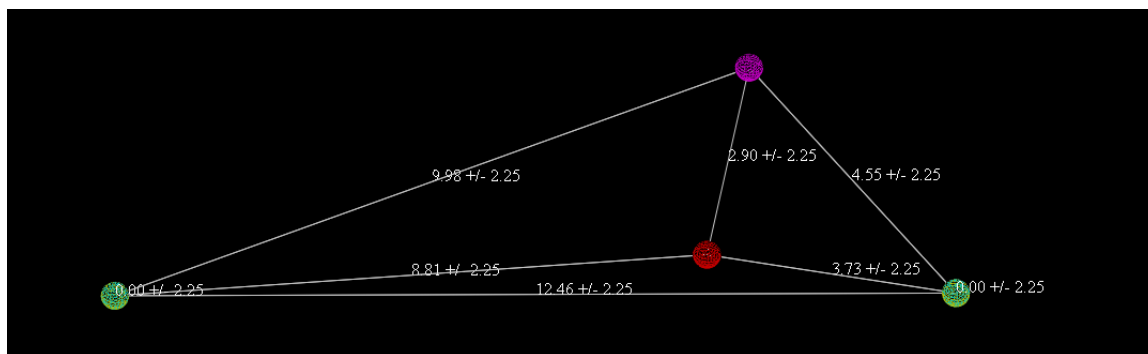


Figure 4.6 DISCOtech pharmacophore derivation of substituted aminobutyl-benzamides (compounds 19-28). Purple sphere = lone pair, red sphere = N atom and green spheres = hydrophobic points.

Figures 4.7 – 4.9 depict the pharmacophore development for the benzamide-isoquinoline series. The series consisted of mostly poor activities, with the exception of two molecules with high bioactivity, which may account for the difficulty in modeling the pharmacophore. It was found that a three point pharmacophore was more appropriate for this class specifically; the hydrophobic area on the other side of nitrogen, when chosen as a binding feature, was difficult to include in the program.

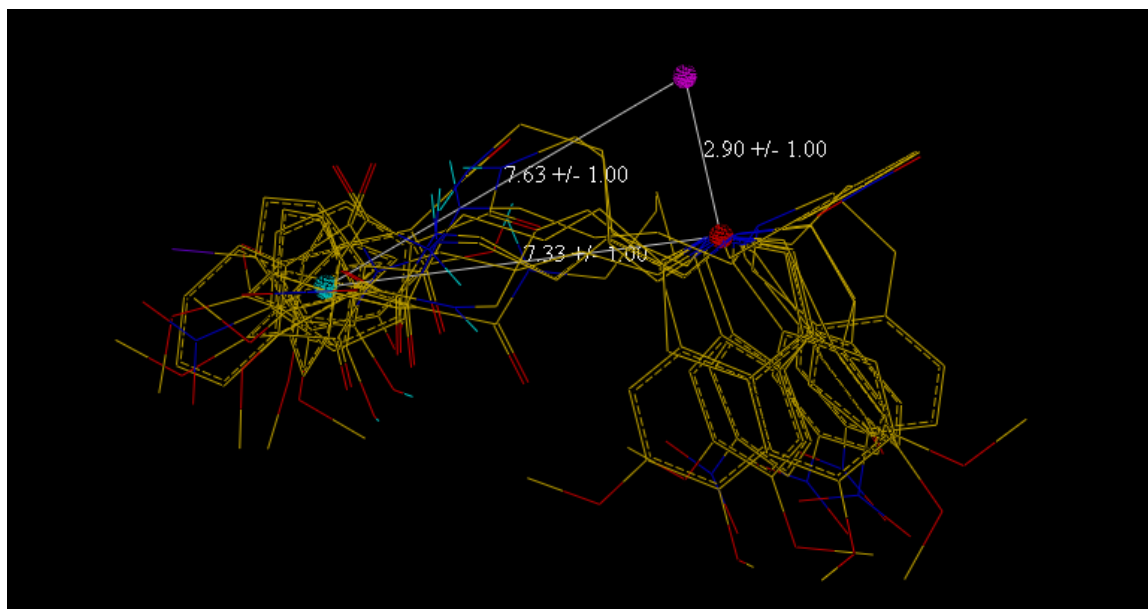


Figure 4.7 DISCOtech pharmacophore derivation of substituted benzamide-isoquinoline derivatives (compounds 29-37, hydrogen atoms hidden). Purple sphere = lone pair, red sphere = N atom and blue-green sphere = hydrophobic point.

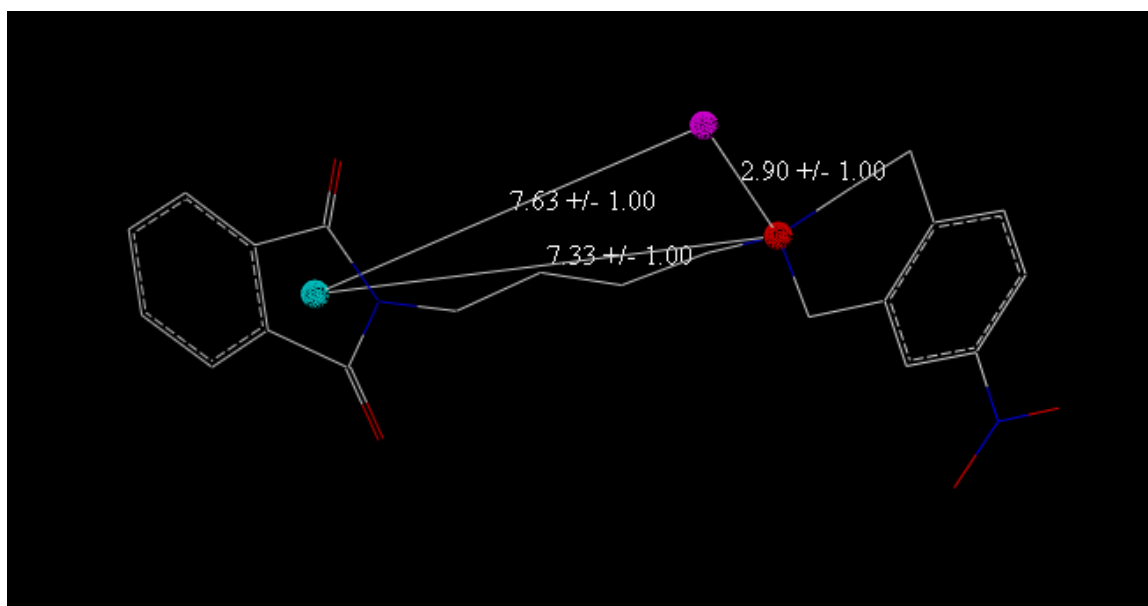


Figure 4.8 DISCOtech pharmacophore derivation of substituted benzamide-isoquinoline derivatives (compounds 29-37), overlay with compound 37 - hydrogen atoms hidden. Purple sphere = lone pair, red sphere = N atom and blue-green sphere = hydrophobic point.

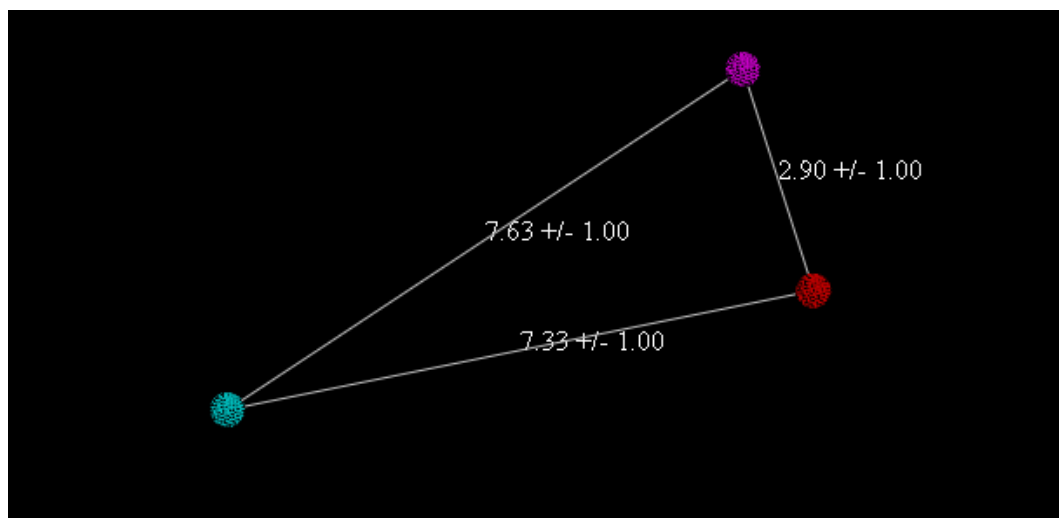


Figure 4.9 DISCOtech pharmacophore derivation of substituted benzamide-isoquinoline Derivatives (compounds 29-37). Purple sphere = lone pair, red sphere = N atom and blue-green sphere = hydrophobic point.

Figures 4.10 - 4.12 present another pyramid-type pharmacophore, in this case for the trishomocubane series, however the distances between the N and hydrophobic groups is much smaller as compared to the previous sigma classes studied thus far.

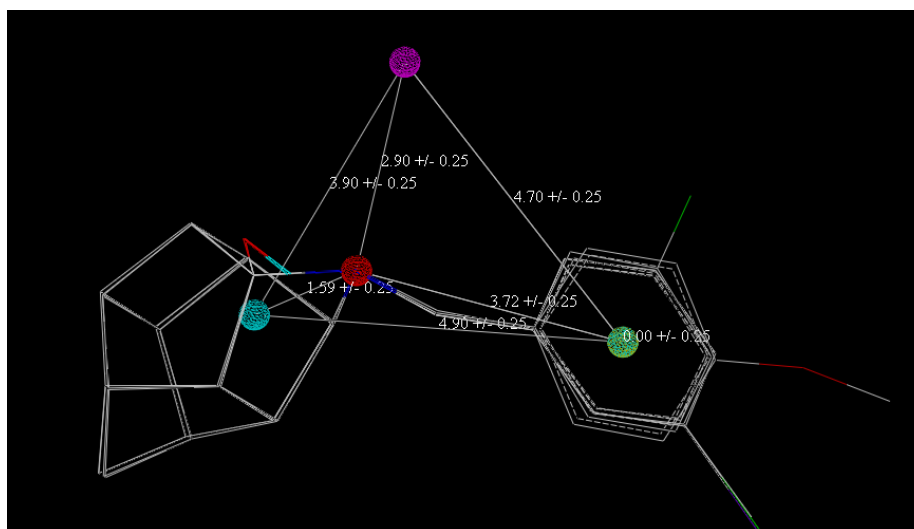


Figure 4.10 DISCOtech pharmacophore derivation of substituted trishomocubane subset (compounds 38-42, hydrogen atoms hidden). Purple sphere = lone pair, red sphere = N atom and blue/green spheres = hydrophobic points.

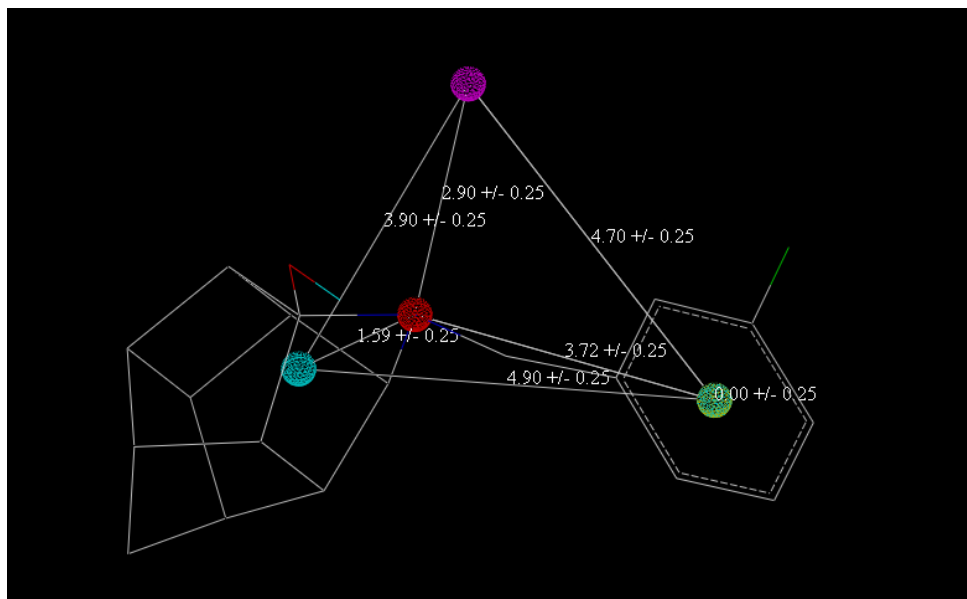


Figure 4.11 DISCOtech pharmacophore derivation of substituted trishmocabane subset (compounds 38-42), overlay with reference molecule compound 52 (hydrogen atoms hidden). Purple sphere = lone pair, red sphere = N atom and blue/green spheres = hydrophobic points.

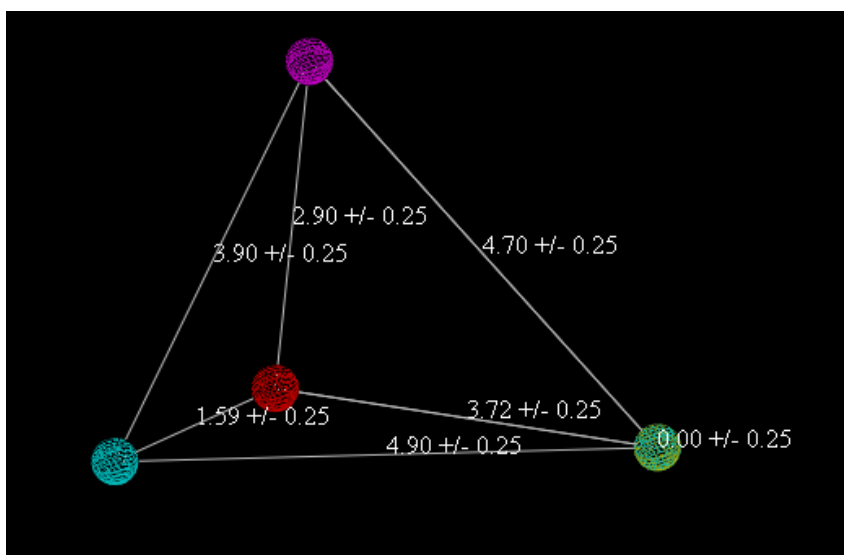


Figure 4.12 DISCOtech pharmacophore derivation of substituted trishmocabane subset (compounds 38-42). Purple sphere = lone pair, red sphere = N atom and blue/green spheres = hydrophobic points.

Figures 4.13 through 4.15 present the pharmacophore model for 1-alkyl-4-benzylpiperazine derivatives studied in this work. Similarly, it presents a 4-point pharmacophore, however, the distances between the N atom and hydrophobic groups are a little less than the earlier classes (with the exception of the trishomocubanes), though there is the question of the hydrophobic area being the area before the phenyl or whether it is the phenyl ring (which would mean a slightly longer distance). The model developed here was the “cleanest” version with very good overlap for the conformers generated by DISCOtech. Note that it is slightly different in molecule conformation (overall) vs the previous molecules; though the pharmacophore is a pyramid-type, the piperazine is not as “straight” as noted for the other cyclohexyl-type rings in previous molecules. In fact, the way the piperazine piece lines up is similar to the close alignment of the N atoms observed in the sigma 1 pharmacophore development and CoMFA studies, which may explain why this class also shows high activity for sigma 1. Some of the other classes in this study for sigma 2 are more selective for sigma 2 than sigma 1.

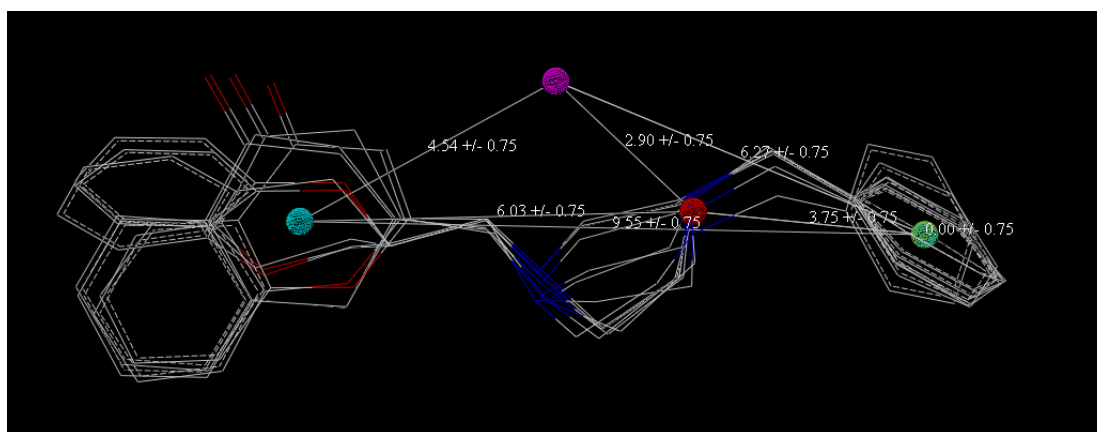


Figure 4.13 DISCOtech pharmacophore derivation of 1-alkyl-4-benzylpiperazine derivatives subset (compounds 43-49, hydrogen atoms hidden). Purple sphere = lone pair, red sphere = N atom and blue/green spheres = hydrophobic points.

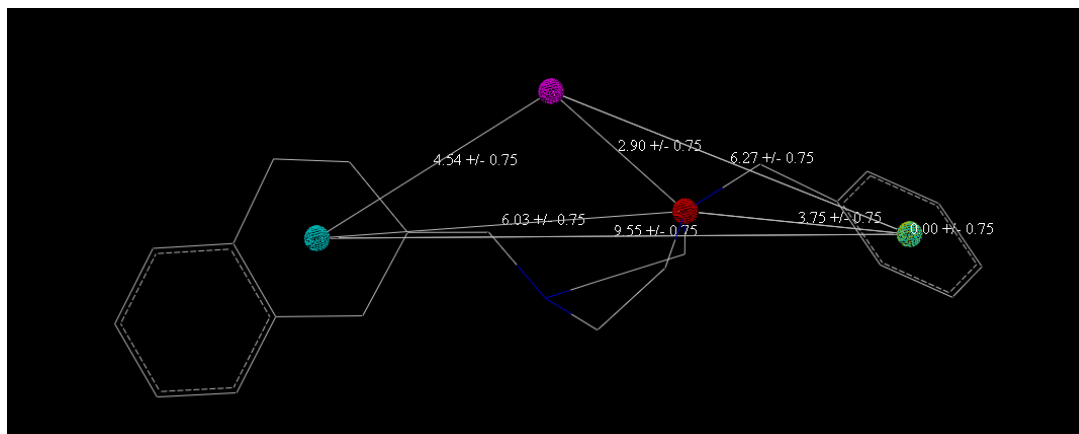


Figure 4.14 DISCOtech pharmacophore derivation of 1-alkyl-4-benzylpiperazine derivatives subset (compounds 43-49), overlay with compound 43 - hydrogen atoms hidden. Purple sphere = lone pair, red sphere = N atom and blue/green spheres = hydrophobic points.

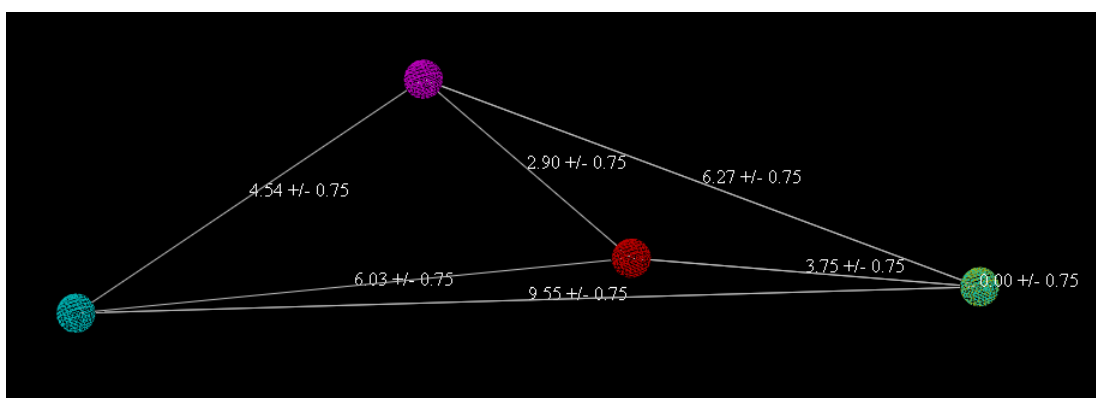


Figure 4.15 DISCOtech pharmacophore derivation of 1-alkyl-4-benzylpiperazine derivatives subset (compounds 43-49). Purple sphere = lone pair, red sphere = N atom and blue/green spheres = hydrophobic points.

Figures 4.16 – 4.18 represent the comprehensive pharmacophore development for sigma 2, where lead compounds were selected from each class along with some rigid references to yield a representative pharmacophore for the sigma 2 subtype; the compounds chosen were compounds 5, 19, 37, 45, 50, 51 and 52. Compound 5, PB 28 – the most active sigma 2 ligand – was used as the reference in the pharmacophore generation in DISCOtech. Note that the distance between the lone pair and the N atom is 2.9 Å,

whereas the distance between the N atom and one hydrophobic point is 2.9 Å and the other distance is 5.47 Å. The other part of the triangle piece, on the opposite side of 5.47 Å length is 6.37 Å, the distance between the lone pair and the hydrophobic point, whereas the distance between the lone pair and the phenyl group on the right side of the figures is 4.8 Å. The distance between the two hydrophobic groups is 8.17 Å. As discussed during the 1-alkyl-4-benzylpiperazine model explanation, generally the sigma 2 pharmacophore does not depict close or directional overlay of the N from the cyclohexyl/piperazine piece of the molecules; in general there is a pharmacophoric point there, but it is also weighted by the two (instead of one) pharmacophoric hydrophobic points on either side of it. This is a key point because this pharmacophore shape was applied to the CoMFA studies for sigma 2 with successful results, as the models were considered robust by the criteria in Section 2.2.2. Therefore, it seems that the main difference between the sigma 1 and sigma 2 pharmacophores is the matter of 3-points vs 4 points due to the additional hydrophobic group. This was observed visually in the sigma 2 CoMFA alignments in Figures 4.23 and Figures 4.24 where the hydrophobic groups are more clearly clustered on both sides of the N as opposed to only the one hydrophobic cluster, the thiophene/phenyl overlay seen in the sigma 1 CoMFA alignments.

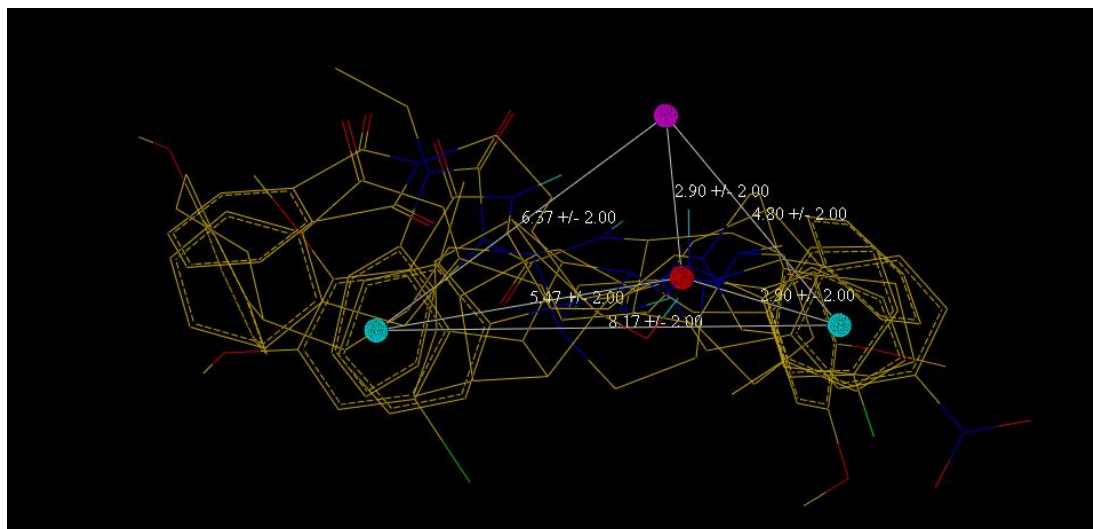


Figure 4.16 Comprehensive DISCOtech pharmacophore derivation for Sigma 2 (compounds 5, 19, 37, 45, 50, 51 and 52 – hydrogen atoms hidden). Purple sphere = acceptor site, red sphere = positive nitrogen and blue-green spheres = hydrophobic centers.

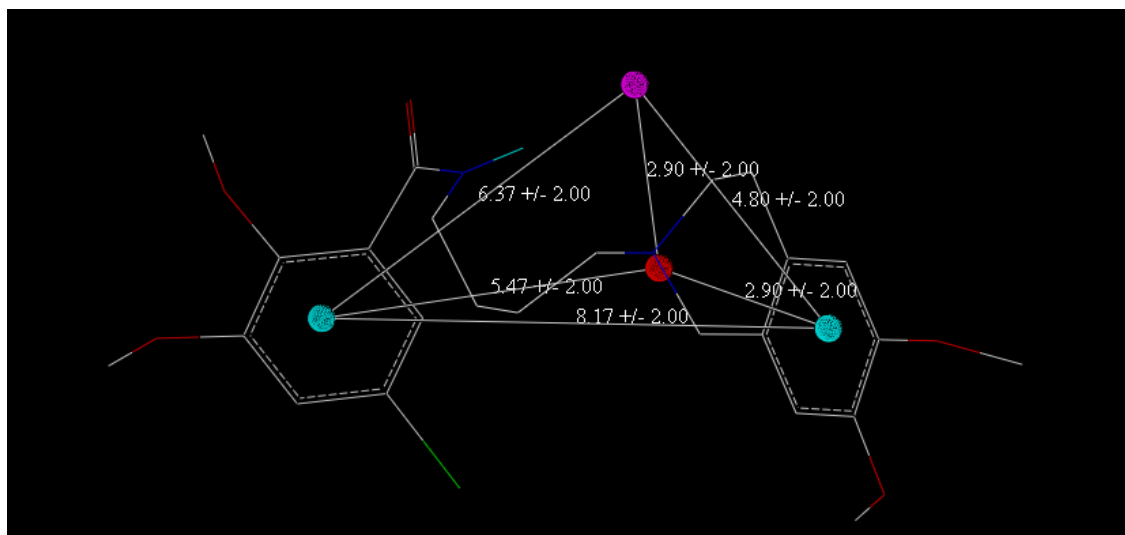


Figure 4.17 Comprehensive DISCOtech pharmacophore derivation for Sigma 2, overlay with compound 5 (hydrogen atoms hidden). Purple sphere = acceptor site, red sphere = positive nitrogen and blue-green spheres = hydrophobic centers.

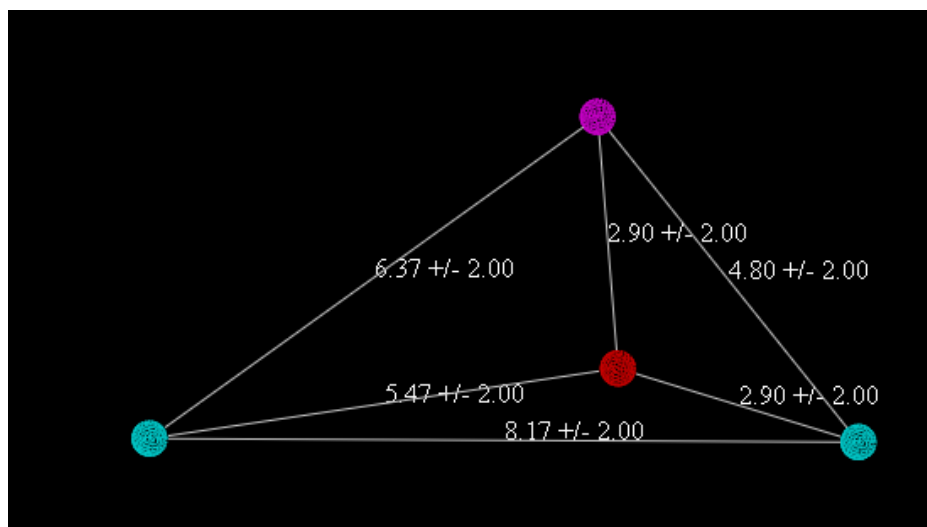


Figure 4.18 Comprehensive DISCOtech pharmacophore derivation for Sigma 2. Purple sphere = acceptor site, red sphere = positive nitrogen and blue-green spheres = hydrophobic centers.

The current comprehensive pharmacophore model for sigma 2 in Figures 4.16 through 4.18 was compared with previous sigma 2 pharmacophores from the Gund group. Patel had a three-point pharmacophore, which encompasses part of the current pharmacophore, with the N atom and hydrophobic group (2010). Figure 4.19 highlights some similarities in the distances between the models.

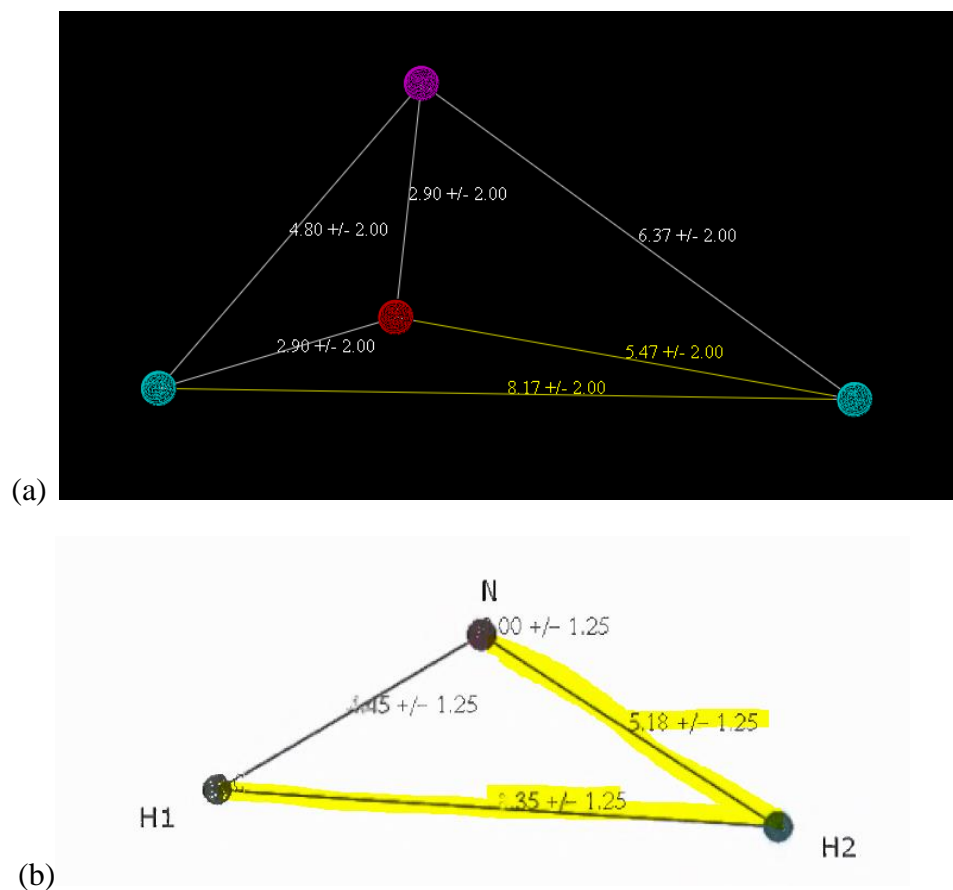


Figure 4.19 Comparison of Comprehensive DISCOtech pharmacophore (a) from Figure 4.17 with pharmacophore derived by Patel (b).

Source: (b) Patel, 2010

The current comprehensive pharmacophore model for sigma 2 in Figures 4.16 through 4.18 was compared to Jung's model. Jung had a three-point pharmacophore, which encompasses part of the current pharmacophore, with the N atom and hydrophobic group (2003). Figure 4.20 highlights the similarities in the distances between the models.

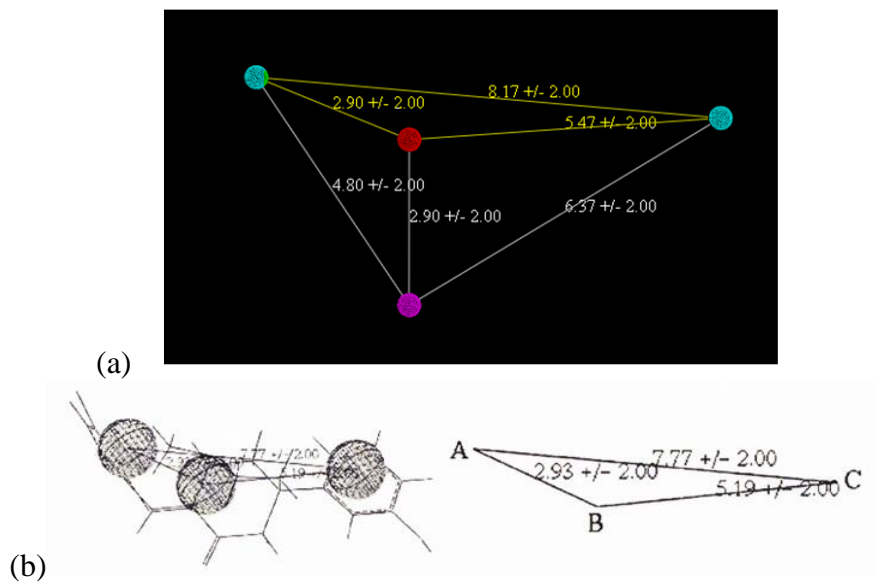


Figure 4.20 Comparison of Comprehensive DISCOtech pharmacophore (a) from Figure 4.17 with pharmacophore derived by Jung (b).
 Source: (b) Jung, 2003

The current comprehensive pharmacophore model for sigma 2 in Figures 4.16 through 4.18 was compared to Wirpsza's model. Wirpsza had a four point pharmacophore, similar to the current pharmacophore (2008). Note that nearly all the distances are very close with the exception of the distance between the hydrophobic groups. This can be explained by the fact that compound 5, PB 28, was used as the reference for the current work since it was deemed to be the most active compound for sigma 2, whereas Wirpsza used the default reference in DISCOtech which could mean a smaller distance between the hydrophobic groups if that molecule was not as active. Figure 4.21 highlights the similarities in the distances between the models.

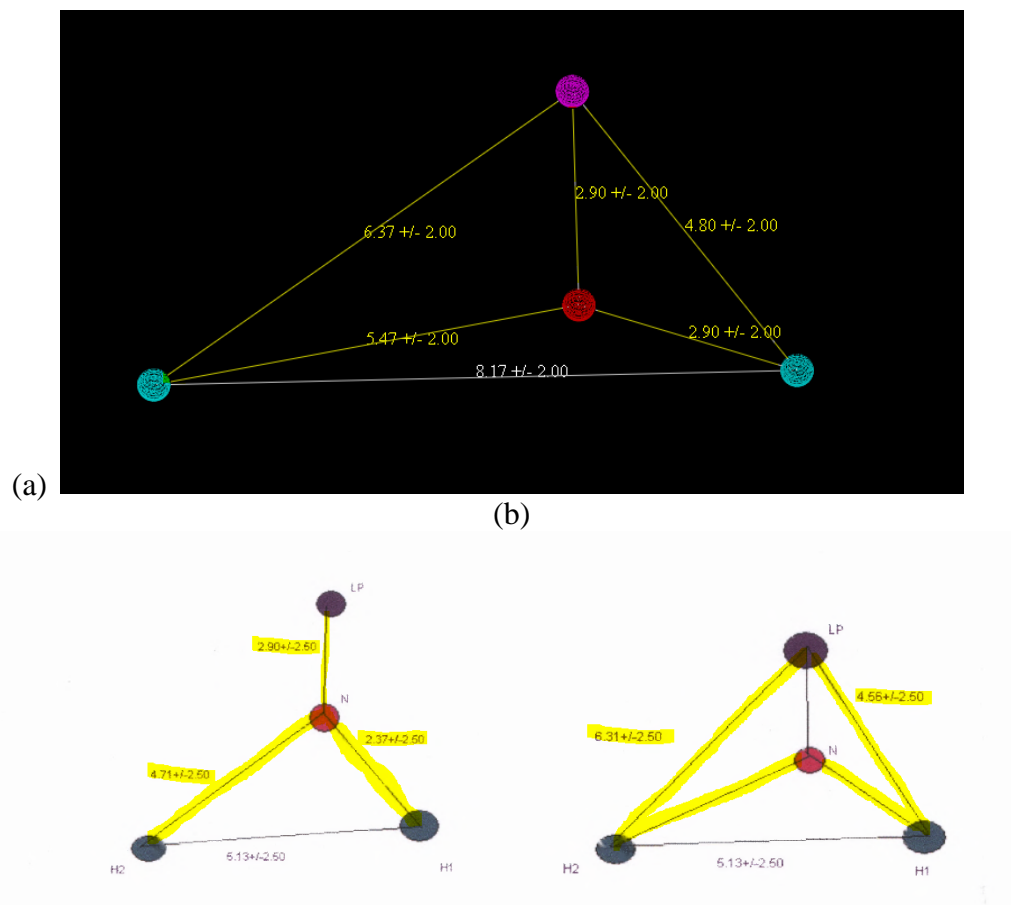


Figure 4.21 Comparison of Comprehensive DISCOtech pharmacophore (a) from Figure 4.17 with pharmacophore derived by Wirpsza (b).
Source: (b) Wirpsza, 2008

This study aimed to resolve the model differences from the past by the Gund group and was able to do so successfully; the current pharmacophore in Figures 4.16 – 4.18 could be considered a “hybrid” model which includes aspects of all of the other models, including all of the classes the other researchers studied while using the most active reference for DISCOtech to yield a more representative, active pharmacophore model. This model was compared with those seen in the literature. Rhoades and colleagues recently published a paper about a comprehensive sigma 2 pharmacophore (2014). They

note that the other models they compared with from other researchers were very molecule/class-specific (Rhoades et al., 2014). Therefore, the researcher for this study compared with Rhoades' model who aimed to develop a representative sigma 2 pharmacophore (2014). The work done by Rhoades and colleagues was very extensive, with approximately 100 pharmacophore models which they ranked, clustered and analyzed (Rhoades et al., 2014). Figure 4.22 is the best model for comparison for our case, as "Group 2" as explained, was the best ranked as it had ties to analysis yielding high q^2 values, however the application of the robust criteria was not explicitly observed in the paper (it is unclear if it had been performed as there is no mention to Golbraikh and colleagues, however other statistical values were calculated and discussed) (Rhoades et al., 2014). Nevertheless, Figure 4.22 depicts two pharmacophores by Rhoades and colleagues with some similarity around P1 (positive nitrogen), however the hydrophobic point locations are different and they have chosen donor sites, not an acceptor site associated with the N atom as chosen in this study. The approach Rhoades and colleagues took was different than the one taken here where they do not have a very active molecule such as PB 28 in the study. Further, the energy/calculation levels associated with the QSAR/electrostatics taken by Rhoades is not clear. Each researcher has a different approach and therefore there are variations in the models. From the current work, the leading pharmacophore in Figure 4.16 – 4.18 is postulated, especially since it was applied during the CoMFA model alignment quite successfully.

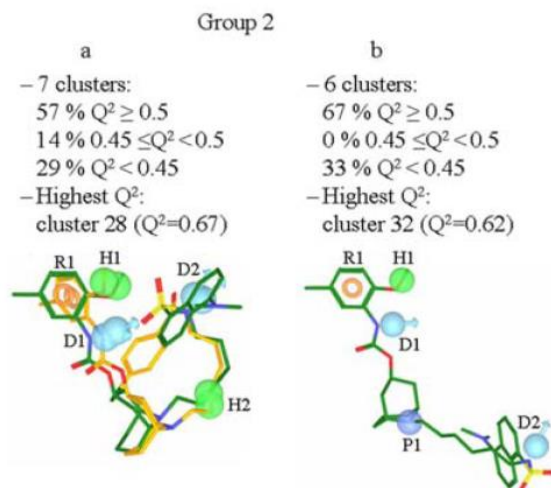


Figure 4.22 Pharmacophore models by Rhoades and colleagues. R1 = aromatic, H1/H2 = hydrophobic, D1/D2 = donor sites and P1 = positively charged site.

Source: Rhoades et al., 2014.

4.5 Comparative Molecular Field Analysis

4.5.1 Geometry Optimization and Electrostatic Studies

Each molecule in this study was optimized and saved at the *ab initio* HF/6-31G* and density functional B3LYP/6-31G* levels with electrostatic charges corresponding to each calculation level. Once each molecule was optimized, it was saved as a “.mol2” file with “electrostatic” to carry the corresponding geometry and calculated electrostatic charges into SYBYL-X 2.1.

4.5.2 Alignment

Alignment of the HF/6-31G* and B3LYP/6-31G* optimized geometries for the sigma 2 ligands was an essential step in generating a CoMFA model for each calculation level, respectively. A key point is that this was a rigid alignment approach with the intent to maintain the bound conformation of each molecule at the calculation level being studied. Many researchers, however, use flexible alignment approaches; as an example, Caballero and researchers state that their 3D-QSAR models rely on the arbitrary alignment of conformationally flexible ligands (2012). Since part of the objective of this study was to observe the results, comparing *ab initio* with density functional methods, and also since the conformation is unknown for each molecule when it binds to the sigma 2 receptor, the assumption was made that the energy should be minimized. Therefore the *ab initio* and density functional methods calculated energy minimized geometries while also calculating the electrostatic charges. The resulting molecules were then rigidly aligned to each other.

The approach to alignment for the sigma 2 ligands consisted of first applying the DISTILL RIGID tool for the 1-aralkyl-4-benzylpiperazine molecules since those conformations were very close visually and therefore very tight alignment could be initiated for the sigma 2 ligands with that class. Then compound 5 (PB 28), considered the template molecule overall for the CoMFA alignment especially since it was the reference compound in the comprehensive pharmacophore model, was aligned with the already aligned 1-aralkyl-4-benzylpiperazine class. Then DISTILL RIGID was applied to the 1-cyclohexylpiperazines. The lead compound from the benzamide-isoquinoline derivatives was aligned to compound 5, with the remaining molecules then aligned to the

lead via ALIGN DATABASE. The same approach was taken for the aminobutylbenzamides. Trishmocabanes were aligned via the nitrogen atom to compound 5. References were similarly aligned via the “match atoms” function using the N and surrounding carbon atoms. Then the benzamide-isoquinoline derivatives were further aligned via the “match atoms function” choosing the phenyl ring and N and surrounding carbon atoms. The q^2 for HF/6-31G* and B3LYP/6-31G* were 0.528 and 0.544, respectively.

Consistent with the robust criteria described in Section 2.2, 5 molecules were chosen as the test set with the remaining 26 molecules acting as the training set. Additional details are provided in Section 4.5.3. The final alignment of all 31 molecules can be viewed in Figure 4.23 for HF/6-31G* and Figure 3.24 for B3LYP/6-31G*. The resulting alignments led to robust models as described in Section 2.2.2. Additional details about the CoMFA models are described in Section 4.5.3.

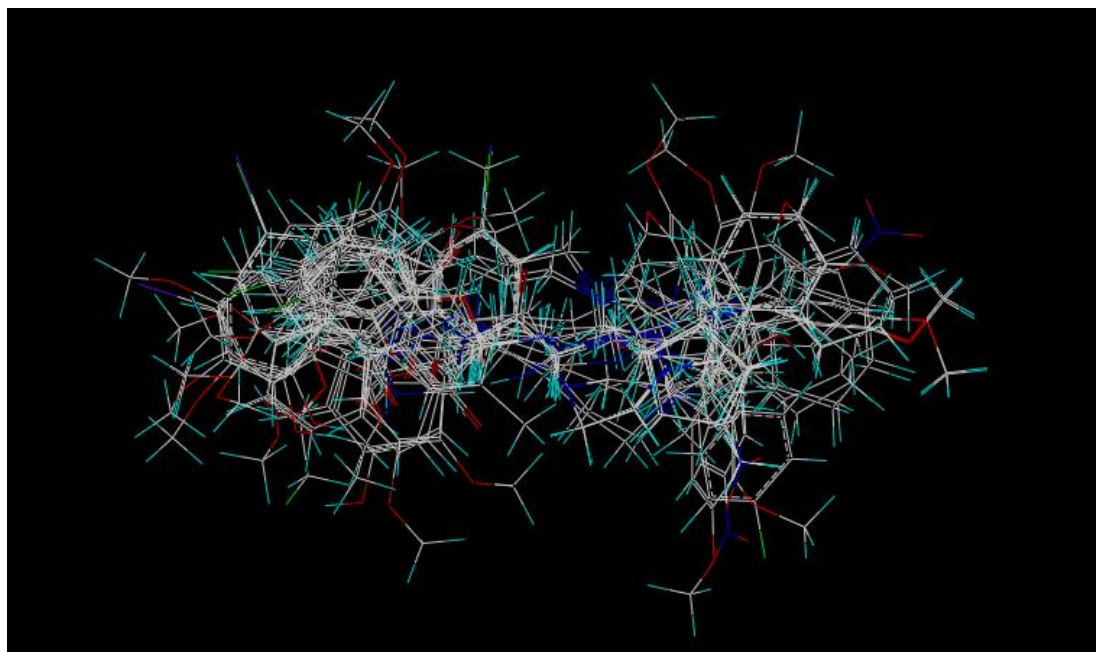


Figure 4.23 Alignment of all 31 sigma 2 ligands at the HF/6-31G* calculation level.

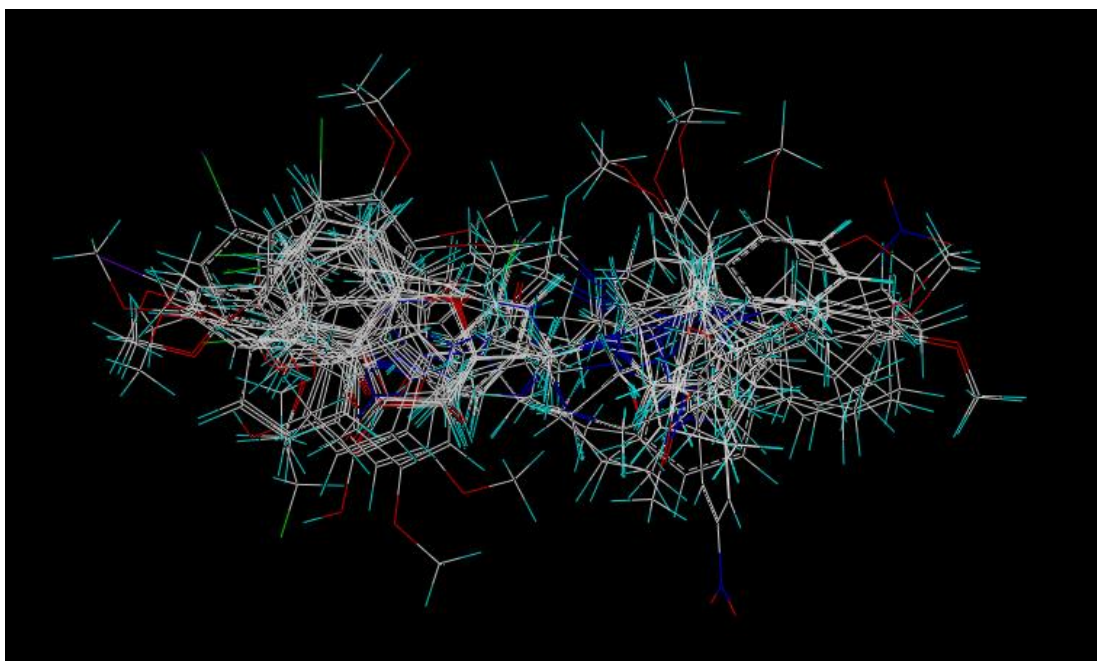


Figure 4.24 Alignment of all 31 sigma 2 ligands at the B3LYP/6-31G* calculation level.

4.5.3 Quantitative Structure Activity Data Analysis

The CoMFA models were initiated by first conducting the molecular alignment as described in Section 4.5.2. Each activity (K_i) value was converted to a pK_i value using Equation 2.4. The training set for the CoMFA ensured a range of at least 3 log units in terms of pK_i , as is suggested in the field and demonstrated by other researchers (Bolden et al., 2013). The training set ranged from -3.1462 to 0.4685 whereas the test set ranged from -2.9379 to -0.48 log units. The histograms of the pK_i vs number of molecules are shown in Figures 4.25A and 4.25B.

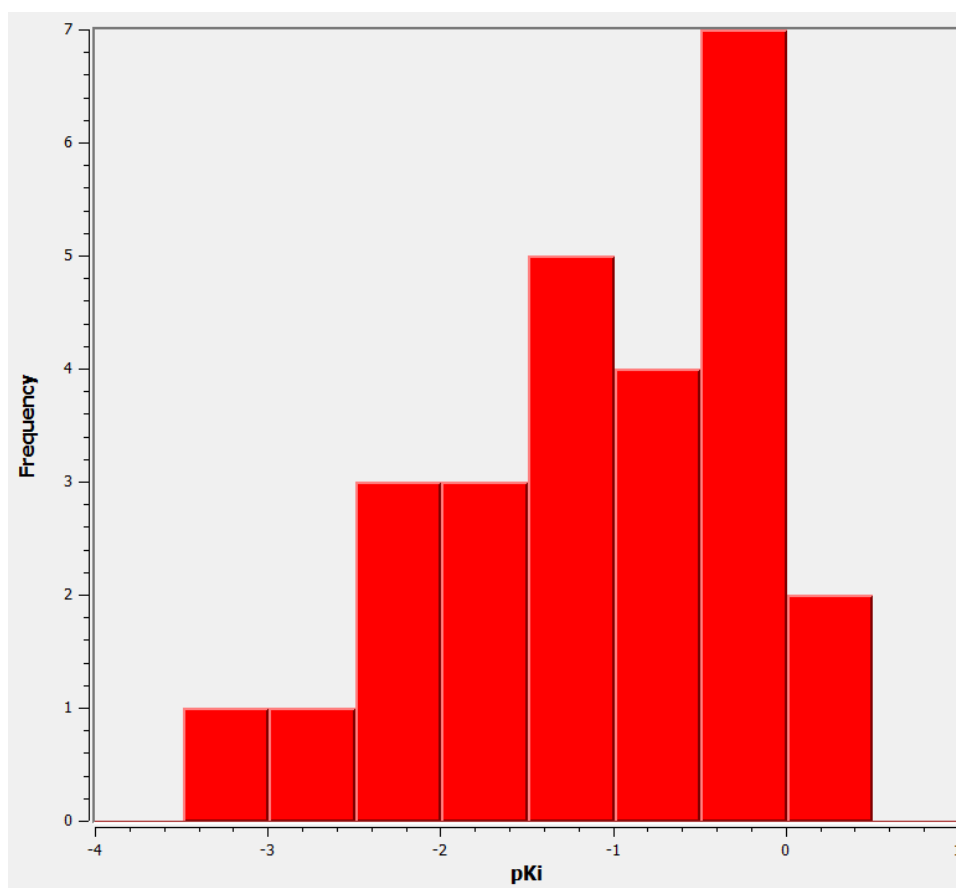


Figure 4.25A Histogram of frequency vs pK_i for sigma 2 ligands in training set.

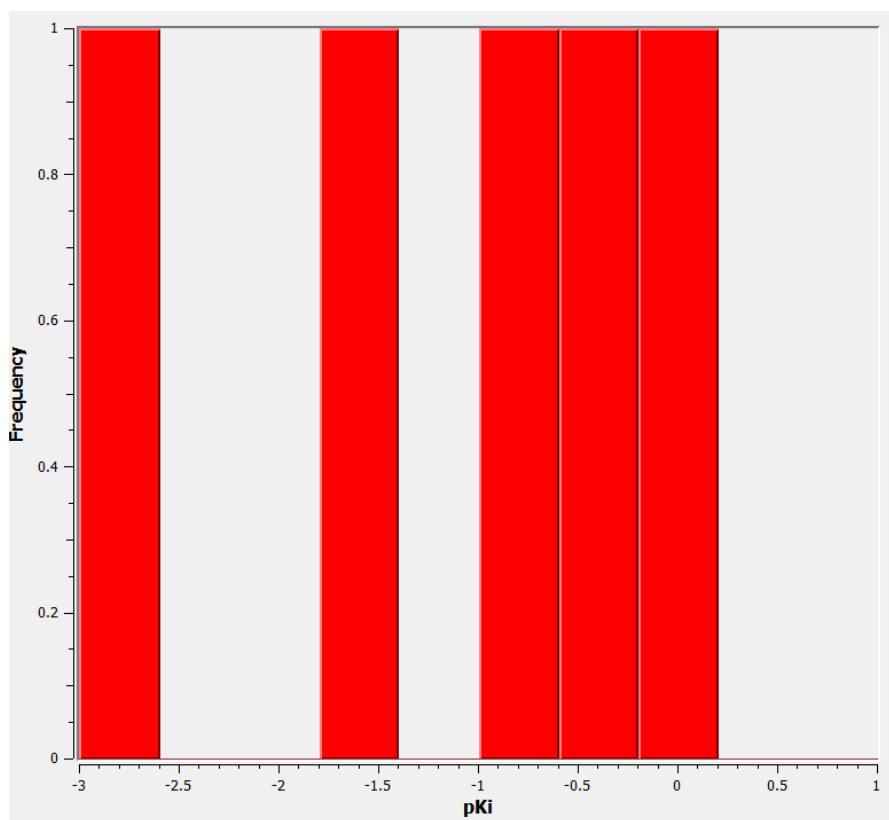


Figure 4.25B Histogram of frequency vs pK_i for sigma 2 ligands in test set.

The CoMFA models were constructed using the default settings in SYBYL-X 2.1. Therefore, an sp^3 hybridized carbon atom was probed with a +1.0 unit charge which extended at least 4 Å beyond each molecule, 2.0 Å grid spacing and the default 30 kcal/mol energy cutoff for steric and electrostatic fields. The CoMFA column, combined with the literature pK_i values, generated the Partial Least Squares cross-validated q^2 for each set, resulting in a predicted bioactivity (pK_i) value for each training set molecule. The test set, molecules which were not used to create the model, was used to validate the model by comparing predicted bioactivities generated with the experimental results. The resulting sigma 1 dataset at HF/6-31G* with 36 molecules in the training set resulted in a q^2 value of 0.528; the predicted bioactivity values for that set is in Table 4.7. The

resulting sigma 1 dataset at B3LYP/6-31G* with 26 molecules in the training set resulted in a q^2 value of 0.544; the predicted bioactivity values for that set is in Table 4.7. Table 4.8 shows the results for the test set.

Table 4.7: Experimental and Predicted Bioactivities (pK_i) by the Training Set of Sigma 2 Compounds using *ab initio* and Density Functional Calculation Methods

Compounds	Lit. pK _i	Predicted pK _i	
		HF/6-31G*	B3LYP/6-31G*
5	0.4685	0.0313	0.5584
6	-0.734	-0.6151	-0.7734
7	-0.0864	-0.4827	-0.1277
13	-0.4249	-0.0658	-0.4706
14	-0.0492	-0.0078	-0.0809
19	-0.9138	-0.7067	-0.9242
20	-0.4314	-0.6527	-0.4761
22	0.0862	-0.1115	0.0781
23	-2.8657	-2.9031	-2.8122
25	-2.4983	-2.698	-2.5214
29	-1.4278	-1.6768	-1.423
33	-3.1461	-3.1	-3.1764
37	-1.3276	-1.307	-1.3004
38	-2.1335	-1.9038	-2.2583
40	-1.6021	-1.6407	-1.5547
41	-1.7324	-1.6586	-1.6701
42	-2.0334	-1.7699	-1.9121
43	-0.2304	-0.3102	-0.1726
44	-0.1703	-0.3759	-0.2927
45	-0.2014	-0.2972	-0.1155
47	-1.4082	-0.5968	-1.3412
48	-0.6767	-0.5132	-0.7251
49	-0.7284	-0.6895	-0.7325
50	-1.4502	-1.5098	-1.4138
51	-1.5051	-1.2912	-1.4476
52	-1.301	-1.6708	-1.4377

Table 4.8: Experimental and Predicted Bioactivities (pK_i) by the Test Set of Five Sigma 2 Compounds using *ab initio* and Density Functional Calculation Methods

Compounds	Lit. pK_i	HF/6-31G*	B3LYP/6-31G*
			Predicted pK_i
4	0.1675	-0.1008	0.0541
31	-2.9379	-2.1729	-2.0907
39	-1.4771	-1.6445	-1.5026
46	-0.48	-0.5441	-1.0786
53	-0.9814	-1.3519	-1.2244

The Partial Least Squares Analysis (PLS), as described in Section 2.2.1, was used by applying the SAMPLS algorithm in SYBYL-X 2.1 developed by Bruce Bush. The optimum number of components was determined by the SYBYL-X 2.1 in the output report from the SAMPLS algorithm and is shown in **bold** in Table 4.8. For the HF/6-31G* calculation level, the QSAR module used 2 components for the model, however SAMPLS, during the PLS application, stated 4 components was the optimum. In this case the originally chosen 2 component model was used, especially since the q^2 value decreased at the next component addition as observed in Table 4.9. The number of optimal components identified in Table 4.8 was then applied without cross-validation yielding the results in Table 4.10. The R^2 values for HF/6-31G* and B3LYP/6-31G* without cross-validation, using the optimal number of components for each, respectively, at 5 and 4 yielded 0.920 and 0.995. Note that Table 4.10 also presents the electrostatic and steric contributions to the CoMFA field.

Table 4.9: Optimal Component Number and q^2 by “Leave-One-Out” using SAMPLS by the Training Set of 26 Molecules

Lev.	Term	C. 1	C. 2	C. 3	C. 4	C. 5	C. 6	C. 7	C. 8	C. 9	C. 10
HF	s.e.e.	0.754	0.676	0.699	0.705	0.727	0.763	0.792	0.834	0.869	0.897
	q^2	0.387	0.528	0.517	0.531	0.525	0.503	0.492	0.469	0.457	0.458
B3	s.e.e.	0.762	0.728	0.724	0.727	0.726	0.734	0.751	0.780	0.809	0.842
	q^2	0.374	0.453	0.481	0.501	0.527	0.540	0.544	0.535	0.530	0.522

s.e.e. is standard error of estimates.

Table 4.10: QSAR Reports by Non-Crossvalidation Using SAMPLS by the Training Set of 26 Molecules

Calculation Level	S.E.E.	R^2	F Values	Steric.	Electro.
HF/6-31G*	0.279	0.920	(n1 = 2, n2 = 23) 131.471	0.422	0.578
B3LYP/6-31G*	0.080	0.995	(n1 = 7, n2 = 18) 499.198	0.393	0.607

s.e.e. is standard error of estimates.

The application of the robust criteria as described in Section 2.2.3 is shown in Figures 4.26 and 4.27 for HF/6-31G* in the graphs of predicted pK_i values vs experimental pK_i values. The training set and tests were subject to Equations 2.5 – 2.9; those equations were used to calculate and confirm that the HF/6-31G* CoMFA model meets the robust criteria as defined by Golbraikh and colleagues in Table 4.11 (2002, 2003).

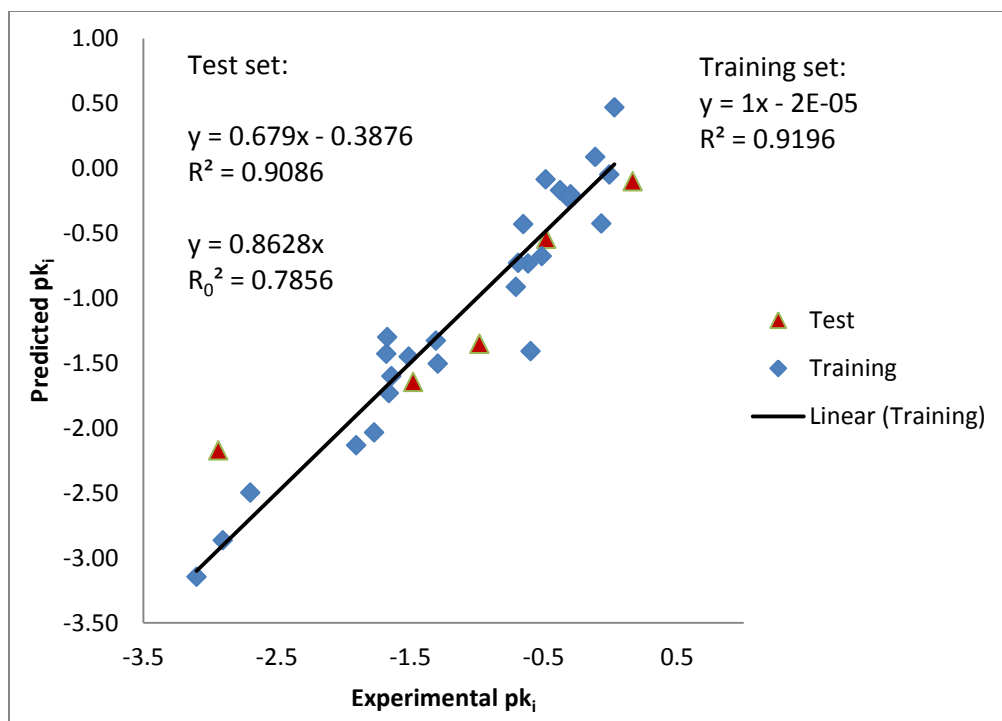


Figure 4.26 Graph of Predicted pK_i vs Experimental pK_i by the CoMFA model at HF/6-31G*.

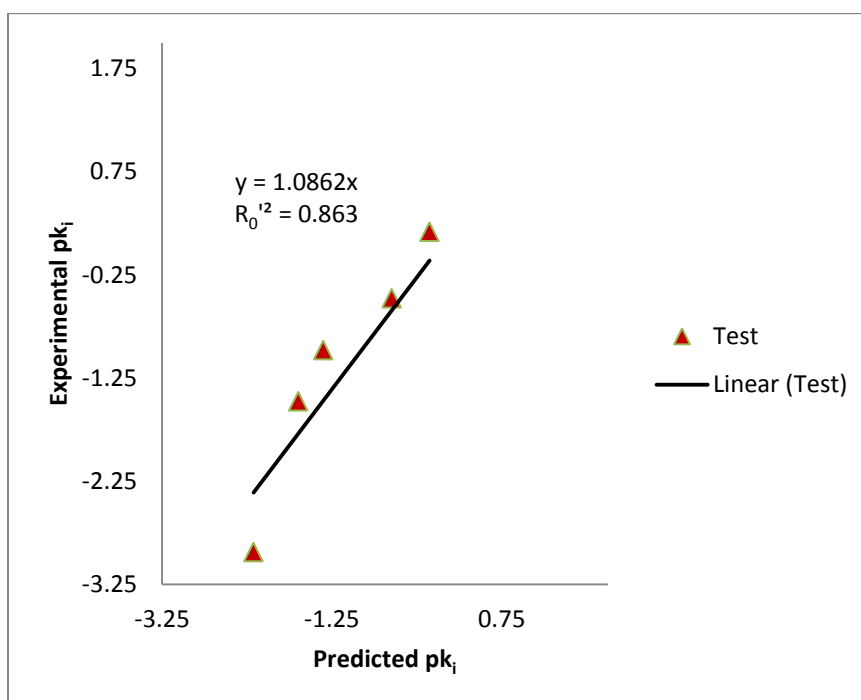


Figure 4.27 Graph of Experimental pK_i vs Predicted pK_i for Test Set by the CoMFA model at HF/6-31G*.

Table 4.11: Results for QSAR Robust Criteria Equations 2.5 – 2.9 for HF/6-31G* (Sigma 2)

Equations (2.5 – 2.9)	Value
$q^2 > 0.5$	$q^2 = 0.528$
$R^2 > 0.6$	$R^2 = 0.91$
$\frac{(R^2 - R_0'^2)}{R^2} < 0.1$ and $0.85 \leq k \leq 1.15$	$\frac{(R^2 - R_0'^2)}{R^2} = 0.05$ and $k = 1.09$
$ R_0^2 - R_0'^2 < 0.3$	$ R_0^2 - R_0'^2 = 0.08$

The application of the robust criteria as described in Section 2.2.3 is shown in Figures 4.28 and 4.29 for B3LYP/6-31G* in the graphs of predicted pK_i values vs experimental pK_i values. The training set and tests were subject to Equations 2.5 – 2.9; those equations were used to calculate and confirm that the B3LYP/6-31G* CoMFA model meets the robust criteria as defined by Golbraikh and colleagues in Table 4.12 (2002, 2003).

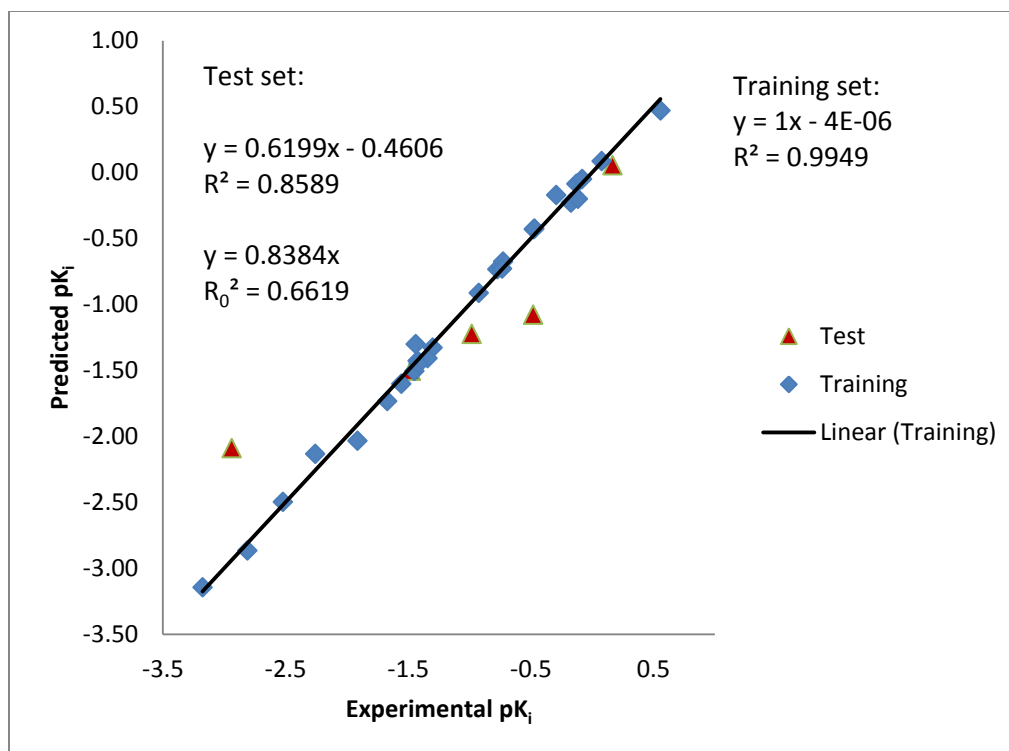


Figure 4.28 Graph of Predicted pK_i vs Experimental pK_i by the CoMFA model at B3LYP/6-31G*.

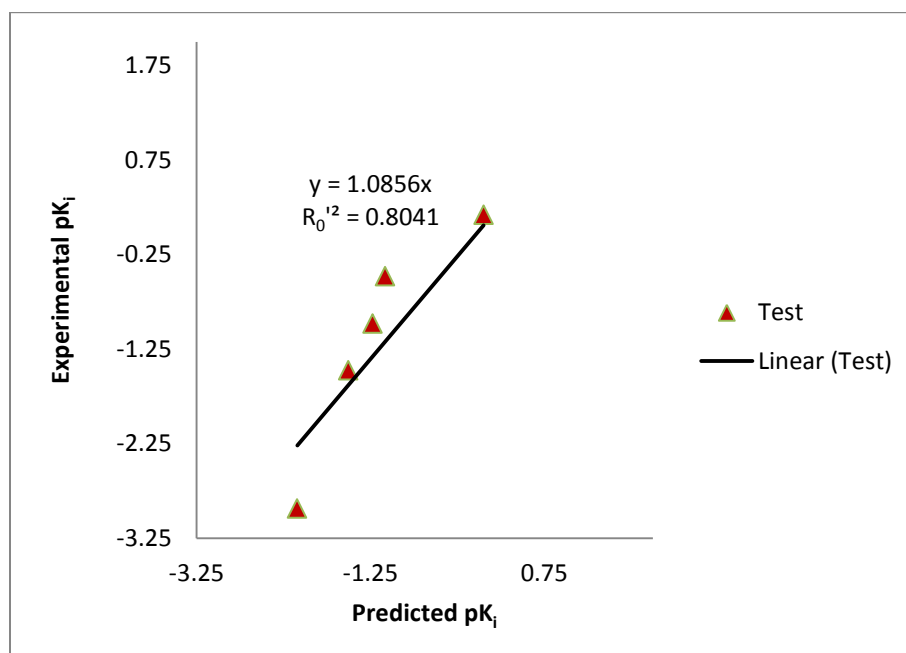


Figure 4.29 Graph of Experimental pK_i vs Predicted pK_i for Test Set by the CoMFA model at B3LYP/6-31G*.

Table 4.12: Results for QSAR Robust Criteria Equations 2.5 – 2.9 for B3LYP/6-31G* (Sigma 2)

Equations (2.5 – 2.9)	Value
$q^2 > 0.5$	$q^2 = 0.544$
$R^2 > 0.6$	$R^2 = 0.995$
$\frac{(R^2 - R_0^2)}{R^2} < 0.1$ and $0.85 \leq k \leq 1.15$	$\frac{(R^2 - R_0^2)}{R^2} = 0.06$ and $k = 1.09$
$ R_0^2 - R_0'^2 < 0.3$	$ R_0^2 - R_0'^2 = 0.14$

In summary, the bioactivity prediction for both models at HF/6-31G* and B3LYP/6-31G* were considered robust via PLS and the criteria set by Golbraikh and colleagues (2002, 2003). Therefore, the model can serve as a means to predict other compounds for sigma 2 activity.

4.5.4 Contour Maps of CoMFA Models

Contour maps from the CoMFA models were explored with the objective to understand the desired sterics and electrostatics that could enhance the activity of a molecule, enabling the design of new ligands. In the maps, green represents steric bulk desirable whereas yellow represents steric bulk undesirable. In terms of electrostatics, the maps depict red for negative charge desirable whereas blue represents positive charge as desirable. The differences observed in the CoMFA contour maps between HF/6-31G* and B3LYP/6-31G* were also explored.

Figure 4.30 and Figure 4.31 show the contour maps for compound 5 (PB 28), which served as the template for the CoMFA model as well as the reference compound

for the DISCOtech pharmacophore generation for the representative sigma 2 model. The right side of Figures 4.30 and 4.31 show that electronegativity is preferable above the cyclohexyl as well as bulk surrounding that area; on the left side it shows bulk around the rings as well as a mix of positive and negative charge desirable. The calculation levels for the CoMFA contour maps appear to be in good agreement visually.

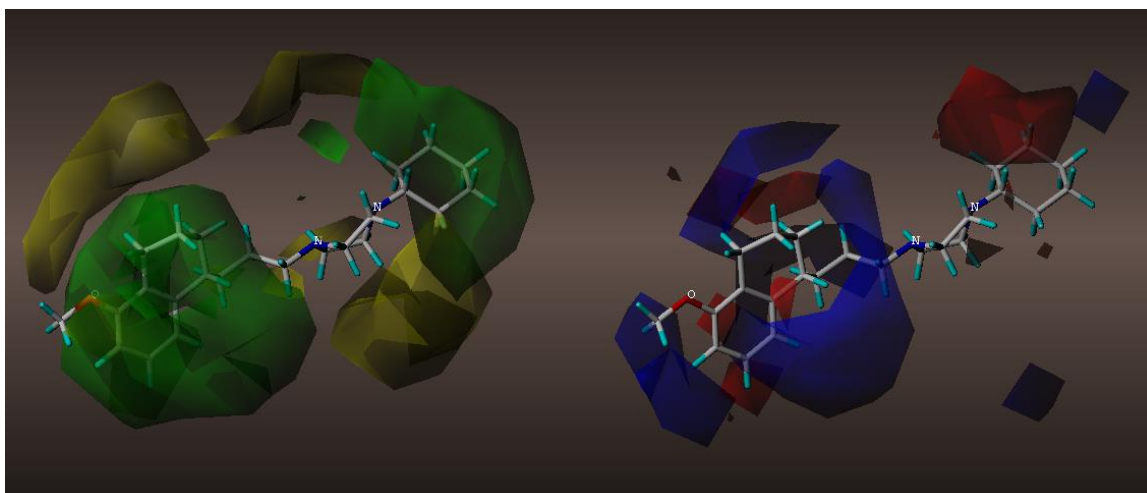


Figure 4.30 CoMFA contour map of compound 5 (PB28) at HF/6-31G*.

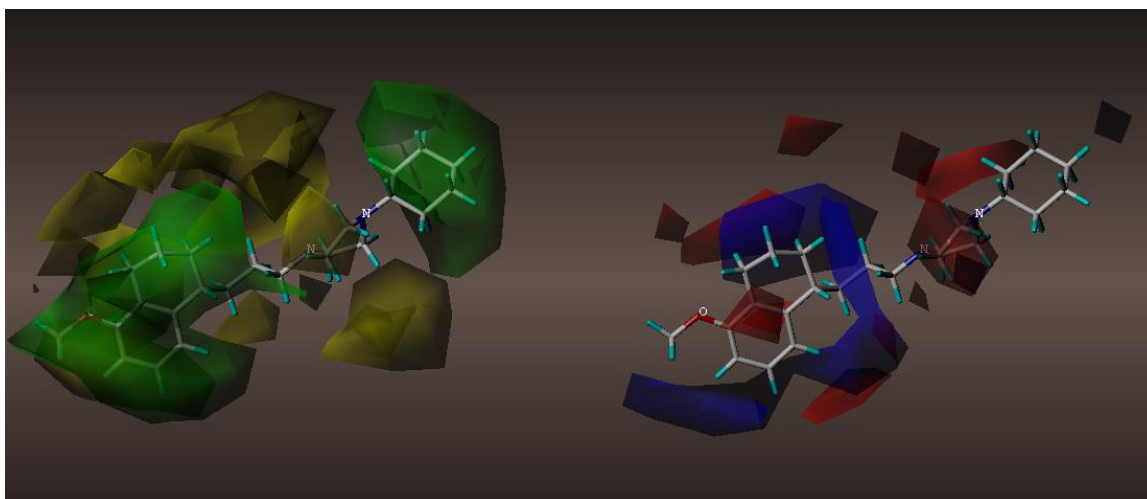


Figure 4.31 CoMFA contour map of compound 5 (PB28) at B3LYP/6-31G*.

The CoMFA contour maps for compound 19 were observed, as this molecule, based on its aforementioned extremely high selectivity for sigma 2, is an excellent candidate for bioactivity improvement. Figures 4.32 and 4.33 demonstrate the possibilities to add electronegativity on the right side as well as bulk, in addition to there being opportunities on the left side around the rings, to add bulk and positivity. This was explained further in Section 4.6.

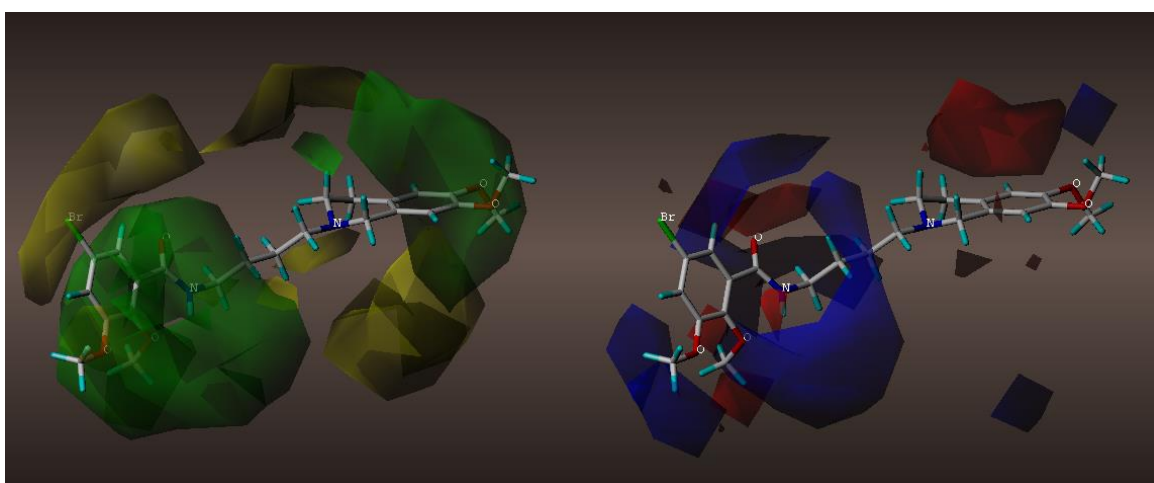


Figure 4.32 CoMFA contour map of compound 19 at HF/6-31G*.

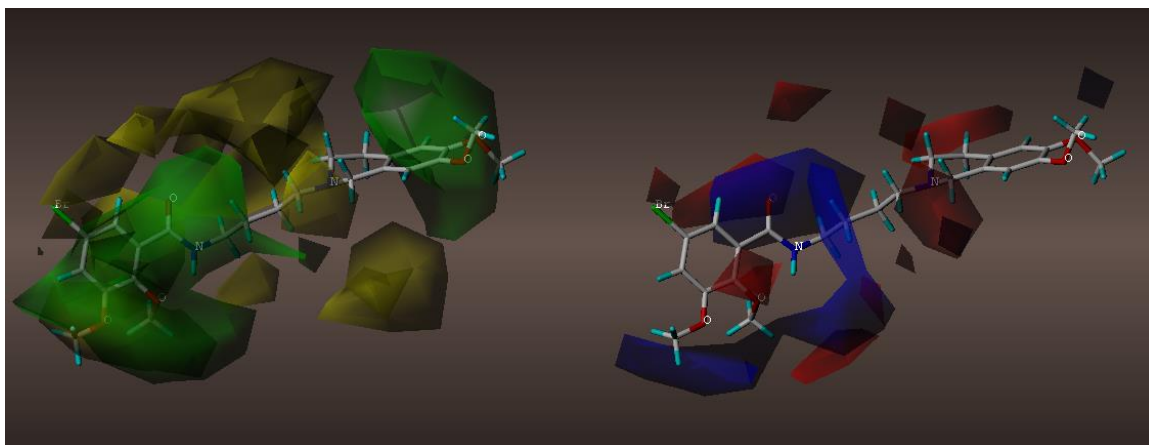
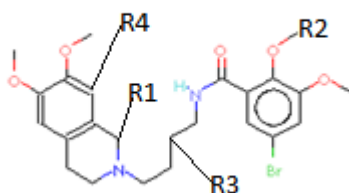


Figure 4.33 CoMFA contour map of compound 19 at B3LYP/6-31G*.

4.6 Design of New Sigma 2 Ligands

Utilizing the analysis conducted in Section 4.5.4, the design of new ligands was conducted on compound 19, with various combinations to increase electronegativity or positivity as well as bulk in various locations. There were four main locations considered based on the CoMFA contour maps as shown in Table 4.13, with improved bioactivity values noted in **bold**. Note that the literature pK_i for compound 19 is -0.9138.

Table 4.13: Compound 19-based New Ligands



Comp.	R1	R2	R3	R4	HF/6-31G*	B3LYP/ 6-31G*
					Predicted pK_i	
19	H	CH ₃	H	H	-0.7067	-0.9242
53	Cl	CH ₃	H	H	-0.2655	-0.4803
54	Cl	tbutyl	H	H	-0.1777	-0.3961
55	COOH	CH ₂ -NH ₂	NH ₂	H	-0.3564	-0.4336
56	COOH	CH ₃	H	H	-0.3028	-0.6155
57	H	tbutyl	H	H	-0.5156	-0.833
58	F	CH ₃	H	H	-0.2448	-0.6145
59	H	CH ₃	NH ₂	H	-0.7367	-0.6311
60	H	CH ₂ -NH ₂	H	H	-0.4522	-0.4811
61	Cl	C(CH ₃)(CH ₂ NH ₂)(CH ₂ NH ₂)	H	H	-0.6485	-1.1311
62	H	CH ₃	H	tbutyl	-0.7117	-0.8609

The best R-group combinations, yielding highest activity improvements, were selected for discussion. In the case of adding bulk (tbutyl) at the R2 location and Cl at the R1 location, the predicted pK_i improved from -0.7067 to -0.1777 for HF/6-31G* and from -0.9242 to -0.3961 for B3LYP/6-31G*. As explained in Chapter 3, higher pK_i means increased bioactivity. A pK_i value could mean a K_i value of 1.5 nM which is an improvement over the literature value of 8.2 nM for the molecule. The corresponding contour maps are in Figures 4.34 and 4.35.

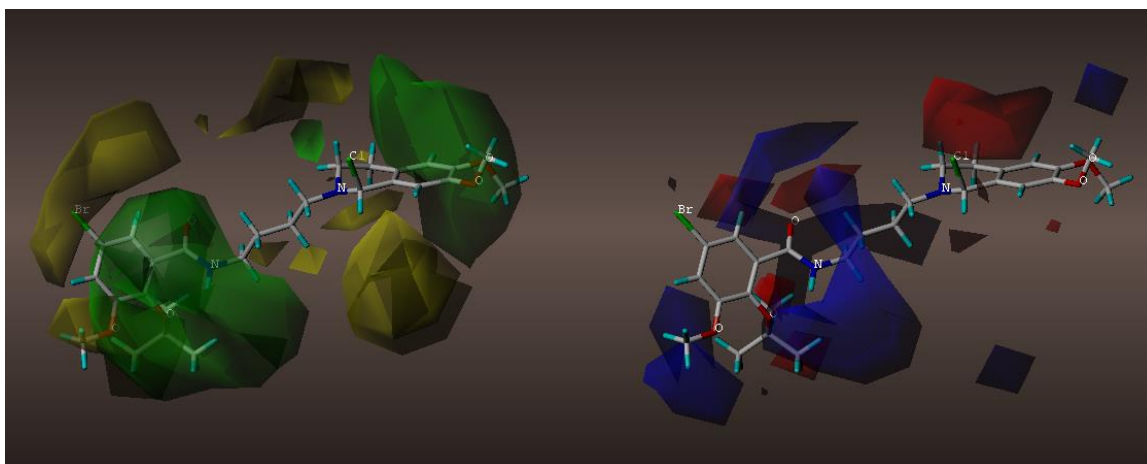


Figure 4.34 CoMFA contour map of compound 54 at HF/6-31G*.

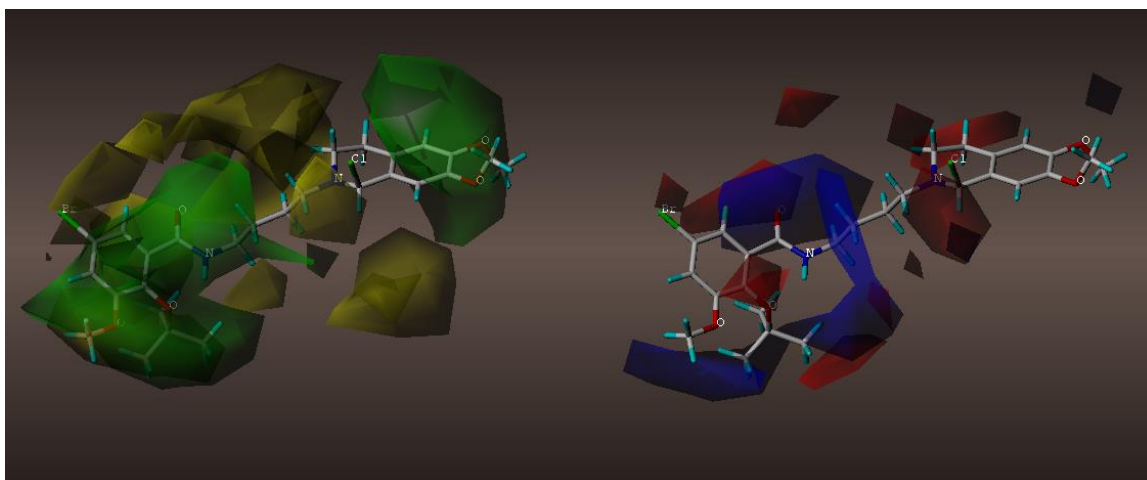


Figure 4.35 CoMFA contour map of compound 54 at B3LYP/6-31G*.

Another promising combination, yielding high activity improvement, was the case of adding N atoms (increasing positivity) at R2 and R3. There was fairly good overlap of these additions into the blue areas of the contour map. The predicted pK_i improved from -0.7067 to -0.3564 for HF/6-31G* and -0.9242 to -0.4336. The corresponding contour maps are in Figures 4.36 and 4.37.

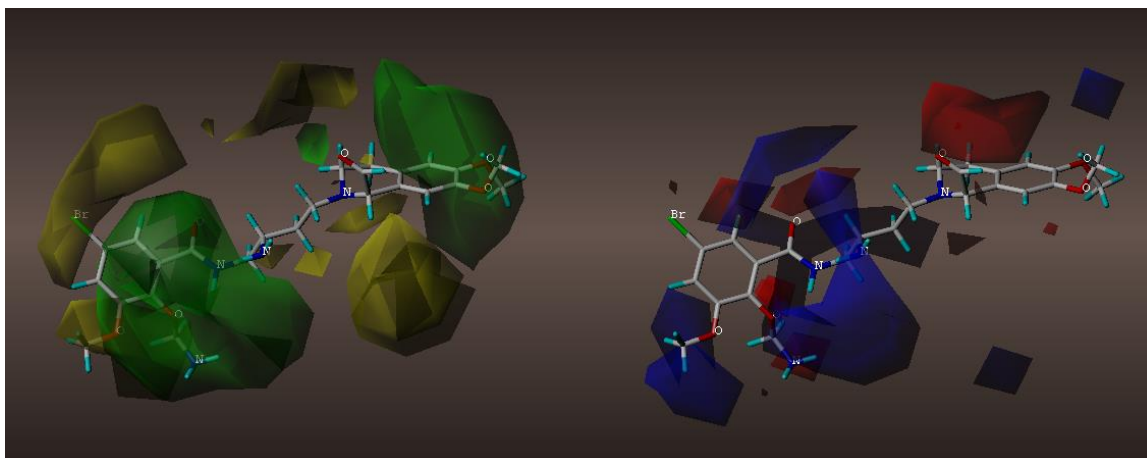


Figure 4.36 CoMFA contour map of compound 55 at HF/6-31G*.

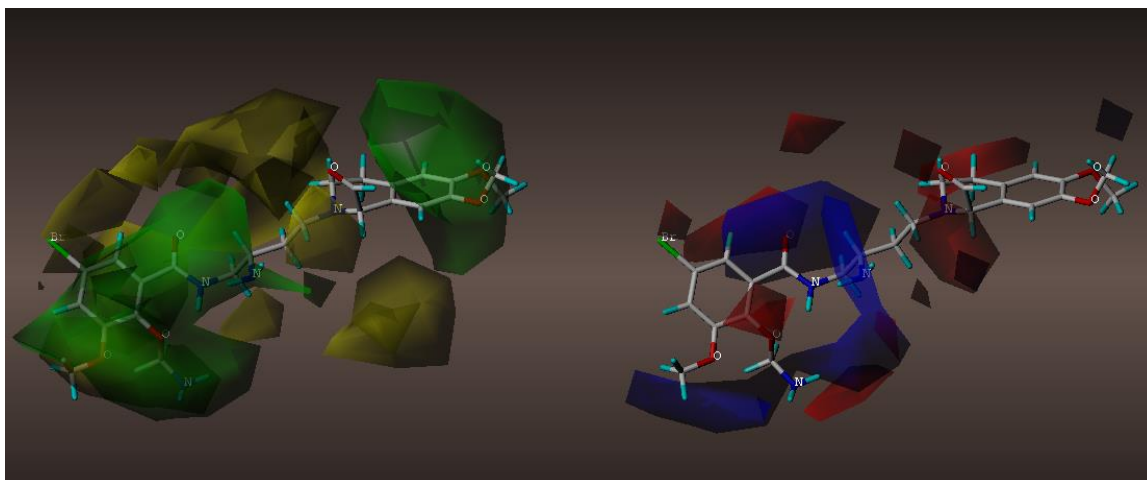


Figure 4.37 CoMFA contour map of compound 55 at B3LYP/6-31G*.

The case of increasing electronegativity on the right cyclohexyl ring with the addition of a Cl atom helped increase bioactivity for compound 19 as well on both calculation levels as demonstrated with compound 58. The predicted pK_i value went from -0.7067 to -0.2655 for HF/6-31G* and -.9242 and -0.4803 for B3LYP/6-31G*. The corresponding contour maps are in Figures 4.38 and 4.39.

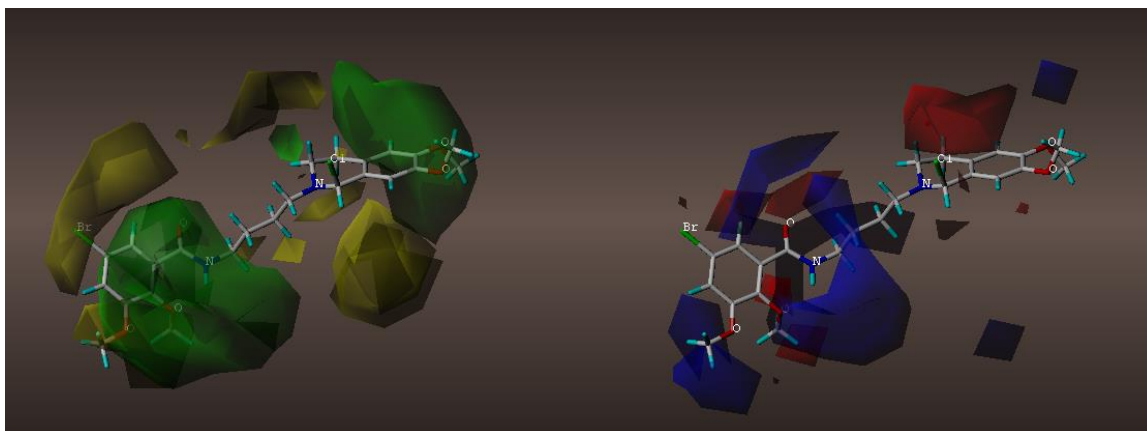


Figure 4.38 CoMFA contour map of compound 53 at HF/6-31G*.

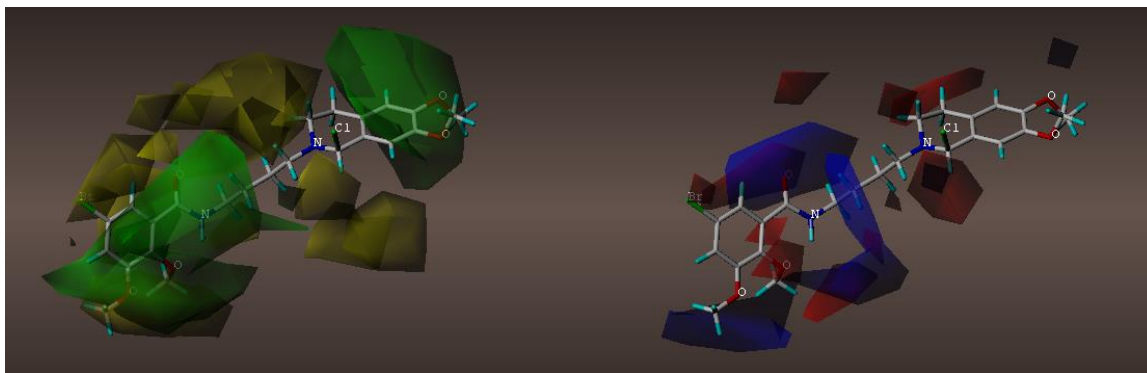


Figure 4.39 CoMFA contour map of compound 53 at B3LYP/6-31G*.

Certainly these are promising results, lending to the possibility that the newly predicted highly active ligands could be synthesized and potentially used in the future as drug candidates, particularly as potentially highly selective sigma 2 compounds since these were designed from compound 19. Highly active, selective sigma 2 compounds are rare as evidenced by the data set and by other researchers. In fact, even compound 5, PB 28, does not have a very high selectivity (σ_1/σ_2): 40 vs 1573 for compound 19. Therefore, we can see the value for improving activity for compound 19; initial results were excellent with a possible high activity at 1.5 nM. Additional contour maps for newly designed ligands are located in the APPENDIX.

CHAPTER 5

COMPARISON OF SIGMA 1 AND SIGMA 2 RECEPTOR LIGANDS

5.1 Sigma 1 and Sigma 2 Receptor Ligand Differences

Part of the objective of this study was to determine what differentiates a ligand from being bioactive for a sigma 1 receptor vs a sigma 2 receptor. As mentioned in Chapter 3 and 4, there were noted differences in the comprehensive pharmacophores. Figures 3.20 and 4.18 represent the two different comprehensive pharmacophores. As stated, these pharmacophores drove the alignment techniques used for the corresponding CoMFA models which were considered robust and highly predictive for bioactivity. Therefore, one can presume that these pharmacophores generated by DISCOtech are viable models, in addition to the consistent framework they had from previous work in the Gund group. Particularly for sigma 2, the current model postulated resolves the previous models into a hybrid model and again shows strong representation for different classes of compounds, with a highly active reference.

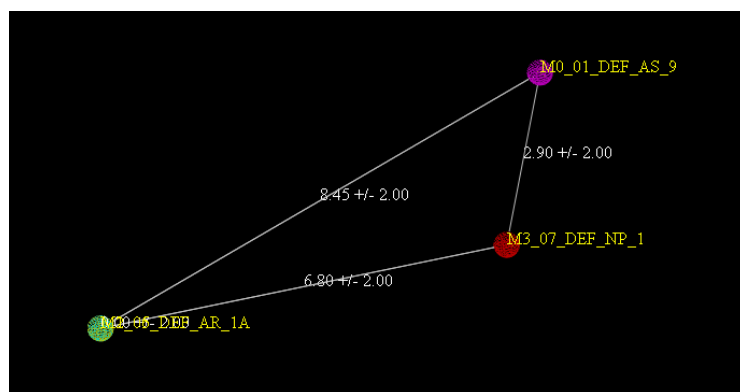


Figure 3.20 (repeat) Comprehensive DISCOtech pharmacophore derivation for Sigma 1. Purple sphere = acceptor site, red sphere = positive nitrogen and green sphere = aromatic/hydrophobic center.

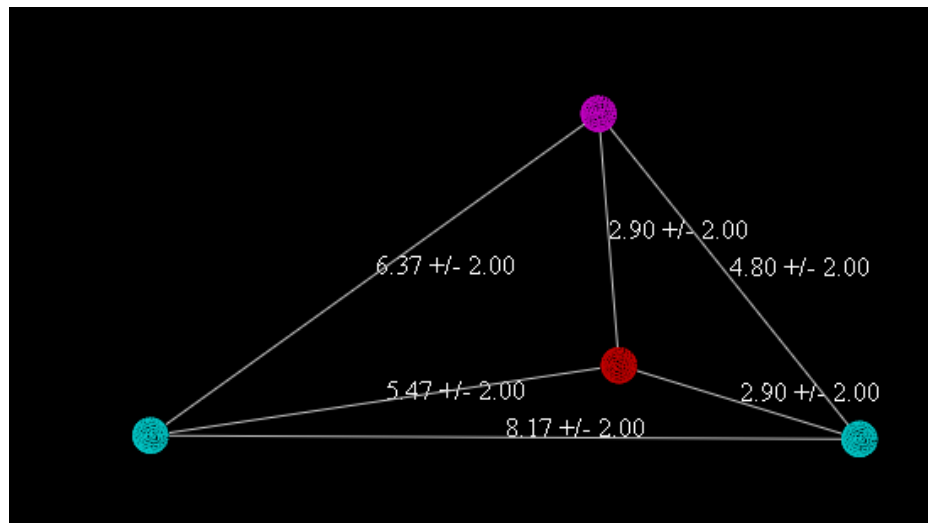


Figure 4.18 (repeat) Comprehensive DISCOtech pharmacophore derivation for Sigma 2. Purple sphere = acceptor site, red sphere = positive nitrogen and blue-green spheres = hydrophobic centers.

The following Figures 5.1 - 5.4, demonstrate the test compound, Haloperidol, in the HF/6-31G* and B3LYP/6-31G* CoMFA contour maps. Interestingly, Haloperidol in sigma 1 maps appears to have slightly more distribution of bulk on both ends of the molecule and somewhat around the molecule. Haloperidol in sigma 2 maps, however, appears to have more distinct bulk forms, one on each side of the molecule and not

necessarily around the whole molecule. Further, sigma 2 appears to favor more positivity as evidenced by the color blue in the map.

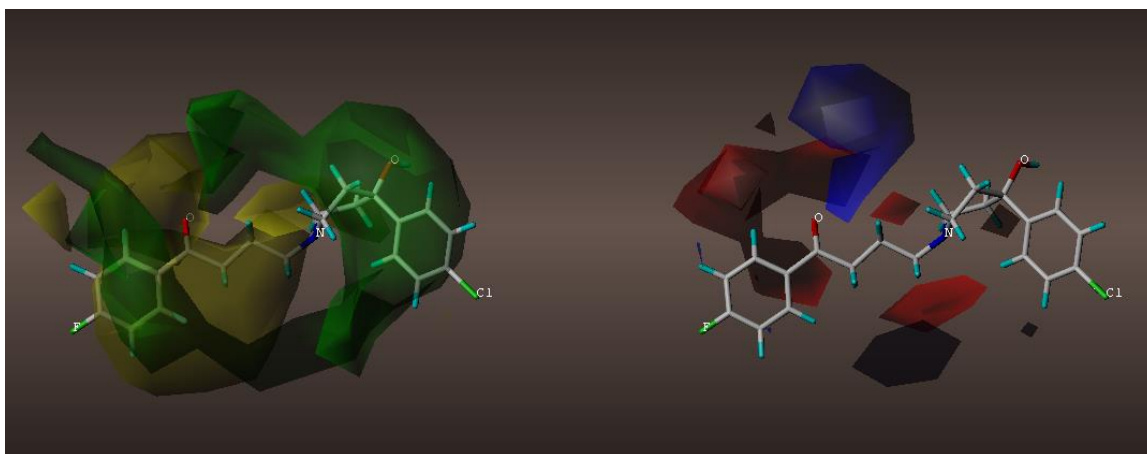


Figure 5.1 Haloperidol at HF/6-31G* sigma 1 CoMFA contour map.

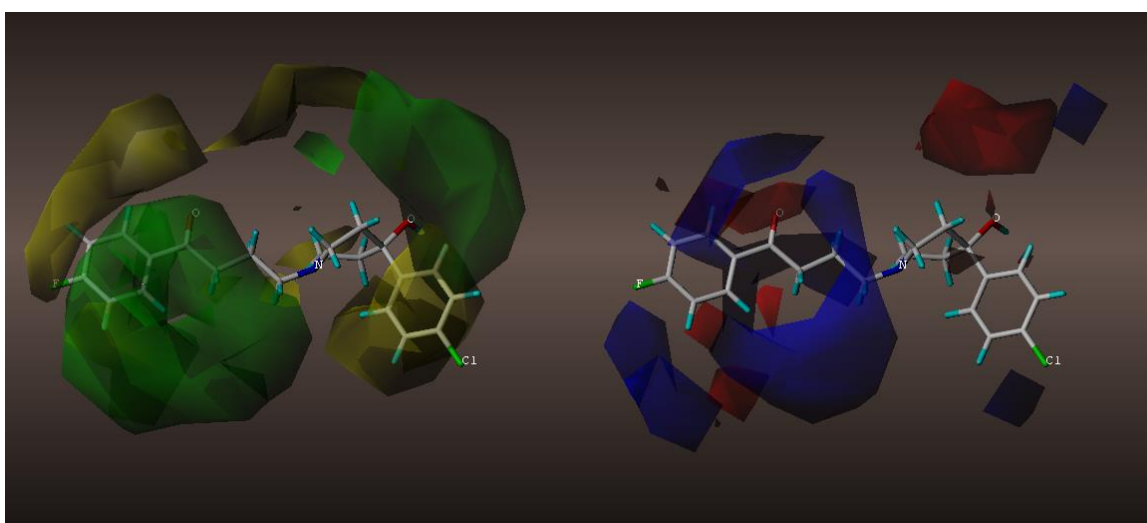


Figure 5.2 Haloperidol at HF/6-31G* in sigma 2 CoMFA contour map.

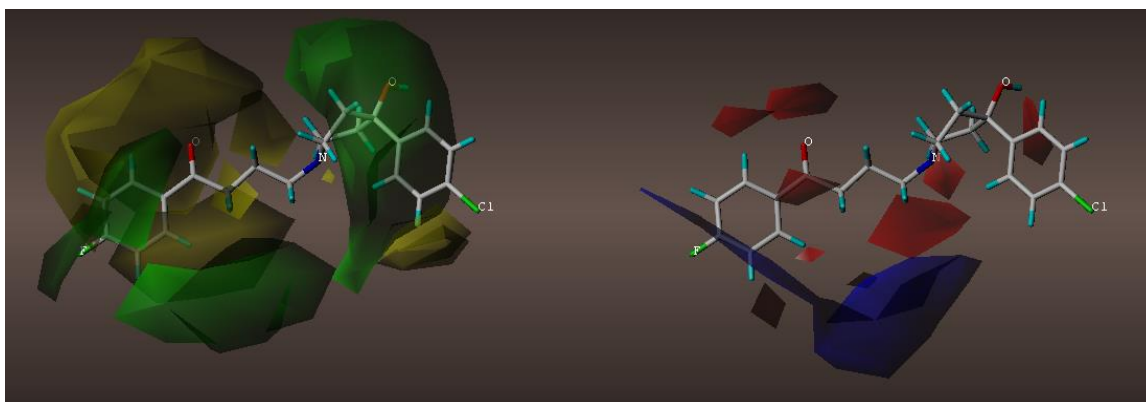


Figure 5.3 Haloperidol at B3LYP/6-31G* in sigma 1 CoMFA contour map.

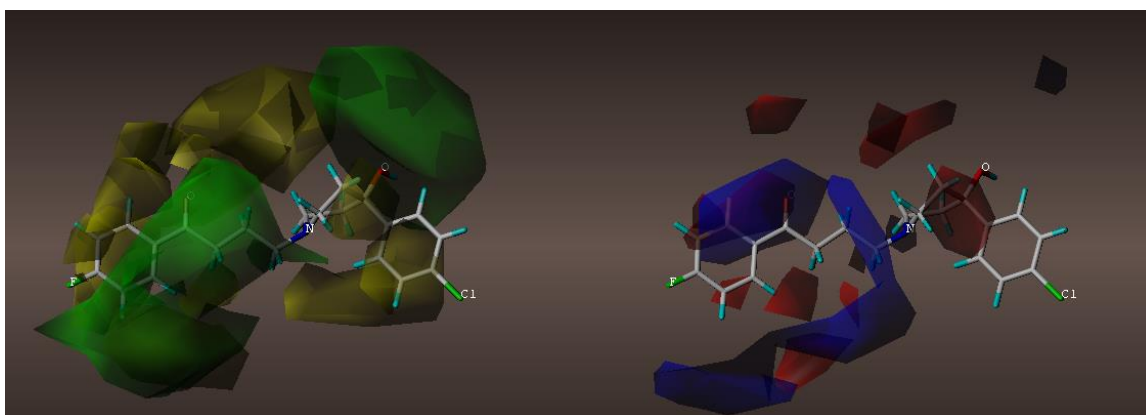


Figure 5.4 Haloperidol at B3LYP/6-31G* in sigma 2 CoMFA contour map.

CHAPTER 6

SUGGESTIONS FOR FURTHER WORK

Following the completion of the analysis around the sigma 1 and sigma 2 ligands studied in this work, the researcher concludes that the objectives of the study were met – from deriving pharmacophores for both receptor ligand subtypes, to designing comprehensive pharmacophores, to applying the designed comprehensive pharmacophores to the CoMFA alignments and models, to yielding robust CoMFA models and consequently useful contour maps which led to the understanding of the differences of sigma 1 and sigma 2 receptor ligands in addition to enabling the design of several new, highly bioactive ligands. Additionally, some comparison to previous work in the Gund group as well as other researchers' models globally was conducted.

Future work should encompass delving further into the analysis around sigma 1 vs sigma 2. Now that these CoMFA models have been confirmed as highly robust and predictive, they could be used for additional screening work for design of new ligands or prediction of bioactivity for various molecules. For instance, perhaps molecules could be designed to shift to either sigma 1 or sigma 2 activity depending on the need. If that design process could yield successful results, then it would be clear that there is indeed understanding of the differences between sigma 1 and sigma 2. Further, the models could be used to test other compounds for sigma 1 or sigma 2 prior to being synthesized in the lab.

Many researchers appear to modify the design of a ligand by varying ring size or shifting a substituent. Another approach could be to test those ideas in the CoMFA

models or more importantly, consider the bulk and electrostatics according to the models for the design initially.

Further work should be done to understand if flexible alignment is truly appropriate or sound. Many researchers claim this to be the case and in general the software programs expect that one will be mostly conducting flexible alignment. Perhaps some studies to conduct flexible alignment while measuring the energy differences and simultaneously comparing the results to the data generated here may be a first step in that process.

Finally, pharmacophore and CoMFA models can be expanded to include additional classes as new data is published.

APPENDIX A

ADDITIONAL CONTOUR MAPS FOR SIGMA 1 LIGANDS

The figures in APPENDIX A represent additional contour maps of the lead compounds for each sigma 1 class as well as the entire training set.

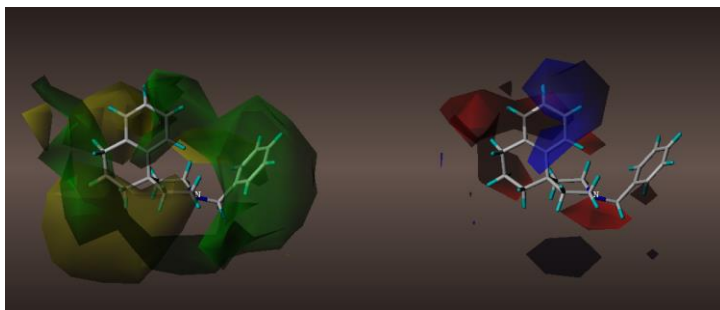


Figure A.1 Contour map of sigma 1 compound 1 at HF/6-31G*.

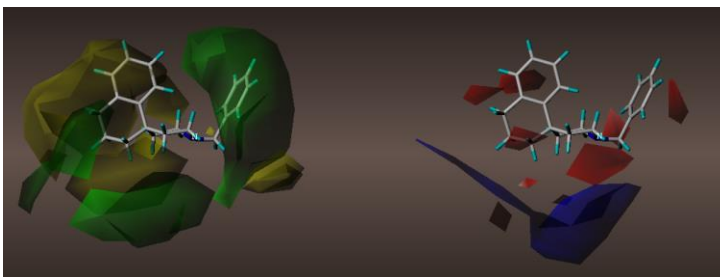


Figure A.2 Contour map of sigma 1 compound 1 at B3LYP/6-31G*.

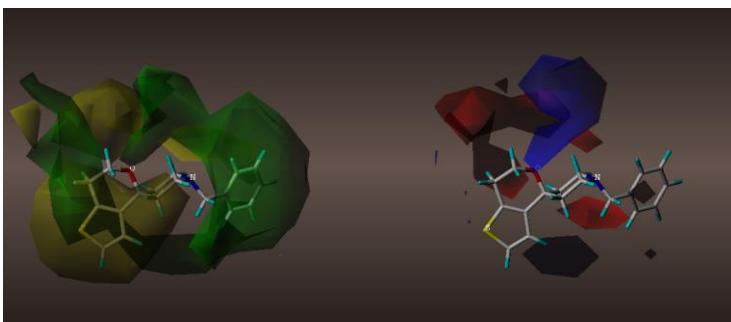


Figure A.3 Contour map of sigma 1 compound 9 at HF/6-31G*.

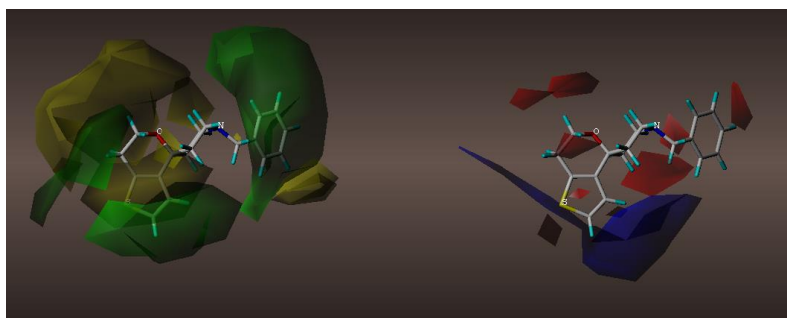


Figure A.4 Contour map of sigma 1 compound 9 at B3LYP/6-31G*.

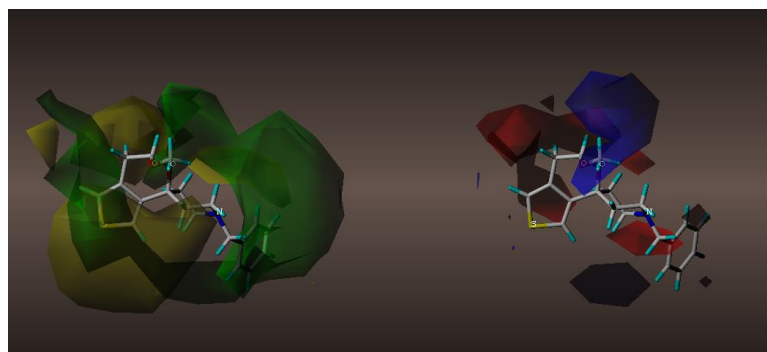


Figure A.5 Contour map of sigma 1 compound 22 at HF/6-31G*.

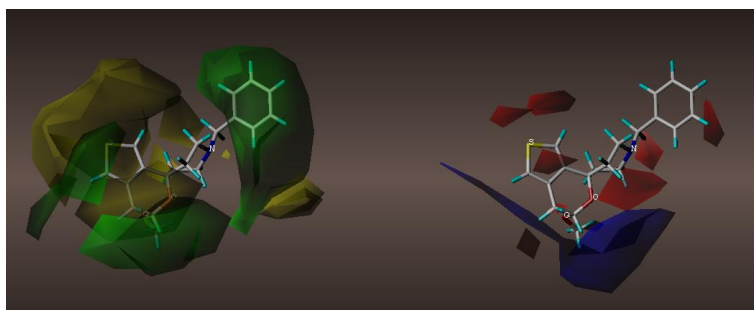


Figure A.6 Contour map of c sigma 1 compound 22 at B3LYP/6-31G*.

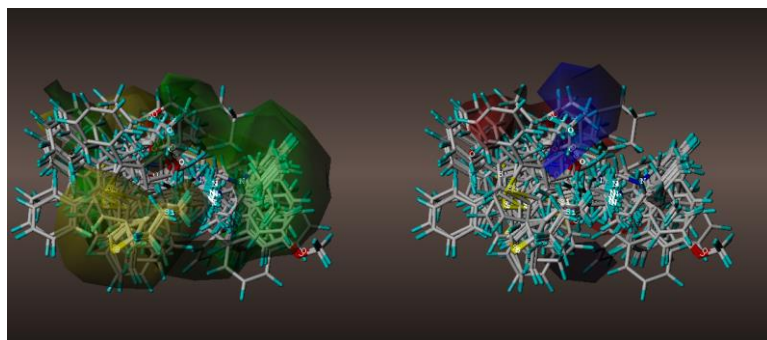


Figure A.7 Contour map of sigma 1 training set at HF/6-31G*.

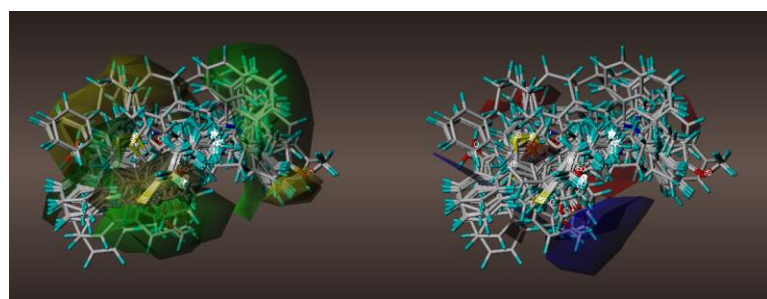


Figure A.8 Contour map of sigma 1 training set at B3LYP/6-31G*.

APPENDIX B

ADDITIONAL CONTOUR MAPS FOR SIGMA 2 LIGANDS

The figures in APPENDIX B represent additional contour maps of the lead compounds for each sigma 2 class as well as the contour maps of the entire training set.

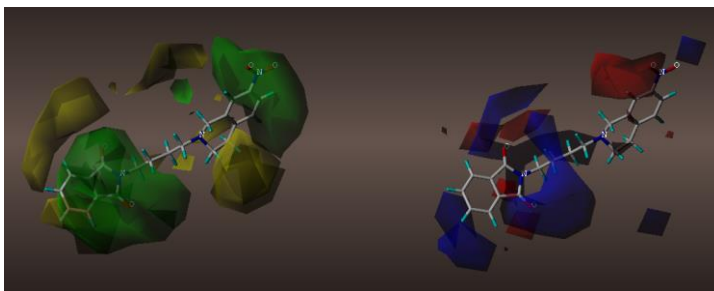


Figure B.1 Contour map of sigma 2 compound 37 at HF/6-31G*.

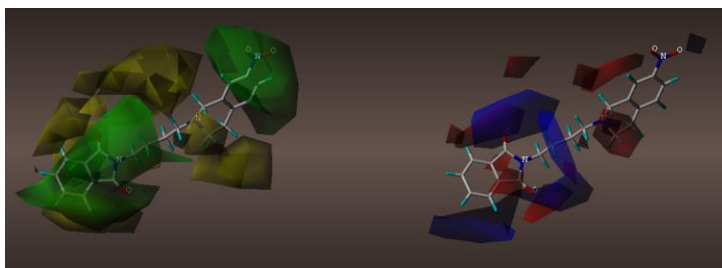


Figure B.2 Contour map of sigma 2 compound 37 at B3LYP/6-31G*.

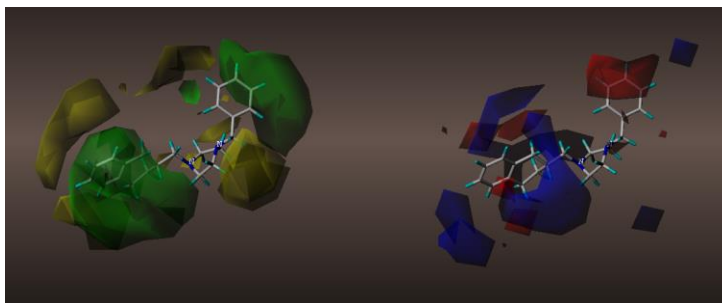


Figure B.3 Contour map of sigma 2 compound 43 at HF/6-31G*.

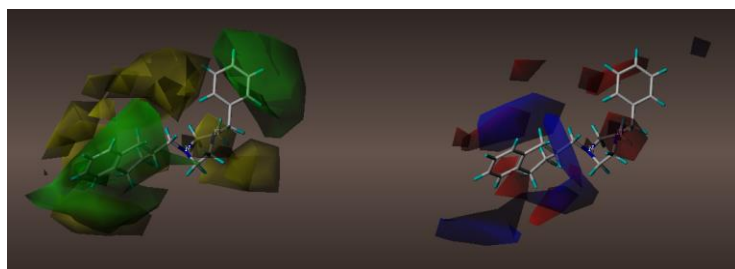


Figure B.4 Contour map of sigma 2 compound 43 at B3LYP/6-31G*.

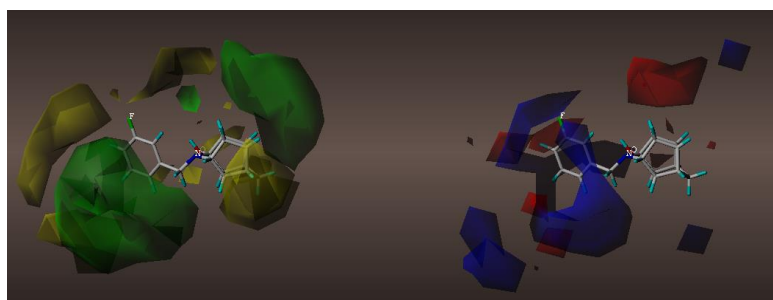


Figure B.5 Contour map of sigma 2 compound 52 at HF/6-31G*.

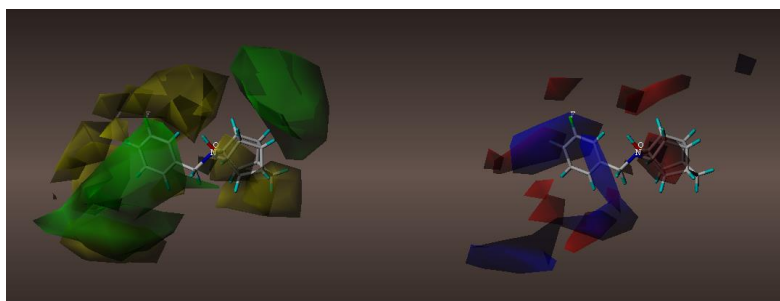


Figure B.6 Contour map of sigma 2 compound 52 at B3LYP/6-31G*.

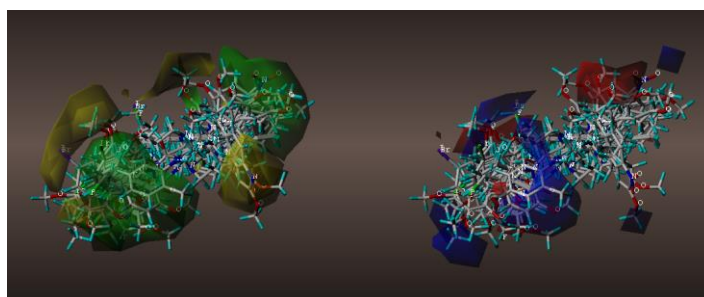


Figure B.7 Contour map of sigma 2 training set at HF/6-31G*.

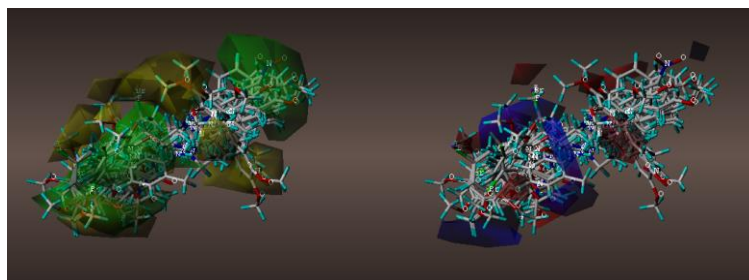


Figure B.8 Contour map of sigma 2 training set B3LYP/6-31G*.

APPENDIX C

ADDITIONAL CONTOUR MAPS FOR NEWLY DESIGNED SIGMA 2

LIGANDS

The figures in APPENDIX C represent additional contour maps of the newly designed sigma 2 ligands.

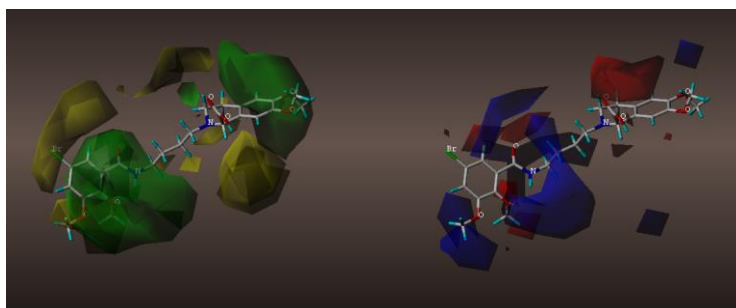


Figure C.1 Contour map of sigma 2 compound 56 at HF/6-31G*.

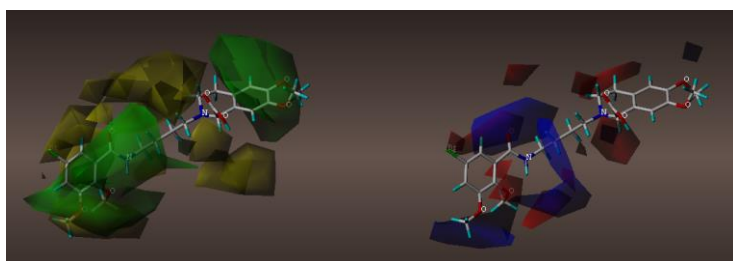


Figure C.2 Contour map of c sigma 2 compound 56 at B3LYP/6-31G*.

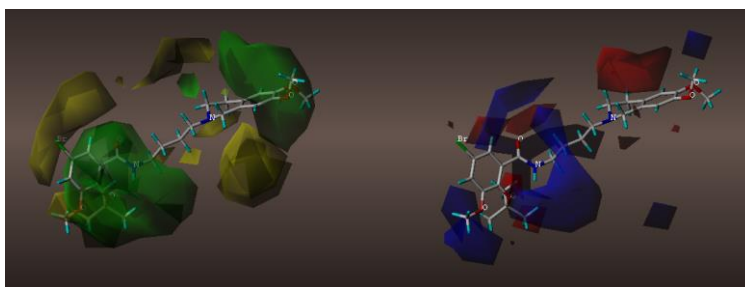


Figure C.3 Contour map of sigma 2 compound 57 at HF/6-31G*.

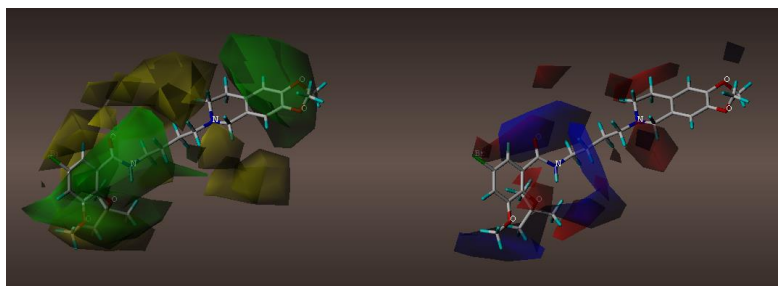


Figure C.4 Contour map of sigma 2 compound 57 at B3LYP/6-31G*.

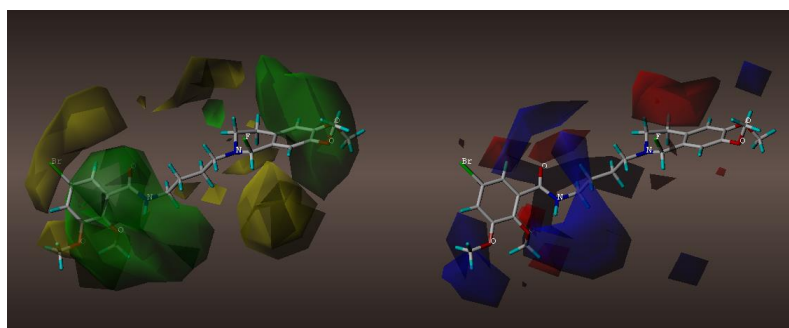


Figure C.5 Contour map of sigma 2 compound 58 at HF/6-31G*.

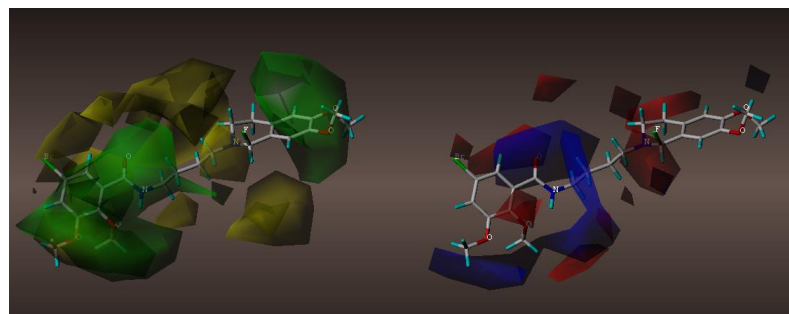


Figure C.6 Contour map of sigma 2 compound 58 at B3LYP/6-31G*.

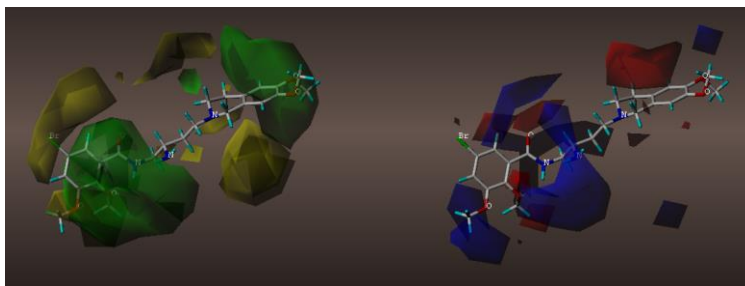


Figure C.7 Contour map of sigma 2 compound 59 at HF/6-31G*.

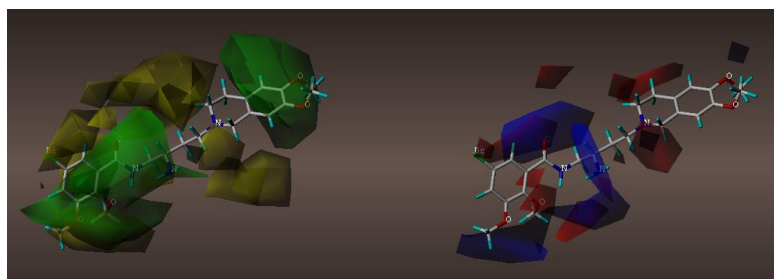


Figure C.8 Contour map of sigma 2 compound 59 at B3LYP/6-31G*.

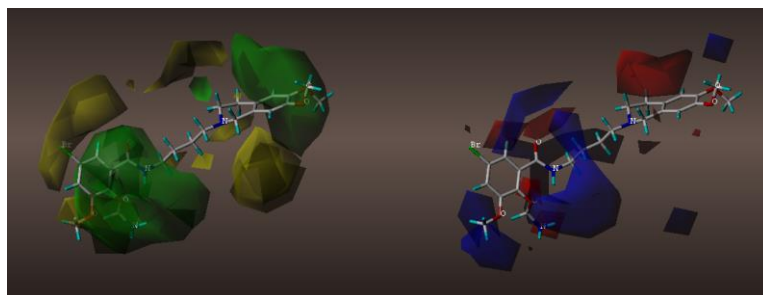


Figure C.9 Contour map of sigma 2 compound 60 at HF/6-31G*.

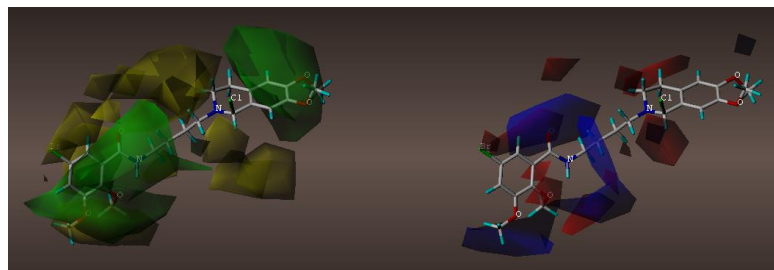


Figure C.10 Contour map of sigma 2 compound 60 at B3LYP/6-31G*.

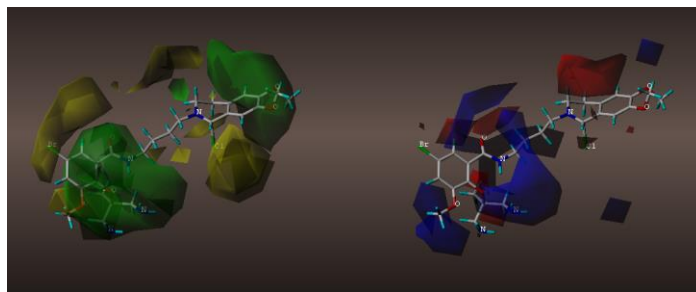


Figure C.11 Contour map of sigma 2 compound 61 at HF/6-31G*.

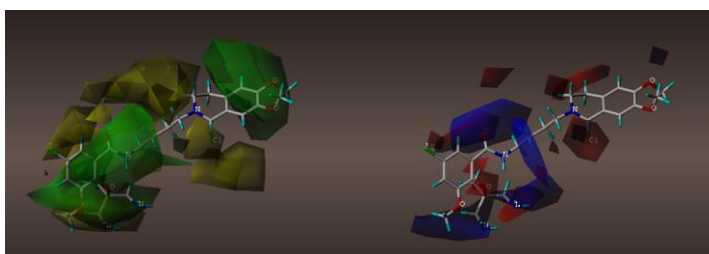


Figure C.12 Contour map of sigma 2 compound 61 at B3LYP/6-31G*.

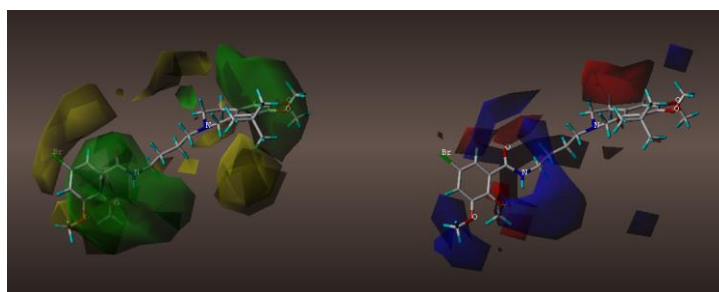


Figure C.13 Contour map of sigma 2 compound 62 at HF/6-31G*.

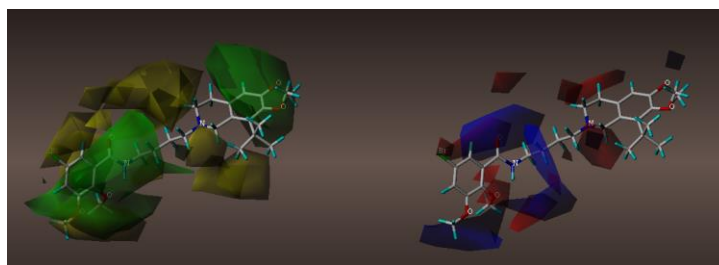


Figure C.14 Contour map of sigma 2 compound 62 at B3LYP/6-31G*.

REFERENCES

- Abate, C., Ferorelli, S., Contino, M., Marottoli, R., Colabufo, N.A., Perrone, R., and Berardi, F. *European Journal of Medicinal Chemistry*, **2011**, 46, 4733-4741.
- Abate, C. Niso, M., Marottoli, R. Riganti, C., Ghigo, D., Ferorelli, S., Ossato, G., Perrone, R., Lacivita, E., Lamb, D. and Berardi, F. *Journal of Medicinal Chemistry*. **2014**, 57, 3314-3323.
- Akunne, H.C., Whetzel, S.Z., Wiley, J. N., Corbin, A.E., Ninteman, F.W., Teclé, H., Pei, Y., Pugsley, T.A. and Heffner, T. G. *Neuropharmacology*. **1997**, 36(1), 51-62.
- Berardi, F., Ferorelli, S., Abate, C., Colabufo, N.A., Contino, M., Perrone, R. and Tortorella, V. *Journal of Medicinal Chemistry*. **2004**, 47, 2308-2317.
- Berg, J., Tymoczko, J., and Styrrer, L. *Biochemistry*. W.H. Freeman and Company : New York, New York, 2005; pp 1002-1026.
- Bolden, S., Boateng, C.A., Zhu, X.Y., Etukala, J.R., Eyunni, S.K., Jacob, M.R., Khan, S.I. and Ablordepey, S.Y. *Bioorganic and Medicinal Chemistry*. **2013**, 21, 7194-7201.
- Bonhaus, D.W., Loury, D. N., Jakeman, L.B., To, Z., DeSouza, A., Eglén, R.M. and Wong, E.H.F. *Journal of Pharmacology and Experimental Therapeutics* . **1993**, 267 (2), 961-970.
- Brune, S., Priel, S. and Wünsch, Bernhard. (2013). *Journal of Medicinal Chemistry*. **2013**, 56 (24), 9809-9912.
- Caballero, J., Zilocchi, S., Tiznado, W., Rossi, Daniela and Collina, S. *Molecular Simulation*. **2012**, 38, 227-235.
- Cannon, J. *Pharmacology for Chemists (2nd ed)*. Oxford University Press: New York, New York, 2007. pp 57-72.
- Cheng, Y. and Prusoff, W. *Biochemical Pharmacology*. **1973**, 22 (23), 3099-3108.
- Clark, M. and Cramer, R.D. III. *Quantitative Structure Activity Relationship*. **1993**, 12, 137-145.
- Cobos, E.J., Entrena, J.M., Nieto, F.R., Cendán, C.M. and Del Pozo, E.D. *Current Neuropharmacology*, **2008**, 6, 344-366.
- Collina, S., Loddò, G., Urbano, M., Linati, L., Callegari, A., Ortuso, F., Alcaro, S., Laggner, C., Langer, T., Prezzavento, O., Ronsisvalle, G. and Azzolina, O. *Bioorganic and Medicinal Chemistry*, **2007**, 15, 771-783.
- Cornish-Bowden, A. *Principles of Enzyme Kinetics*. Butterworths: Boston, Massachusetts, 1976. pp 52-76.
- Costatino, L. Gandolfi, F., Sorbi, C., Franchini, S., Prezzavento, O., Vittorio, F., Ronisvalle, G., Leonardi, A., Poggesi, E. and Brasili, L. *Journal of Medicinal Chemistry*. **2005**, 48, 266-273.

- Dessalew, N., Bharatam, P.V., and Singh, S.K. *QSAR and Combinatorial Science*. **2006**, 1, 85-91.
- Fan, K-H., Lever, J. and Lever, S. *Bioorganic and Medicinal Chemistry*. **2011**, 19, 1852-1859.
- Glennon, R.A. *Mini-Reviews in Medicinal Chemistry*, **2005**, 5, 927-940.
- Golbraikh, A. and Tropsha, A. Beware of q²! *Journal of Molecular Graphics and Modelling*. **2002**, 20, 269-276.
- Golbraikh, A., Shen, M., Xiao, Z., Xiao, Y.-D., Lee, K.-H., and Tropsha, A. *Journal of Computer-Aided Molecular Design*. **2003**, 17, 241-253.
- Gund, T.M., Floyd, J. and Jung, D. *Journal of Molecular Graphics and Modelling*. **2004**, 22, 221-230.
- Gund, T.M., Shukla, K. and Su, T-P. *Journal of Mathematical Chemistry*, **1991**, 8, 309-325.
- Gund, T.M., Shukla, K., Su, T-P. and Parish, D. *Multiple Sigma and PCP Receptor Ligands*; Kamenka, J-M and Domino, E., Ed.; NPP Books: Ann Arbor, Michigan, 1992; pp 53-57.
- Hajipour, A., Guo, L., Pal, A., Maviyutov., T. and Ruoho, A. *Bioorganic and Medicinal Chemistry*. **2011**, 19, 7435-7440.
- Hanner, M., Moebius, F.F., Flandorder, A., Knaus, H.G., Striessnig, J., Kempner, E., Glossman, H. *Proceedings of the National Academy of Sciences of the United States of America*. **1996**, 93, 9072-8077.
- Harel, D., Schepmann, D., Wünsch, B. *European Journal of Medicinal Chemistry*, **2013**, 69, 490-497.
- Höltje, H-D. Pharmacophore Identification and Receptor Mapping. *The Practice of Medicinal Chemistry*; Wermuth, C.G., Ed.; Academic Press: New York, New York, 1996; pp 437-455.
- Hornick, J., Vangveravong, S., Spitzer, D., Abate, C., Berardi, F., Goedegebuure, P., Mach, R. and Hawkins, W. *Journal of Experimental and Clinical Cancer Research*, **2012**, 31:41.
- Jasper, A., Schepmann, D., Lehmkuhl, K., Vela, J.M., Buschmann, H., Holenz, J. and Wünsch, B. *European Journal of Medicinal Chemistry*, **2012**, 53, 327-336.
- Jbilo, O., Vidal, H., Paul, S., De Nys, N., Bensaid, M., Silve, S., Carayon, P., Davi, D., Galieue, S., Bourrie, B., Guillemot, J. C., Ferrara, P., Loison, G., Maffrand, J. P., Le Fur, G. and Casellas, P. *Journal of Biological Chemistry*. **1997**, 272, 27107.
- Jung, D., Floyd, J and Gund, T.M. *Journal of Computational Chemistry*, **2004**, 25,1385-1398.

- Jung, D. Pharmacophore Derivation Using DISCOtech and Comparison of Semi-Empirical, Ab Initio and Density Functional CoMfa Study for Sigma 1 and Sigma 2 Receptor-Ligands. Ph.D. Thesis. New Jersey Institute of Technology, May 2003.
- Laggner, C., Schieferer, C., Fiechtner, B., Poles, G., Hoffman, R.D., Glossman, H., Langer, T., and Moebius, F. *Journal of Medicinal Chemistry*, **2005**, 4754-4764.
- Leach, A.R. *Molecular Modelling Principles and Applications*. Addison Wesley Longman Limited: Singapore, 1996. pp 543-582.
- Manallack, D.T., Wong, M.G., Costa, M., Andrews, P. and Beart, P. *Molecular Pharmacology*, **1988**, 34, 863-879.
- Marriott, K-S., Morrison, A.Z., Moore, M., Olubajo, O. and Stewart, O. *Bioorganic and Medicinal Chemistry*, **2012**, 20, 6856-6861.
- Martin, Y-C. and Lin, C.T. *The Practice of Medicinal Chemistry*; Wermuth, C.G., Ed.; Academic Press: New York, New York, 1996; pp 460-480.
- Meyer, C. Schepmann, D., Yanagisawa, S., Yamaguchi, J., Itami, K., and Wünsch, B. *European Journal of Organic Chemistry*. **2012**, 5972-5979.
- Meyer, C. Schepmann, D., Yanagisawa, S., Yamaguchi, J., Laurini, E., Itami, K., Pricl, S. and Wünsch, B. *Journal of Medicinal Chemistry*. **2012**, 55, 8047-8065.
- Nguyen, V.H. Kassiou, M., Johnston, G.A.R., Macdonald, C.J. *European Journal of Pharmacology*. **1996**, 311, 233-240.
- Park, H.R., Park, K-s, Choo, J., and Chong, Y. *Bulletin of the Korean Chemical Society*. **2009**, 30, 2117-2120.
- Patel, Hemantbhai. Development of Pharmacophore and CoMFA Study of Rigid and Flexible Sigma 2 Receptor Ligands. M.S. Thesis. New Jersey Institute of Technology, January 2010.
- Patrick, G. *Introduction to Medicinal Chemistry* (3rd ed). Oxford University Press: New York, New York, 2005. pp 185-703.
- Quaglia, W., Giannella, M., Piergentili, A., Pigini, M., Brasili, L., Di Toro, R., Rossetti, L., Spampinato, S. and Melchiorre, C. *Journal of Medicinal Chemistry*. **1998**, 41, 1557-1560.
- Rack, E., Fröhlich, R., Schepmann, D. and Wünsch, B. *Bioorganic and Medicinal Chemistry*, **2011**, 19, 3141-3151.
- Sharma, R. *Enzyme Inhibition: Mechanisms and Scope, Enzyme Inhibition and Bioapplications* [Online], **2012**. <http://www.intechopen.com/books/enzyme-inhibition-and-bioapplications/enzyme-inhibition-mechanisms-andscope> (accessed July 15, 2014).
- Rhoades, D.J., Kinder, D.H. and Mahfouz, T.M. *Medicinal Chemistry*. **2014**, 10, 98-121.
- Silverman, R. *The Organic Chemistry of Drug Design and Drug Action*. Elsevier Academic Press: New York, New York, 2004. pp 122-165.

- Spartan '14. Wavefunction, Inc., Irvine, CA 92612 in collaboration with Q-Chem, Pleasanton, CA, 2014.
- Su, T. P., Wu, X. Z., Cone, E. J., Shukia, K., Gund, T. M., Dodge, A. L. and Parish, D. W. *Journal of Pharmacology and Experimental Therapeutics*. **1991**, 259, 543-50.
- SYBYL X-2.1, Certara, L.P. St. Louis, MO, 2014.
- Tacke, R., Bertermann, R., Burschka, C., Dörrich, S., Fischer, M., Müller, B., Meyerhans, G., Schepmann, D., Wünsch, B., Arnason, I., and Bjornsson, R. *ChemMedChem*. **2012**, 7, 523-532.
- Wang, X., Li, Y., Deuther-Conrad, W., Xie, F., Chen, X., Cui, M-C., Zhang, X-J., Zhang, J-M., Steinbach, J., Brust, P., Liu, B-L. and Jia, J-M. *Bioorganic and Medicinal Chemistry*. **2013**, 21, 215-222.
- Wirsza, L. Development of Pharmacophore and CoMFA Studies for Sigma 2 Receptor Ligands. M.S. Thesis. New Jersey Institute of Technology, August 2008.
- Zamanillo, D., Romero, L., Merlos, M., Vela, J.M. *European Journal of Pharmacology*. **2013**, 716, 78-93.
- Zhang, L., Tsai, K.-C., Du, L., Fang, H., Li, M. and Xu, W. *Current Medicinal Chemistry*. **2011**, 18, 923-930.